Kink Oscillations of Expanding Coronal Loops in the Presence of Bulk Flow

Alexander Alexandrovich Shukhobodskiy

Submitted for the degree of Doctor of Philosophy

School of Mathematics and Statistics

September 2018

Supervisor: Robert von Fáy-Siebenbürgen

Co-Supervisor: Michael S. Ruderman

University of Sheffield

To my family.

Abstract

Transverse coronal loop oscillations were first observed by TRACE in 1998 and reported by Aschwanden et al. (1999) and Nakariakov et al. (1999). One important property of transverse coronal loop oscillations is that they are usually strongly damped with the damping time being comparable with the oscillation period. However, sometimes this is not the case. At present, a generally accepted mechanism of this damping is resonant absorption. Observations show that very often oscillating coronal loops are in a highly dynamic state. In particular, they can cool quickly with a characteristic cooling time of the order of a few periods of kink oscillation. It was later showed theoretically that cooling causes amplification and may result in existence of oscillations for which amplitude does not vary in time. Although the coronal loop expansion is relatively small, the ratio of the loop cross-section radii at the apex and at the foot-points still can be about 1.5. These leads to particular interest the effect of expansion on kink oscillations. A coronal loop is modelled as a cylindrical magnetic flux tube. The tube consists of a core region and a thin transitional region at the tube boundary. The plasma density monotonically decreases from its value in the core region to the value outside the tube. Both the plasma density and velocity of background flow vary along the tube and in time. Using multiscale expansions, the system of two equations describing the kink oscillations was derived. This model is studied both analytically by employing Wentzel-Kramer-Brillouin (WKB) method and numerically. We found out that the expansion of cross-section enhances the amplification of amplitude of kink oscillations and decreases the frequency of the oscillations. In addition we showed theoretically that a coronal loop cooling may lead to amplification of amplitude or non-monotonic amplitude profile even in presence of resonant damping. That result is particularly interesting from the coronal seismology point of view, since it is a good candidate for physical mechanism behind recent observation of kink oscillations of coronal loops with amplified and varying amplitudes.

Contents

List of Tables

List of Figures

List of Symbols

A	amplitude of kink oscillation
$\boldsymbol{B}$	background magnetic field
$\boldsymbol{b}$	perturbation of the magnetic field
$C_k = \sqrt{\frac{2B^2}{\mu_0(\rho_i+\rho_e)}}$	kink speed
$g \approx 274 ms^{-2}$	gravity acceleration
H	atmospheric scale height
k_B	Boltzmann constant
L	characteristic scale of spacial variation along the tube
L_c	arbitrary constant with the dimension of length
$l(z)$	thickness of the transitional region at z
m	mean mass per particle
P	magnetic pressure perturbation
p	kinetic pressure
$R(z)$	radius of a magnetic flux tube at z
R_f	radius at a magnetic flux tube footpoint
T	temperature of plasma
$\boldsymbol{U}$	background flow velocity
$\boldsymbol{u}$	velocity perturbation
$V_A = \sqrt{\frac{B^2}{\mu_0\rho}}$	Alfvén speed
$W = rB\xi_\perp$	scaled displacement perpendicular to the magnetic field
$w = B\xi_\perp$	scaled displacement perpendicular to the magnetic field
$\beta = \frac{2\mu_0 p}{B^2}$	plasma-beta
$\eta = \frac{\xi_\perp}{R(z)}\Big\|_{\psi=\psi_i}$	dimensionless displacement of the internal region boundary
$\vartheta = \frac{R(z)}{R_f}$	expansion factor
ι	coefficient of shear viscosity
μ_0	magnetic permeability of free space
ξ	plasma displacement
$\xi_\perp$	plasma displacement perpendicular to the magnetic field
ξ_ϕ	angular plasma displacement
ρ	plasma density
ρ_e	density in the external region
ρ_i	density in the internal region
ρ_t	density in the transition region
ψ	magnetic flux function
$\omega(t)$	oscillation frequency

Chapter 1

Introduction

§ 1.1 Sun Structure and Coronal Loops

1.1.1 Sun Structure

The Sun is a marvellous object, which we all can observe in everyday life. It gives us almost all the energy to sustain life in our planet. It is a subject of great interest for humanity starting from the ancient times. For example, there is historical evidence of recording solar eclipses by ancient Chinese and Greeks. However, until recently, the observational tools were not able to produce detailed picture of the Sun. The new era of observations started by launching space instruments. This revolutionised observations and helped us to have better understanding of the Sun. The first instrument to give us the moderately detailed impression of solar surface and atmosphere is known as SkyLab which was launched in 1973. SkyLab was able to obtain images in soft x-ray wavelength (2.34 – 4.4nm). Afterwards more space missions were launched with even better suits of instruments. These instruments were able to produce images with wider and better resolved spectra and higher quality resolution.

Now, we describe the structure of the Sun. It is assumed that the Sun consists of plasma. Plasma is a state of matter in which a fluid is highly ionised, which results in high electrical conductivity, so that electric and magnetic field govern the behaviour of the matter. Solar structure may be summarised as follows (see e.g. Priest, 2014). The Sun consists of a few different layers (see Figure 1.1). These layers are united into two distinct groups: internal region and solar atmosphere. The former cannot be seen directly and consists of the core, the radiative zone, the tachocline and the convection zone. On the contrary, the latter is visible and consists of the photosphere, the chromosphere, the transition zone and the corona. The theory suggests that about 50% of the solar mass, $M_\odot \approx 1.99 \times 10^{30}$ kg, is located inside the core. However, its radius is only 25% of the radius of the Sun, $R_\odot = 695.5$ Mm. It is estimated that 99% of nuclear fusion occurs in this region, giving the enormous amount of energy, with estimate of core temperature $T_{cs} = 1.5 \times 10^7$ K. The produced energy is carried by different processes to the surrounding plasma. The other internal regions, with exception of the tachocline, are named by the proposed main energy transfer mechanism. The closest layer to the core is known as the radiative zone, with the main mechanism of energy transfer as radiation and estimated thickness $0.45R_\odot$. The next layer is known as the tachocline. This is a very thin transition region between the radiative zone and the convection zone with estimated thickness of $0.04R_\odot$. The main property the tachocline is known to posses is high shear stress. That is because the two adjacent layers: the radiative zone and convection zone, posses different rotational behaviours, with the first rotating more like a solid and with the second rotating as a liquid. The next layer is known as convection zone, where convection is assumed to be the main mechanism of the energy transfer. That means that, in this layer, hot plasma is literally moving outward of the the Sun center to the cooler parts of the Sun. The estimated thickness for this zone is $0.3R_\odot$. The next layer is on the surface of the Sun and the first visible layer is known as the photosphere. Its estimated thickness is $7 * 10^{-4} R_\odot$ Mm, which makes it relatively thin compare to other Sun's regions. However, it is relatively dense if one

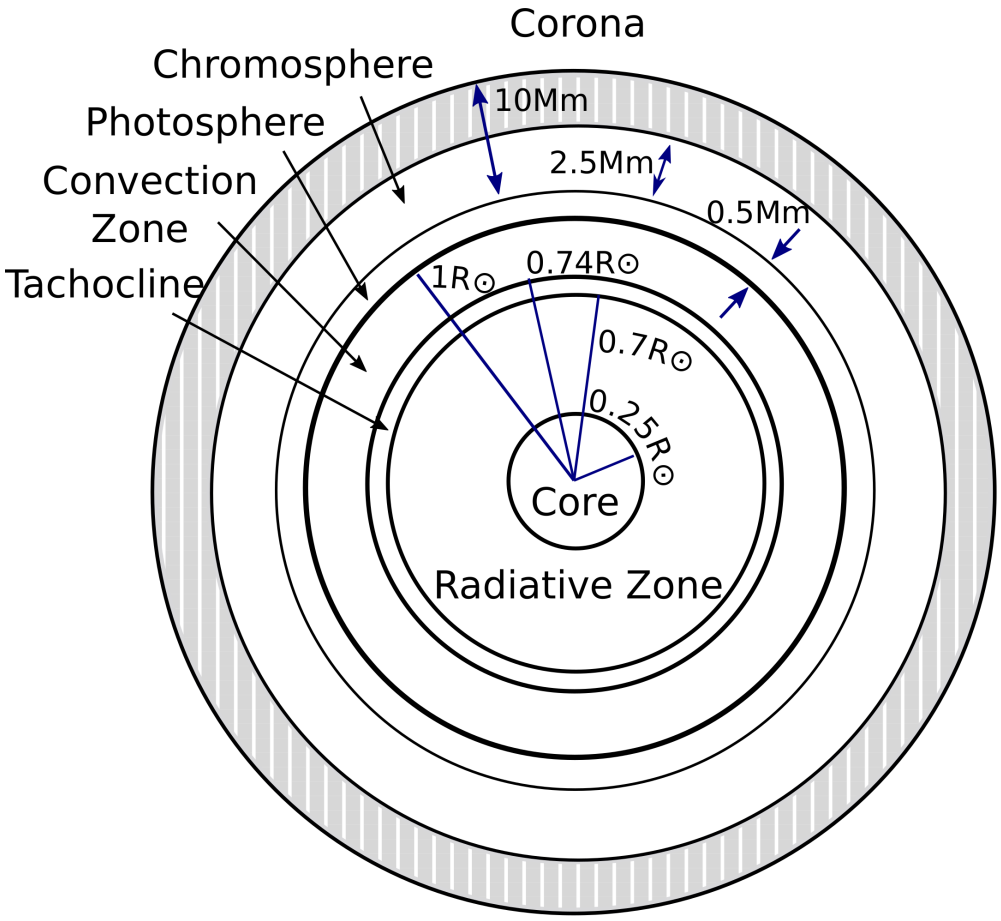

Figure 1.1: The graphical representation of the Sun's structure. The length and distances are not up to scale. The region between chromosphere and corona may varies between 2.5 – 15 Mm and indicated as pinstripes region.

compares it with densities of the solar atmosphere, the chromosphere and the corona. The typical density for photosphere is 10^{-9} kg/m^3, where chromospheric, lower corona and higher corona densities are typically 10^4, 10^8 and 10^{12} times lower, respectively. The thickness of solar chromosphere varies around the Sun with estimated variation of $0.003 - 0.02 R_\odot$ Mm. The transition zone is the thin layer of the atmosphere, where the temperature rises from the chromospheric values to that of the lower corona. The corona is the outer layer of the solar atmosphere with a strong magnetic field and low density. This layer is, normally, not visible without special equipments. Nevertheless, in case of a solar eclipse it is possible to see it even with bare eye. The low solar corona is normally considered to be present within $1 - 3$ $R_\odot$ from the Sun center, where the higher solar corona is further away from the center. For better understanding of the processes discussed later, it is convenient to introduce the plasma-beta β,

$$\beta = \frac{2\mu_0 p}{B^2}, \tag{1.1}$$

where μ_0 is the magnetic field permeability, p is the kinetic pressure and B is the strength of the magnetic field. This parameter enables us to understand what types of forces are dominant in the region of study. Also, $P = B^2/2\mu_0$ is known as the magnetic pressure. The corona has low plasma-beta, $\beta \ll 1$ in the low corona and active regions, while β varies in the high corona.

The solar corona is an object of high interest for research as it has temperatures between 1 MK and 10 MK, while in the photosphere $T \approx 6$ kK (see e.g. Eddy et al., 1979). So far the difference in temperatures remains a mystery and it is one of the major problems of solar physics, known as coronal heating problem. However, there are two main mechanisms suggested to solve this problem. One is the magnetic reconnection of current sheets (see e.g. Priest, 1999) and the other is the dissipation of magnetic waves generated in the convection zone (see e.g. Roberts, 2000).

1.1.2 Coronal Loops

To describe what is a coronal loop, it is important to define a magnetic field line. A field line is a curve, for which the tangent line at each point is parallel to the magnetic field direction. The Sun's surface contains many closed field lines, the ones that are filled with a relatively dense plasma are known as coronal loops (see Figure 1.2). These structures are normally observed in various parts of electromagnetic spectrum, such as soft X-rays, EUV (extreme ultraviolet) and visible spectrum. The temperature of coronal loops varies from 0.1 MK to 5 MK and are classified as cool loops for temperatures between 0.1 MK and 1MK (observed in UV(ultraviolet) spectrum by, e.g. SOHO (Solar and Heliospheric Observatory) launched in 1996), warm loops for temperatures between 1 MK and 2 MK (observed in EUV spectrum by, e.g. TRACE (Transitional Layer and Solar Corona) launched in 1998) and hot loops with temperatures greater the than 2 MK (observed in the soft X-rays spectrum, by e.g. Skylab). The length of loops also varies from 0.1 Mm to 1000 Mm. To be able to understand what follows we need to define what is a kink oscillation. Two normal modes of oscillation which are considered in this thesis are the kink mode and the sausage mode. These modes have simple mathematical formulation. We apply Fourier analysis to perturbed variables in governing equations. In the cylindrical polar coordinates, this means that perturbations will be proportional to the exponent term of a form $\exp[i(kz + m\phi - \omega(t))]$. Here k is the longitudinal wavenumber, m is wavenumber and $\omega(t)$ is the oscillation frequency. In case $m = 0$ oscillation mode is known as sausage mode, for $m = 1$ it is known as kink mode (there are also modes for $m > 1$ known as flute modes).

Known properties of kink oscillations may be summarised as follows: oscillations have boundaries of a plasma object going in phase, they are weakly compressible, have little variation in cross-section, density and thus produce the motion of the coronal loops. On the other hand, sausage modes are highly compressible, the boundaries of a plasma object are moving out of phase and pulsate. In what follows we focus on magnetic flux tubes of cylindrical shape. The schematic representation for kink and

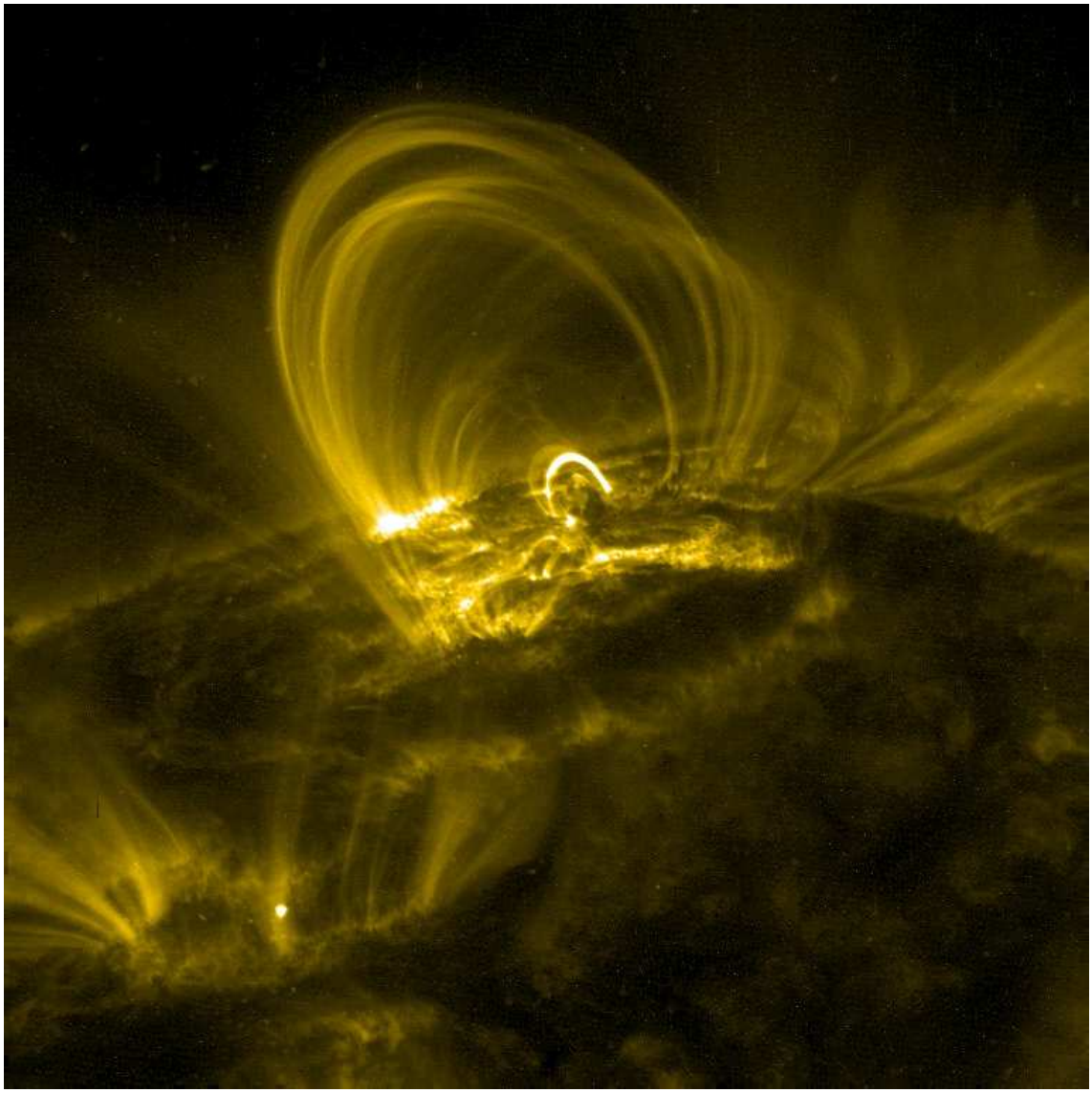

Figure 1.2: Image of the Sun obtained by TRACE on 8 of September 2005. In the 171 Å

sausage waves for the case of flux tube is shown in Figure 1.3. The cylindrical shape is a relatively good approximation as theoretical results obtained using it correlate with the one obtained with observation (see e.g. Goossens et al., 2005). Nevertheless, since our observations are limited, we do not know for sure if this shape is correct or even that the loop is monolithic and does not consist of separate discrete threads.

The transverse coronal loop oscillations were first observed by TRACE in 1998 and were reported by Aschwanden et al. (1999) and Nakariakov et al. (1999). It has also been seen that usually kink oscillations of coronal loops are heavily damped (see e.g. Nakariakov et al., 1999), however, sometimes this is not the case (see e.g. Wang

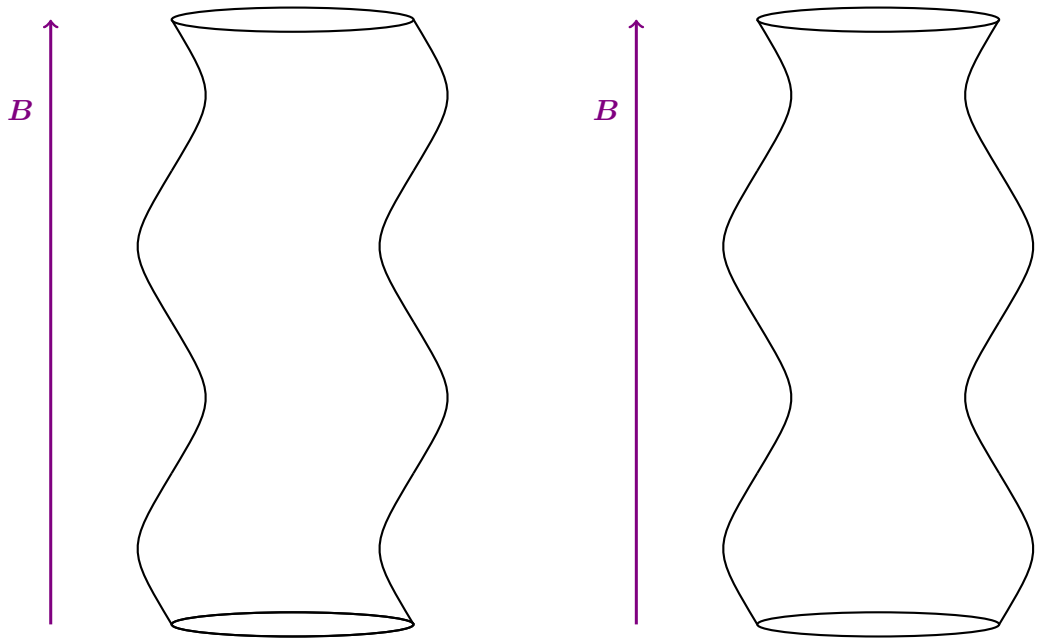

Figure 1.3: Kink oscillation ($m = 1$) and Sausage oscillations ($m = 0$) in a presence of background magnetic field $\boldsymbol{B}$

et al., 2012; Anfinogentov et al., 2013; Nisticò et al., 2013). It is still not known why there is such a fast decay of kink oscillations. Although there is a good candidate for explanation, which is resonant absorption (see e.g. Ruderman and Roberts, 2002; Goossens et al., 2002). Resonant absorption occurs when the external driving waves reach location, where their frequency matches the local Alfvén or cusp frequency (see e.g. Goossens et al., 2011 and references therein). The latest absorb the energy from the driving waves at the resonance layer. This results in a stronger wave which propagates perpendicular to the direction of the magnetic field. As a result, the energy will be dissipated and heating will occur. Cool chromosphere plasma entering the coronal loop may cause flows inside the magnetic flux tube (see e.g. Ofman and Wang, 2008; Chae et al., 2008). Therefore, the effects of resonant absorption on kink oscillations of an expanding magnetic flux tube in a presence of the bulk flow will be of a great interest to study.

§ 1.2 Previous Work and Observations

After transverse coronal loop oscillations were first observed by TRACE in 1998 and reported by Aschwanden et al. (1999) and Nakariakov et al. (1999), they received ample attention in the solar physics community. Since then, these oscillations were routinely observed during various space missions (see e.g. Erdélyi and Taroyan, 2008; Duckenfield et al., 2018; Su et al., 2018; Abedini, 2018, and references therein).

An important property of transverse coronal loop oscillations is that they are

strongly damped with the damping time being comparable with the oscillation period. At present, a generally accepted mechanism of this damping is resonant absorption. It was suggested by Hollweg and Yang (1988) ten years before the first observation of transverse coronal loop oscillations that they can be strongly damped by resonant absorption. Hollweg and Yang (1988) studied resonant absorption using planar geometry, but then translated their result to cylindrical geometry and obtained the correct expression for the decrement in the thin tube approximation. Later, Goossens et al. (1992) studied the damping of kink oscillations of magnetic flux tubes due to resonant absorption in the general case. Ruderman and Roberts (2002) applied the theory of wave damping due to resonant absorption to the first observation of coronal loop kink oscillations. They showed that the observed damping of these oscillations can be used to obtain information about the internal structure of coronal magnetic loops. Ruderman and Roberts (2002) modelled a coronal loop as a magnetic tube consisting of an internal core of radius R and a transitional or boundary layer of thickness ℓ between the dense core plasma and the rarefied surrounding plasma. They obtained that the decrement is proportional to ℓ/R. Using the data on the oscillation damping reported by Nakariakov et al. (1999) Ruderman and Roberts (2002) obtained that $\ell/R = 0.23$. Goossens et al. (2002) used observations of eleven cases of damped kink oscillations of coronal magnetic loops to estimate ℓ/R. They obtained values of ℓ/R between 0.16 and 0.49. Since then, observations of damped coronal loop oscillations are continuously used to obtain information on the loop internal structure (e.g. Ruderman and Erdélyi, 2009; Goossens et al., 2011).

In the earlier studies of kink oscillations of coronal magnetic loops, a very simple model of a homogeneous magnetic cylinder was used (e.g. Ryutov and Ryutova, 1976; Edwin and Roberts, 1983). In this model, the tube has a sharp boundary. That means that there will be no singularity which will include dissipative terms in the analyitcal solution, so such models do not describe resonant absorption. To describe resonant absorption, the model with sharp boundary was modified by including a transitional layer at the tube boundary. By adding the transitional layer with varying density, the analytical solution will have a singularity, which will lead to inclusion of dissipative terms to proceed with analytical results (see e.g. Ruderman, 2011b). Later, more realistic models of coronal loops were studied. Such modification to the earlier homogeneous mangetic flux tube model was obtained by considering the following: curved magnetic flux tubes (see e.g. Ruderman, 2003), twisted magnetic flux tubes (see e.g. Ruderman, 2007), expanding magnetic flux tubes (see e.g. Ruderman et al., 2008), magnetic flux tubes in a presence of background flows (see e.g. Ruderman, 2010) and magnetic flux tubes with variable density (see e.g. Dymova and Ruderman, 2006a). In particular, the variation of the plasma density along the tube was taken into account. Dymova and Ruderman (2006a) investigated the resonant damping of kink oscillations of a magnetic tube with such density variation. The main result that they obtained is the following: if the ratio of densities in the tube core and in the surrounding plasma is constant, and the ratio of density inside the boundary layer and in the tube core does not vary along the tube, then the ratio of the damping time and oscillation period is not affected by the density variation along the tube.

Although the coronal loop expansion is relatively small, the ratio of the loop cross-section radii at the apex and at the foot-points still can be about 1.5 (Klimchuk, 2000; Watko and Klimchuk, 2000). On the other hand, in the chromosphere the expansion of vertical magnetic flux tubes can be as large as a few hundred (e.g. Tsuneta et al., 2008). Hence, to account for magnetic flux tube expansion is important. Ruderman et al. (2008) and Verth and Erdélyi (2008) derived the equation describing kink oscillations of an expanding magnetic flux tube. They considered a magnetic flux tube with a sharp boundary meaning that the equation that they derived does not describe resonant damping. Ruderman et al. (2017) generalised this derivation to include a siphon flow, temporal variation of the plasma parameters, and a transitional layer at the tube boundary.

Observations show that very often oscillating coronal loops are in a highly dynamic state. In particular, they can cool quickly with a characteristic cooling time of the order of a few periods of kink oscillation (e.g. Aschwanden and Terradas, 2008). Morton and Erdélyi (2009, 2010) found that cooling results in the decrease of the period of the coronal loop kink oscillations, while similar results were found by Al-Ghafri et al. (2014) for longitudinal oscillations. Ruderman (2011a) showed that cooling causes the amplification of coronal loop kink oscillations. Ruderman (2011b) studied the competition between cooling and resonant damping. He showed that this competition can result in the existence of kink oscillations with the amplitude not varying in time. Recently, Ruderman et al. (2017) studied the effect of tube expansion on kink oscillations of cooling coronal loops. Shukhobodskiy and Ruderman (2018) studied the effect of damping of the resonant absorption on the amplification due to cooling.

§ 1.3 Motivation

In previous section we discussed previous works done in the area of kink oscillations of coronal loops. Although we have good analytical models we still have numerous observations, which are hard to explain by applying the current analytical knowledge on the observed features the good candidate will be non-damped and amplified kink oscillations of coronal loops. Thus, it will be a particularly interesting to add new degree of complexity in existing models to be able obtain better physical understanding behind the processes involved in such complex phenomena. As a result, the main aim of this thesis is to obtain a model for kink oscillations of an expanding coronal loops in a presence of background flow under cold plasma approximation. This approximation means that magnetic forces are dominant compared to internal energy. Thus, we can assume $\beta = 0$.

To have a better understanding of why such a model is proposed, we will briefly describe two previous models, which will intuitively lead to our case.

First of all, we start from the work done by Ruderman et al. (2008). These authors considered straight cylindrical magnetic flux tube with variable cross-section with equilibrium configuration given by Figure 1.4. Here, $R(z)$ is cross-section radius, $\boldsymbol{B}$ is background magnetic field ρ_i, ρ_e are internal and external densities and L is the length of the tube. Ruderman et al. (2008) showed that for ideal MHD (Magnetohydrodynamics)

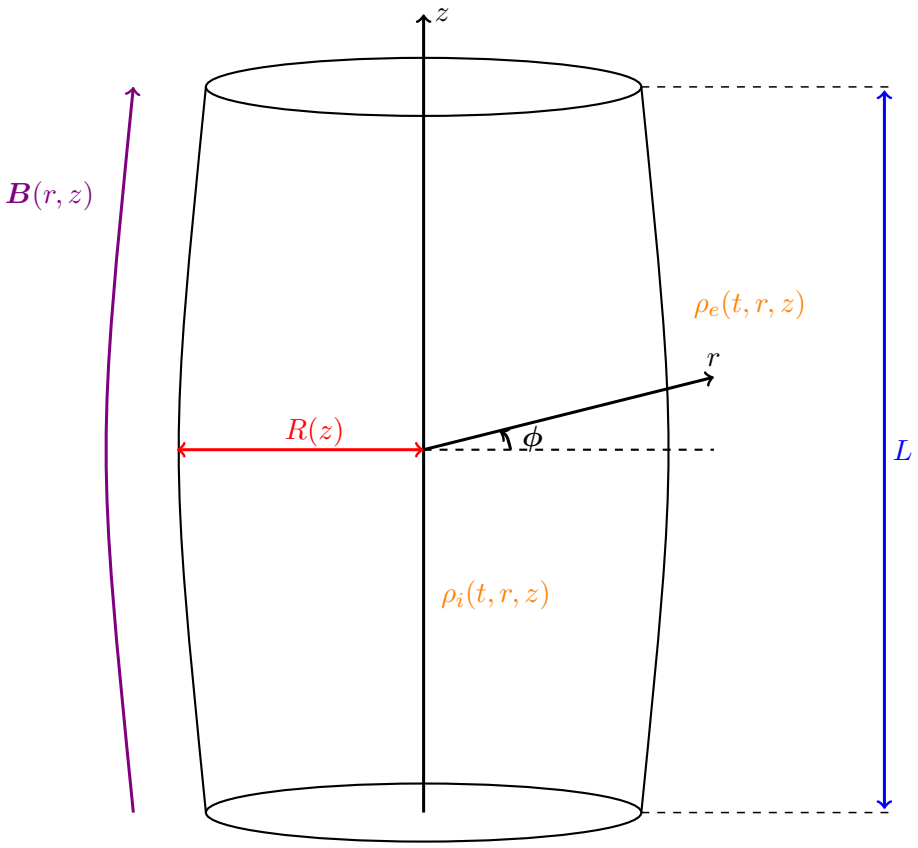

Figure 1.4: Equilibrium configuration of the straight expanding the magnetic flux tube

equations, under cold plasma and thin tube approximations, the background magnetic field $\boldsymbol{B}$ is potential ($\boldsymbol{B} = \nabla \times \boldsymbol{\Psi}$, where $\boldsymbol{\Psi}$ is the magnetic vector potential). It was also assumed that $\boldsymbol{B} \to B_\infty \mathbf{e}_z$ as $r \to \infty$, where B_∞ is a positive constant and $\mathbf{e}_z$ is a unit vector in the z direction. The following model satisfying the potential magnetic field was considered

$$\psi = (1/2)B_\infty r^2 + \psi_* r J_1(r/l)\cosh(z/L_c), \tag{1.2}$$

where ψ_* and L_c are arbitrary constants, $J_1(x)$ is the Bessel function of the first kind and first order and magnetic flux function ψ is defined by the following equation:

$$B_r = -\frac{1}{r}\frac{\partial \psi}{\partial z}, \quad B_z = \frac{1}{r}\frac{\partial \psi}{\partial r}. \tag{1.3}$$

As a result, the expression for cross-section expansion $R(z)$ was obtained

$$R(z) = R_f \lambda \sqrt{\frac{\cosh(L/2L_c) - 1}{\cosh(L/2l_c) - \lambda^2 + (\lambda^2 - 1)\cosh(z/L_c)}}. \tag{1.4}$$

The above equation will be used in the thesis to model the cross-section expansion under different equilibrium configurations to study various effects. In addition Equation (1.4)

Ruderman et al. (2008) derived equations which are governing the model proposed. This equation reads as follows:

$$\frac{\partial^2 u}{\partial t^2} = \frac{h\sqrt{h}}{\rho}\left[\frac{h}{\mu_0}\frac{\partial^2}{\partial z^2}\left(\frac{u}{\sqrt{h}}\right) - \sqrt{2\psi}\left(\frac{h'}{2}\frac{\partial Q}{\partial z} + h^2\frac{\partial Q}{\partial \psi}\right)\right] \tag{1.5}$$

$$\frac{\partial^2 \xi_\phi}{\partial t^2} = \frac{h\sqrt{h}}{\rho}\left[\frac{1}{\mu_o}\frac{\partial^2(\xi_\phi\sqrt{h})}{\partial z^2} - \frac{h}{\sqrt{2\psi}}\frac{\partial Q}{\partial \phi}\right], \tag{1.6}$$

$$Q = \frac{-1}{\mu_0\sqrt{2h\phi}}\left(\frac{h'\psi}{h^2}\frac{\partial u}{\partial z} + 2\psi\frac{\partial u}{\partial \psi} + u + h\frac{\partial \xi_\phi}{\partial \phi}\right), \tag{1.7}$$

where $u = B\xi_\perp$, $\xi_\perp$ is perpendicular displacement, ξ_ϕ is angular displacement, $\psi = 1/2r^2h(z)$ and $h(z)$ is an arbitrary function such that $R^2(z)h(z) = const.$ Then, again, using the thin tube approximation, Ruderman et al. (2008) derived the equation that determines eigenmodes and eigenfrequencies,

$$\frac{\partial^2 \eta}{\partial z^2} + \frac{\omega^2}{C_k^2}\eta, \quad \eta = 0 \quad \text{at} \quad z = \pm L, \tag{1.8}$$

where

$$C_k^2 = \frac{2B^2(z)}{\mu_0\left[\rho_i(z) + \rho_e(z)\right]} \quad \text{and} \quad \eta = \frac{\xi_\perp}{R(z)}, \tag{1.9}$$

ω is the frequency, and $B(z)$ is the magnetic field strength. Note that Equations (1.5)–(1.9) were obtained under thin tube approximation, author assumed that coronal loop length is much larger than coronal loop diameter.

The second model was studied by Ruderman (2011a), where a straight magnetic tube with constant cross-section and plasma flow driven by density ρ variation (see Figure 1.5) was considered. The density varies in the radial direction between its value inside the tube, ρ_i, and outside the tube, ρ_e, in a transitional layer of thickness l. This additional layer enables to consider effect of the damping due to resonant absorption. The density also varies along the tube and depends on time. Hence, the density is given by

$$\rho = \begin{cases} \rho_i(t,z), & 0 < r < R - l/2, \\ \rho_t(t,r,z), & R - l/2 < r < R + l/2, \\ \rho_e(t,z), & r > R + l/2. \end{cases} \tag{1.10}$$

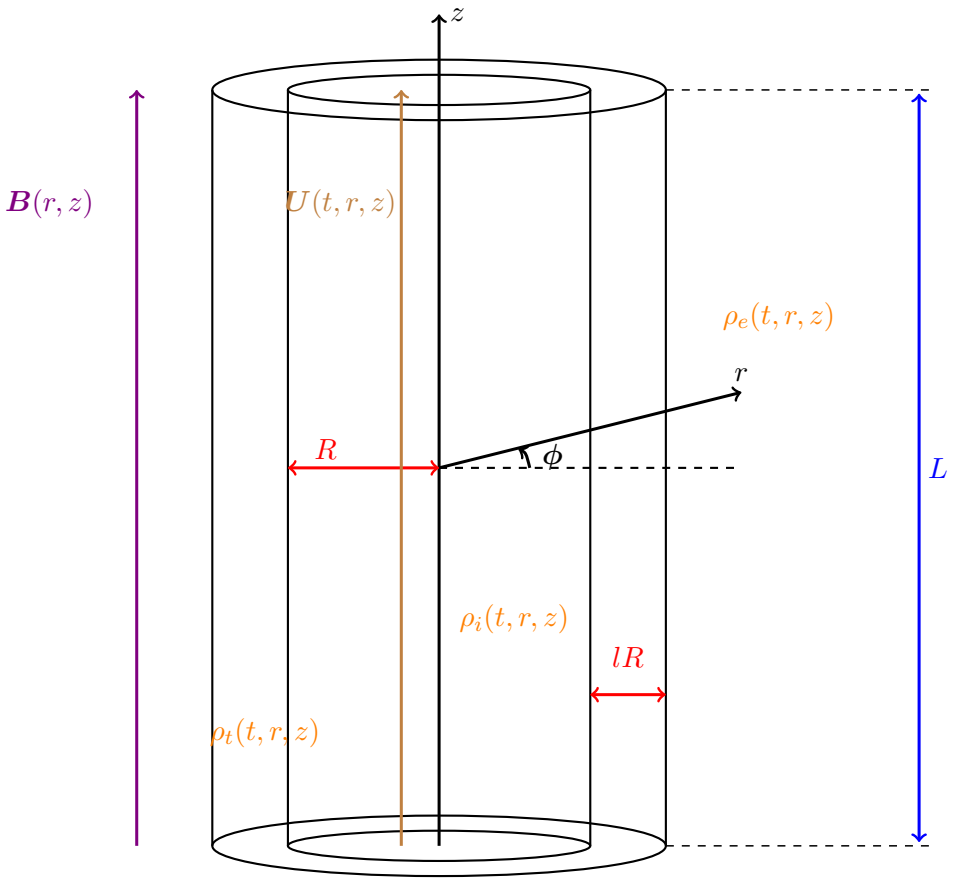

Figure 1.5: Equilibrium configuration of the straight two layered magnetic flux tube in the presence of the background flow

Here the background velocity $\boldsymbol{U}_0(t,r,z)$ satisfies the mass conservation equation,

$$\frac{\partial \rho}{\partial t} + \frac{\partial (\rho U)}{\partial z} = 0. \tag{1.11}$$

It was shown by Ruderman (2011a) that magnetic pressure perturbation P satisfies the equation

$$\frac{1}{r}\frac{\partial}{\partial r}\left(r\frac{\partial P}{\partial r}\right) - \frac{P}{r^2} = 0. \tag{1.12}$$

The pressure perturbation is related to the plasma displacement by $P = -\rho V_A^2 \nabla \cdot \boldsymbol{\xi}$ and V_A^2 is square of Alfvén speed. Solving equation (1.12), then using the WKB (Wentzel-Kramers-Brillouin) approximation and introducing the small parameter $\hat{\nu} = l/R \ll 1$, the equation is similar to equation (1.8) was found under approximation of geometrical optics (the meaning of this approximation will be later explained further in this thesis):

$$\frac{\partial^2 S_0}{\partial z^2} + \frac{\omega^2}{C_k^2} S_0, \quad S_0 = 0 \quad \text{at} \quad z = \pm L/2, \tag{1.13}$$

where the radial component of the plasma displacement inside the tube is given by

$$\xi_{ri} = S(t,z)\exp[i\hat{\nu}^{-1}\Theta(t)], \tag{1.14}$$

where $\Theta(t)$ is arbitrary function and S expands in the series

$$S = S_0 + \hat{\nu}S_1 + \dots. \tag{1.15}$$

Later, Ruderman (2011a) solved Equations (1.13) and (1.14) numerically. The dependence of damping due to resonant absorption on amplification due to cooling for kink oscillations of straight magnetic flux tube was shown. The aim of my work is to study the model which includes both characteristics of model proposed by Ruderman et al. (2008) and Ruderman (2011a), to obtain the governing equations. The obtained result have a particular importance for the observation community especially for the coronal seismology. As the model proposed in this thesis may enables to estimate various properties of a coronal loop, by making very limited number assumptions on initial background conditions and thus making the results more realistic and accurate.

§ 1.4 Outline and Structure

The Thesis is made of 6 chapters. After the introduction, Chapter 2 and Chapter 3 are mainly based on Ruderman et al. (2017). Chapter 4 is mainly based on Shukhobodskiy and Ruderman (2018). Chapter 5 is based on Shukhobodskiy et al. (2018).

Chapter 2 is introducing the equilibrium configuration of the model proposed. Then, using the ideal MHD equations under cold plasma and thin tube approximation, we will derive the set of equations in the parallel, perpendicular and azimuthal components relative to the background magnetic field. At the end, using multiple scale expansion, we will derive the governing equation describing the model proposed under the assumption that the boundaries are thin. Since all the previous models have either presence of a background flow or coronal loops expansion, the current governing equation will enable to consider both of these phenomena simultaneously. Therefore it will help to achieve better understanding behind kink oscillations of coronal loops

In Chapter 3 we study the governing equation obtained in Chapter 2 in the absence of a transitional layer. We will start by modifying the equilibrium configurations proposed in Chapter 3. Then we study the effect of siphon flow, considering the magnetic flux tube as a loop of half-circular shape, and neglecting the effect of geometry on all variables except the density variation. We will also consider the model of cross-section variation proposed by Ruderman et al. (2008). Later, we will obtain the equation describing such configuration. This equation will be solved numerically to obtain the dependence on fundamental frequency, ratio of fundamental frequency and first overtone, and amplitude on background flow for various values of cross-section expansion. These results will be graphically presented. Then we will consider the effect of cooling on kink oscillation. First of all, we will assume that the density varies slowly with time. Again using multi-scale expansion, we will obtain equations describing kink oscillations. We will obtain the quantity known as an adiabatic invariant. These equations will be

studied numerically and the dependences of fundamental frequency, ratio of fundamental frequency and first overtone, and the amplitude on time will be presented and discussed. Although the model we used in this chapter does not include the damping which is usually observed for kink oscillations of coronal loops it provides some important information for coronal seismology. First of all, it allows to neglect relatively slow speed of background flows for kink oscillation of coronal loops. Secondly, it shows the significant effect of coronal loop expansion of oscillations frequency.

In Chapter 4 we will study the governing equation under the assumption of absence of background flow to obtain the decrement for damping of kink oscillation due to resonant absorption. The modified equilibrium configuration will be presented. Then we will introduce viscous MHD equations. These equations will be studied by the means of general Fourier theory. Thus we will able to close the system of governing equations obtained in Chapter 2 for the model with a presence of transitional layer. This will allow us to obtain the decrement for kink oscillation of a magnetic flux tube. We will discuss how the adiabatic invariant will be changed for the resonant model. Finally we will describe properties of the decrement. In particular we conclude that the ratio of decrement to the oscillation frequency for the time independent density profiles is independent of a particular law of density variation along the tube as well as the tube cross-section variation along the tube. This conclusion allows to neglect coronal loops expansion to get information about the radial structure of loops, by observing damping of kink oscillation.

In Chapter 5 we will generalise the results obtained in Chapter 4 by adding the background flow to the model. We will start by using the WKB approximation on governing equation obtained in Chapter 4, to obtain Sturm-Liouville problem. Using general Fourier analysis, we will expand the results obtained in Chapter 4 to close the governing equations. The equation describing the decrement will be obtained and compared with one obtained in Chapter 4. We again will consider the model of cross-section variation proposed by Ruderman et al. (2008). We will assume that the density is slowly varying with time, and considering a loop with a half-circular shape in a fashion similar to Chapter 2. Finally we will obtain the equation describing such configuration, assuming again that the loop geometry affects only the density variation. These equations will be studied numerically. The graphical dependence of amplitude on dimensionless time for various values of expansion factors and various values of the relative strength of resonant damping and amplification caused by cooling will be presented and discussed. The critical value of relative strength of resonant damping and amplification caused by cooling, for which damping due to resonant absorption is in balance with amplification due to cooling, will be presented. Finally the dependence of critical value on expansion factor will be shown and discussed. The model in this chapter have the fewest amount of restrictions with the comparison to the models used in Chapters 3 and 4, which makes analytical and numerical results more realistic. First of all we now are able estimate the radial structure and background flow of kink oscillations of coronal loops by observing the frequency of a coronal loop oscillation, amplitude of the coronal loop oscillation and coronal loops expansion. Secondly, we showed that the cooling is a potential candidate for explanation origin of recently observed non-damped

and amplified of kink oscillation coronal loops. Therefore Chapter 5 has a particular significance for the coronal seismology.

In Chapter 6 the thesis results will be summarised and the discussion on possible further generalisation will be presented.

The structure of Chapters 2–5 will be presented as follows. Each chapter will start from describing the equilibrium state which will be needed to handled. The main body will include all the relevant calculations and assumptions. At the end of each chapter a brief summary will be presented.

Chapter 2

Model Proposed and Governing Equation

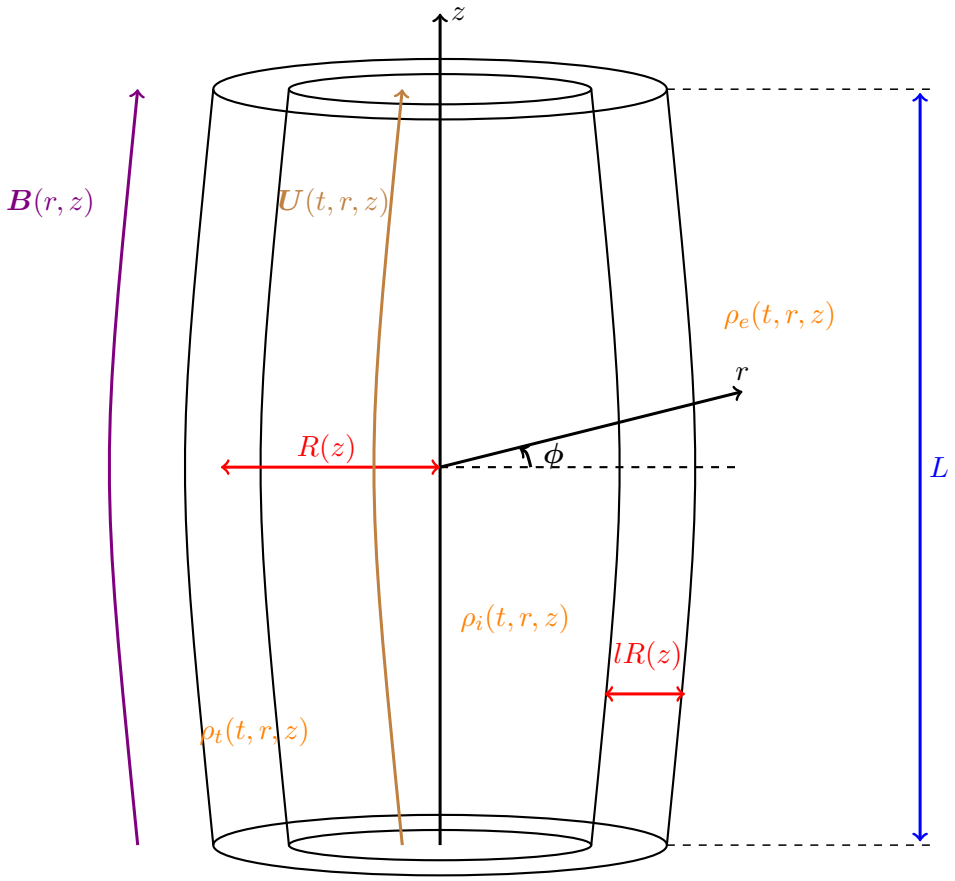

Figure 2.1: Equilibrium configuration of the straight expanding two layered magnetic flux tube in the presence of the background flow

In this thesis we model a coronal loop as a thin straight expanding magnetic flux tube with circular cross-section $R(z)$. Figure 2.1 shows the sketch of equilibrium configuration of the model proposed. In what follows, cylindrical coordinates r, ϕ, z are used. The density inside the tube $\rho_i(t,r,z)$ varies with time along and across the magnetic flux tube as well as the density in surrounding plasma $\rho_e(t,r,z)$ and in transitional layer $\rho_t(t,r,z)$ and is given by

$$\rho = \begin{cases} \rho_i(t,r,z), & 0 \le r \le R(z)(1-l/2), \\ \rho_t(t,r,z), & R(z)(1-l/2) \le r \le R(z)(1+l/2), \\ \rho_e(t,r,z), & r \ge R(z)(1+l/2), \end{cases} \tag{2.1}$$

where l is a constant determining the thickness of a transitional layer. It is assumed that $\rho(t,r,z)$ is a continuous function, and $\rho_t(t,r,z)$ is a monotonically decreasing

function of r. The reason why the tube is split into core and transitional layer is because of the ability to take into account damping due to resonance absorption later in this thesis. The time-independent non-twisted equilibrium magnetic field is $\boldsymbol{B} = (B_r(r,z), 0, B_z(r,z))$. Therefore the divergence-free condition $\nabla\cdot\boldsymbol{B} = 0$ for the magnetic field may be written as

$$\frac{1}{r}\frac{\partial(rB_r)}{\partial r} + \frac{\partial B_z}{\partial z} = 0. \tag{2.2}$$

Thus employing above equation $\boldsymbol{B}$ can be expressed in terms of magnetic flux function ψ as

$$B_r = -\frac{1}{r}\frac{\partial\psi}{\partial z}, \quad B_z = \frac{1}{r}\frac{\partial\psi}{\partial r}. \tag{2.3}$$

In addition, we assume that the boundaries of the transitional layer are magnetic surfaces. Therefore equations $r = R(z)(1 - l/2)$ and $r = R(z)(1 + l/2)$ can be written as $\psi = \psi_i = \text{const}$ and $\psi = \psi_e = \text{const}$, respectively, where indices i and e refer to internal and external values respectively. In what follows, we use the cold plasma approximation and thin tube thin boundary approximation. Therefore it follows from equilibrium configuration that magnetic field must be potential. As a result, we have $\nabla \times \boldsymbol{B} = 0$, which can be rewritten in polar coordinates as

$$\frac{\partial B_r}{\partial z} = \frac{\partial B_z}{\partial r}. \tag{2.4}$$

Substituting Equation (2.3) into Equation (2.4), we express the later equation in terms of magnetic flux function ψ as

$$r\frac{\partial}{\partial r}\left(\frac{1}{r}\frac{\partial\psi}{\partial r}\right) + \frac{\partial^2\psi}{\partial z^2} = 0. \tag{2.5}$$

There is also a time-dependent background flow $\boldsymbol{U} = (U_r(t,r,z), 0, U_z(t,r,z))$. It is assumed that the background flow velocity is parallel to the equilibrium magnetic field, $\boldsymbol{U} \parallel \boldsymbol{B}$. The plasma density and velocity are related by the mass conservation equation

$$\frac{\partial\rho}{\partial t} + \frac{1}{r}\frac{\partial(r\rho U_r)}{\partial r} + \frac{\partial(\rho U_z)}{\partial z} = 0. \tag{2.6}$$

The perturbations of the magnetic field and plasma velocity, $\boldsymbol{b} = (b_r, b_\phi, b_z)$ and $\boldsymbol{u} = (u_r, u_\phi, u_z)$, are described by the linearised MHD equations in the cold plasma approximation,

$$\frac{\partial\boldsymbol{u}}{\partial t} + (\boldsymbol{U}\cdot\nabla)\boldsymbol{u} + (\boldsymbol{u}\cdot\nabla)\boldsymbol{U} = \frac{1}{\mu_0\rho}(\nabla\times\boldsymbol{b})\times\boldsymbol{B}, \tag{2.7}$$

$$\frac{\partial\boldsymbol{b}}{\partial t} = \nabla\times(\boldsymbol{u}\times\boldsymbol{B} + \boldsymbol{U}\times\boldsymbol{b}), \tag{2.8}$$

$$\nabla\cdot\boldsymbol{b} = 0, \tag{2.9}$$

where μ_0 is the magnetic permeability of free space.

§ 2.2 Transformation of the governing equations

In this section we transform the governing equations in terms of the angular and perpendicular components. The term angular and perpendicular will be explained later in this section. Below, we use the following identities (e.g. Korn and Korn, 1961):

$$\begin{aligned} 2(\mathbf{G}\cdot\nabla)\mathbf{F} &= \nabla\times(\mathbf{F}\times\mathbf{G}) + \nabla(\mathbf{F}\cdot\mathbf{G}) - \mathbf{F}(\nabla\cdot\mathbf{G}) + \mathbf{G}(\nabla\cdot\mathbf{F}) \\ &\quad - \mathbf{F}\times(\nabla\times\mathbf{G}) - \mathbf{G}\times(\nabla\times\mathbf{F}), \\ \nabla\cdot(\mathbf{F}\times\mathbf{G}) &= \mathbf{G}\cdot(\nabla\times\mathbf{F}) - \mathbf{F}\cdot(\nabla\times\mathbf{G}), \\ \nabla\times(\mathbf{F}\times\mathbf{G}) &= (\mathbf{G}\cdot\nabla)\mathbf{F} - (\mathbf{F}\cdot\nabla)\mathbf{G} + \mathbf{F}(\nabla\cdot\mathbf{G}) - \mathbf{G}(\nabla\cdot\mathbf{F}), \end{aligned} \tag{2.10}$$

where $\mathbf{F}$ and $\mathbf{G}$ are arbitrary vector-functions.

To be able to proceed further with calculations we use the Lagrangian description and thus consider a particle with the initial position defined by vector $\boldsymbol{a}$. A current position of this particle is $\boldsymbol{x}(t,\mathbf{a})$, so $\boldsymbol{x}(0,\mathbf{a}) = \mathbf{a}$. The trajectory of this particle is given by $\boldsymbol{x} = \boldsymbol{x}(t,\mathbf{a})$. In the unperturbed flow it is $\boldsymbol{x} = \boldsymbol{x}_0(t,\mathbf{a})$. We introduce the plasma displacement $\xi = \boldsymbol{x} - \boldsymbol{x}_0$. In what follows, we consider ξ as a function of Eulerian coordinates, meaning that it is a function of t and $\boldsymbol{x}$. Then, the particle velocity is given by

$$\widetilde{\boldsymbol{U}} = \left.\frac{\partial\boldsymbol{x}}{\partial t}\right|_{\mathbf{a}} = \left.\frac{\partial\boldsymbol{x}_0}{\partial t}\right|_{\mathbf{a}} + \left.\frac{\partial\xi}{\partial t}\right|_{\boldsymbol{x}} + (\widetilde{\boldsymbol{U}}\cdot\nabla)\xi, \tag{2.11}$$

where the subscript $\mathbf{a}$ and $\boldsymbol{x}$ indicate that the derivative with respect to t is calculated at constant $\mathbf{a}$ and constant $\boldsymbol{x}$, respectively. Now, $\partial\boldsymbol{x}_0/\partial t = \boldsymbol{U}(t,\boldsymbol{x}_0)$. Since we use the linear approximation, we can substitute $\boldsymbol{U}(t,\boldsymbol{x}_0)$ for $\widetilde{\boldsymbol{U}}$ in the last term on the right-hand side of Equation (2.11). The Eulerian perturbation of the velocity is $\boldsymbol{u}(t,\boldsymbol{x}) = \widetilde{\boldsymbol{U}}(t,\boldsymbol{x}) - \boldsymbol{U}(t,\boldsymbol{x})$. Then, employing the approximate relation $\boldsymbol{U}(t,\boldsymbol{x}) = U(t,x_0) \approx \boldsymbol{U}(t,\boldsymbol{x}_0) + (\xi\cdot\nabla)\boldsymbol{U}$ (the approximate relation may be obtained using similar technique to the one used in Appendix A.1 for total derivative in Lagrangian representation), we obtain from Equation (2.11) in the linear approximation that the velocity perturbation is given by

$$\boldsymbol{u} = \frac{\partial\xi}{\partial t} + (\boldsymbol{U}\cdot\nabla)\xi - (\xi\cdot\nabla)\boldsymbol{U}, \tag{2.12}$$

where, here and below, the time derivative is calculated at constant $\boldsymbol{x}$. Applying the first identity in Equation (2.10) to last two terms on the right hand side of Equation (2.12), yields

$$\boldsymbol{u} = \frac{\partial\xi}{\partial t} + \nabla\times(\xi\times\boldsymbol{U}) - \xi(\nabla\cdot\boldsymbol{U}) + \boldsymbol{U}(\nabla\cdot\xi). \tag{2.13}$$

Further, we assume that the velocity $\boldsymbol{U}$ is potential, so that $\nabla\times\boldsymbol{U} = 0$. Then, using again the first identity in Equation (2.10), we obtain

$$(\boldsymbol{U}\cdot\nabla)\boldsymbol{u} + (\boldsymbol{u}\cdot\nabla)\boldsymbol{U} = \nabla(Uu_{\parallel}) - \boldsymbol{U}\times(\nabla\times\boldsymbol{u}), \tag{2.14}$$

where $u_{\parallel} = \boldsymbol{b}_0\cdot\boldsymbol{u}$ and $\boldsymbol{b}_0 = \boldsymbol{B}/B$ is the unit vector in the magnetic field direction. Employing this result in Equation (2.7) and taking the scalar product of the obtained

equation with $\boldsymbol{b}_0$ yields

$$\frac{\partial u_\parallel}{\partial t} + \boldsymbol{b}_0 \cdot \nabla(\boldsymbol{U} u_\parallel) = 0. \tag{2.15}$$

We assume that $u_\parallel = 0$ at $t = 0$, then it follows from this equation that $u_\parallel = 0$ for $t > 0$. Taking the scalar product of Equation (2.13) with $\boldsymbol{b}_0$ and using the second identity in Equation (2.10), we obtain

$$\frac{\partial \xi_\parallel}{\partial t} = \frac{1}{B}\nabla \cdot (BU\xi_1) + \xi_\parallel \nabla \cdot \boldsymbol{U} - U\nabla \cdot \xi, \tag{2.16}$$

where $\xi_\parallel = \boldsymbol{b}_0 \cdot \xi$ and $\xi_1 = \xi - \xi_\parallel \boldsymbol{b}_0$.

With the aid of the third identity in Equation (2.10) and divergence-free condition for the magnetic field we have

$$\nabla \times (\xi \times \boldsymbol{B}) = \mathbf{f} - \boldsymbol{B}(\nabla \cdot \xi), \tag{2.17}$$

where

$$\mathbf{f} = (\boldsymbol{B} \cdot \nabla)\xi - (\xi \cdot \nabla)\mathbf{B}. \tag{2.18}$$

Substituting Equation (2.12) into Equation (2.8), yields

$$\frac{\partial \boldsymbol{b}}{\partial t} = \nabla \times (\boldsymbol{U} \times \boldsymbol{b}) - \nabla \times \left[\boldsymbol{B} \times \left(\frac{\partial \xi}{\partial t} + (\boldsymbol{U} \cdot \nabla)\xi - (\xi \cdot \nabla)\boldsymbol{U}\right)\right]. \tag{2.19}$$

With the aid of Equation (2.17) we reduce this equation to

$$\begin{aligned}\frac{\partial}{\partial t}[\boldsymbol{b} - \mathbf{f} + \boldsymbol{B}(\nabla \cdot \xi)] = \nabla \times [U\boldsymbol{b}_0 \times (\boldsymbol{b} - (\boldsymbol{B} \cdot \nabla)\xi] \\ + \nabla \times [\boldsymbol{B} \times (\xi \cdot \nabla)\boldsymbol{U}].\end{aligned} \tag{2.20}$$

Since $\boldsymbol{U} \parallel \boldsymbol{B}$ and using chain rule we obtain the following identity

$$(\xi \cdot \nabla)\boldsymbol{U} = \boldsymbol{B}(\xi \cdot \nabla)\frac{U}{B} + \frac{U}{B}(\xi \cdot \nabla)\boldsymbol{B}, \tag{2.21}$$

Then, we finally arrive at

$$\frac{\partial}{\partial t}[\boldsymbol{b} - \mathbf{f} + \boldsymbol{B}(\nabla \cdot \xi)] = \nabla \times \{U\boldsymbol{b}_0 \times [\boldsymbol{b} - \mathbf{f} + \boldsymbol{B}(\nabla \cdot \xi)]\}. \tag{2.22}$$

It follows from Equation (2.22) that $\boldsymbol{b} - \mathbf{f} + \boldsymbol{B}(\nabla \cdot \xi) = 0$ for $t > 0$ if $\boldsymbol{b} - \mathbf{f} + \boldsymbol{B}(\nabla \cdot \xi) = 0$ at $t = 0$, which is assumed in what follows. As a result, we obtain

$$\boldsymbol{b} = (\boldsymbol{B} \cdot \nabla)\xi - (\xi \cdot \nabla)\boldsymbol{B} - \boldsymbol{B}(\nabla \cdot \xi). \tag{2.23}$$

Then, applying the third identity in Equation (2.10) and recalling that the magnetic field is divergence-free we can rewrite this expression as

$$\boldsymbol{b} = \nabla \times (\xi \times \boldsymbol{B}). \tag{2.24}$$

We now recall that the magnetic pressure perturbation $P = \boldsymbol{B}\cdot\boldsymbol{b}/\mu_0$. Taking the scalar product of Equation (2.24) with $\boldsymbol{B}$, using the second identity in Equation (2.1), and recalling that the equilibrium magnetic field is potential, we easily obtain

$$P = -\frac{1}{\mu_0}\nabla\cdot(B^2\xi_1). \tag{2.25}$$

Substituting Equations (2.14) and (2.24) in Equation (2.7), and taking into account that $u_\parallel = 0$ yields

$$\frac{\partial \boldsymbol{u}}{\partial t} = \boldsymbol{b}_0\times\left(U\nabla\times\boldsymbol{u} - \frac{B}{\mu_0\rho}\nabla\times\nabla\times(\xi\times\boldsymbol{B})\right). \tag{2.26}$$

Equations (2.13), (2.16) and (2.26) constitute the system of equations for ξ.

Further, we introduce the components of the displacement and velocity that are in the planes containing the z-axis and perpendicular to the magnetic field lines,

$$\xi_\perp = \xi_r b_{0z} - \xi_z b_{0r} \quad u_\perp = u_r b_{0z} - u_z b_{0r}. \tag{2.27}$$

Then, recalling that $\boldsymbol{B}$ is solenoidal (solenoidal means the same as divergence-free) and potential, we transform Equations (2.16) and (2.25) to

$$\begin{aligned}\frac{\partial \xi_\parallel}{\partial t} = {}& \frac{\xi_\perp}{B}\left(b_{0z}\frac{\partial(BU)}{\partial r} - b_{0r}\frac{\partial(BU)}{\partial z}\right)\\ & - U^2\left[b_{0r}\frac{\partial}{\partial r}\left(\frac{\xi_\parallel}{U}\right) + b_{0z}\frac{\partial}{\partial z}\left(\frac{\xi_\parallel}{U}\right)\right],\end{aligned} \tag{2.28}$$

$$P = -\frac{B}{\mu_0}\left(\frac{b_{0z}}{r}\frac{\partial(rw)}{\partial r} + \frac{B}{r}\frac{\partial\xi_\phi}{\partial\phi} - b_{0r}\frac{\partial w}{\partial z}\right), \tag{2.29}$$

where $w = B\xi_\perp$. To obtain the expression for $\boldsymbol{u}$ in terms of $\boldsymbol{\xi}$ we use Equation (2.13). First, we take the scalar product of this equation with the vector $(b_{0z}, 0, -b_{0r})$ and use the third identity in Equation (2.10) to obtain the expression for $u_\perp$. Then, we take the ϕ-component of Equation (2.13) to obtain the expression for u_ϕ. As a result we arrive at

$$u_\perp = \frac{1}{B}\frac{\partial w}{\partial t} + \frac{U}{B}\left(\frac{b_{0r}}{r}\frac{\partial(rw)}{\partial r} + b_{0z}\frac{\partial w}{\partial z}\right), \tag{2.30}$$

$$u_\phi = \frac{\partial\xi_\phi}{\partial t} + U\left[rb_{0r}\frac{\partial}{\partial r}\left(\frac{\xi_\phi}{r}\right) + b_{0z}\frac{\partial\xi_\phi}{\partial z}\right]. \tag{2.31}$$

Now, we take the scalar product of Equation (2.26) with the vector $(b_{0z}, 0, -b_{0r})$. Using the third identity in Equation (2.10) yields

$$\begin{aligned}\frac{\partial u_\perp}{\partial t} + U\left[rB_r\frac{\partial}{\partial r}\left(\frac{u_\perp}{rB}\right) + B_z\frac{\partial}{\partial z}\left(\frac{u_\perp}{B}\right)\right] = {}& \frac{B}{\mu_0\rho}\left[\frac{\partial^2 w}{\partial z^2}\right.\\ & \left. + \frac{\partial}{\partial r}\left(\frac{1}{r}\frac{\partial(rw)}{\partial r}\right) + B_z\frac{\partial}{\partial r}\left(\frac{1}{r}\frac{\partial\xi_\phi}{\partial\phi}\right) - \frac{B_r}{r}\frac{\partial^2\xi_\phi}{\partial\phi\partial z}\right].\end{aligned} \tag{2.32}$$

Then, we take the ϕ-component of Equation (2.26) and, again, use the third identity in Equation (2.10) to obtain

$$\begin{aligned}\frac{\partial u_\phi}{\partial t} + U\left(\frac{b_{0r}}{r}\frac{\partial (ru_\phi)}{\partial r} + b_{0z}\frac{\partial u_\phi}{\partial z}\right) = \frac{B}{\mu_0\rho}\left[\frac{B}{r^2}\frac{\partial^2 \xi_\phi}{\partial \phi^2}\right.\\ + \frac{b_{0z}}{r^2}\frac{\partial^2 (rw)}{\partial \phi \partial r} - \frac{b_{0r}}{r}\frac{\partial^2 w}{\partial \phi \partial z} + \frac{b_{0r}}{r}\frac{\partial}{\partial r}\left(r^2 B_r \frac{\partial}{\partial r}\left(\frac{\xi_\phi}{r}\right)\right.\\ \left.\left. + \; rB_z\frac{\partial \xi_\phi}{\partial z}\right) + b_{0z}\frac{\partial}{\partial z}\left(rB_r\frac{\partial}{\partial r}\left(\frac{\xi_\phi}{r}\right) + B_z\frac{\partial \xi_\phi}{\partial z}\right)\right]. \end{aligned} \tag{2.33}$$

Using Equation (2.29) we reduce Equations (2.32) and (2.33) to

$$\begin{aligned}\frac{\partial u_\perp}{\partial t} + U\left[rB_r\frac{\partial}{\partial r}\left(\frac{u_\perp}{rB}\right) + B_z\frac{\partial}{\partial z}\left(\frac{u_\perp}{B}\right)\right]\\ = \frac{B^2}{\rho}\left[b_{0r}\frac{\partial}{\partial z}\left(\frac{P}{B^2}\right) - b_{0z}\frac{\partial}{\partial r}\left(\frac{P}{B^2}\right)\right]\\ + \frac{B^2}{\mu_0\rho}\left(rb_{0r}\frac{\partial}{\partial r}\frac{1}{r} + b_{0z}\frac{\partial}{\partial z}\right)\left(\frac{b_{0r}}{rB}\frac{\partial (rw)}{\partial r} + \frac{b_{0z}}{B}\frac{\partial w}{\partial z}\right), \end{aligned} \tag{2.34}$$

$$\begin{aligned}\frac{\partial u_\phi}{\partial t} + U\left(\frac{b_{0r}}{r}\frac{\partial (ru_\phi)}{\partial r} + b_{0z}\frac{\partial u_\phi}{\partial z}\right) = -\frac{1}{\rho r}\frac{\partial P}{\partial \phi}\\ + \frac{1}{\mu_0\rho}\left(\frac{B_r}{r}\frac{\partial}{\partial r}r + B_z\frac{\partial}{\partial z}\right)\left(rB_r\frac{\partial}{\partial r}\left(\frac{\xi_\phi}{r}\right) + B_z\frac{\partial \xi_\phi}{\partial z}\right). \end{aligned} \tag{2.35}$$

For further details of the derivation of Equations (2.28) – (2.31), (2.34) and (2.35), see Appendix A.2.

We see that Equation (2.28) is detached from the other equations and only serves to determine $\xi_\parallel$. Therefore, we do not use it below. Equations (2.29)–(2.31), (2.34), and (2.35) constitute the system of equations for $\xi_\perp$, ξ_ϕ, $u_\perp$, u_ϕ, and P.

Following the analysis in Ruderman et al. (2008), we use the magnetic flux function ψ as an independent variable instead of r. With the aid of the chain rule we obtain the following relation:

$$\frac{\partial f}{\partial r} = rB_z\frac{\partial f}{\partial \psi}, \quad \left.\frac{\partial f}{\partial z}\right|_r = \left.\frac{\partial f}{\partial z}\right|_\psi - rB_r\frac{\partial f}{\partial \psi}, \tag{2.36}$$

where f is an arbitrary function, and the subscripts r and ψ indicate that the derivative is taken at constant r and constant ψ, respectively. In particular, taking $f = r$ in these relations, we obtain

$$\frac{\partial r}{\partial z} = \frac{B_r}{B_z}, \quad \frac{\partial r}{\partial \psi} = \frac{1}{rB_z}. \tag{2.37}$$

Using Equations (2.36) and (2.37) we transform Equations (2.29)–(2.31), (2.34), and (2.35) to

$$P = -\frac{1}{\mu_0}\left(rB^2\frac{\partial w}{\partial \psi} + \frac{B^2}{r}\frac{\partial \xi_\phi}{\partial \phi} - B_r\frac{\partial w}{\partial z} + B_z\frac{w}{r}\right), \tag{2.38}$$

$$u_\perp = \frac{1}{B}\frac{\partial w}{\partial t} + \frac{U_z}{rB}\frac{\partial (rw)}{\partial z}, \tag{2.39}$$

$$u_\phi = \frac{\partial \xi_\phi}{\partial t} + rU_z\frac{\partial}{\partial z}\left(\frac{\xi_\phi}{r}\right), \tag{2.40}$$

$$\begin{aligned}\frac{\partial u_\perp}{\partial t} + rUB_z\frac{\partial}{\partial z}\left(\frac{u_\perp}{rB}\right) &= \frac{rBB_z}{\mu_0\rho}\frac{\partial}{\partial z}\left(\frac{B_z}{r^2B^2}\frac{\partial (rw)}{\partial z}\right)\\ &+ \frac{B^2}{\rho}\left[b_{0r}\frac{\partial}{\partial z}\left(\frac{P}{B^2}\right) - rB\frac{\partial}{\partial \psi}\left(\frac{P}{B^2}\right)\right],\end{aligned} \tag{2.41}$$

$$\frac{\partial u_\phi}{\partial t} + \frac{U_z}{r}\frac{\partial (ru_\phi)}{\partial z} = \frac{B_z}{\mu_0\rho r}\frac{\partial}{\partial z}\left[r^2B_z\frac{\partial}{\partial z}\left(\frac{\xi_\phi}{r}\right)\right] - \frac{1}{\rho r}\frac{\partial P}{\partial \phi}. \tag{2.42}$$

The system of Equations (2.38)–(2.42) is used in the next section to derive the governing equations for the kink oscillations of a thin expanding flux tube.

§ 2.3 Derivation of the governing equations

We now assume that the magnetic tube is thin, $R(z)/L = \mathcal{O}(\epsilon)$, where $\epsilon \ll 1$ and L is the characteristic scale of spatial variation along the tube. In the case of standing waves L is the tube length, while in the case of propagating waves it is a typical wavelength. In accordance with this we introduce the stretching variable along the tube defined as $Z = \epsilon z$. The characteristic time of the problem is L/V_*, where V_* is the characteristic Alfvén speed. Its ratio to the Alfvénic time determined with respect to the tube radius, R_*/V_*, where R_* is the characteristic value of the tube radius, is of the order of ϵ^{-1}. In accordance with this, we also introduce the stretching time $T = \epsilon t$. The characteristic scale of variation of perturbations in the radial direction is R_*. However, we assume that the characteristic scale of variation of ρ, B, and U outside of the transitional layer, since the tube is thin, i.e in the core of the tube ($r < R(z)(1 - l/2)$) and outside of the tube ($r > R(z)(1 + l/2)$) is L. While the characteristic scale of variation of B is L even in the transitional layer, ρ and U can vary in this layer on the scale lR_*. The ratio of the radial and azimuthal component of the equilibrium magnetic field is of the order of ϵ, and the same estimate is valid for the radial and azimuthal component of the equilibrium flow. In accordance with these estimates, we introduce the scaled radial components of the magnetic field and bulk flow, namely $\widetilde{B}_r = \epsilon^{-1}B_r$ and $\widetilde{U}_r = \epsilon^{-1}U_r$.

Below, we impose the restriction $B_z > 0$. Since the tube is thin, in the vicinity of the magnetic tube we can approximate ψ by the first term of its expansion in the Taylor series. Since the tube axis is a magnetic field line itself, $\psi = \text{const}$ at $r = 0$. Without loss of generality we can take $\psi = 0$ at $r = 0$. Then, it follows from Equation (2.3) that the first term of the Taylor expansion of ψ with respect to r is proportional to r^2 and we can use the approximate expression

$$\psi = \frac{1}{2}r^2h(z). \tag{2.43}$$

Now, it follows from Equation (2.3) that the equilibrium magnetic field is given by

$$B_r = -\frac{r}{2}h'(z), \quad B_z = h(z), \tag{2.44}$$

where the prime indicates the derivative. For the magnetic field magnitude we obtain

$$B = \sqrt{B_r^2 + B_z^2} = B_z + \mathcal{O}\big(\epsilon^2\big) = h(z) + \mathcal{O}\big(\epsilon^2\big). \tag{2.45}$$

It follows from the magnetic flux conservation that

$$h(z)R^2(z) = C = \text{const}. \tag{2.46}$$

For the flow speed we obtain

$$U = \sqrt{U_r^2 + U_z^2} = U_z + \mathcal{O}\big(\epsilon^2\big). \tag{2.47}$$

It follows from symmetry that $\partial U/\partial r = 0$ at $r = 0$. Then, using Taylor's theorem, we obtain in the core region ($r < R(z)(1 - l/2)$)

$$\begin{aligned} U(r,z) &= U(0,z) + \frac{r^2}{2}\frac{\partial^2 U}{\partial r^2}\bigg|_{r=r_*} \\ &= U(0,z) + \mathcal{O}\big(R_*^2/L^2\big) = U(0,z) + \mathcal{O}\big(\epsilon^2\big), \end{aligned} \tag{2.48}$$

where $0 < r_* < R(z)(1-l/2)$. Outside of the tube in its vicinity ($R(z)(1+l/2) < r \ll L$) we have

$$\begin{aligned} U(r,z) &= U(R(z)(1+l/2),z) + r\frac{\partial U}{\partial r}\bigg|_{r=r_*} \\ &= U(0,z) + \mathcal{O}(R_*/L) = U(0,z) + \mathcal{O}(\epsilon), \end{aligned} \tag{2.49}$$

where $R(z)(1 + l/2) < r_* \ll L$. Expressions similar to Equations (2.48) and (2.49) are also valid for ρ outside of the transitional layer and for B everywhere not far from the tube ($r \ll L$). Hence, in the leading order approximation with respect to ϵ, we can consider U and ρ as quantities independent of r outside of the transitional layer, while B can be considered as a quantity independent of r everywhere in the region $r \ll L$.

We now integrate Equation (2.6) over the area of the tube core cross-section, that is over a circle of radius $R(z)(1 - l/2)$. Below, we assume that $l \ll 1$ meaning that we can neglect l in comparison with unity. Then, we obtain

$$R^2\frac{\partial \rho}{\partial t} + R^2\frac{\partial(\rho U_z)}{\partial z} + 2(\rho R U_r)\big|_{r=R} = 0. \tag{2.50}$$

Since the velocity is parallel to the magnetic field, we have with the aid of Equations (2.44) and (2.46)

$$\frac{U_r}{U}\bigg|_{r=R} = \frac{B_r}{B}\bigg|_{r=R} = -\frac{h'R}{2h} = R'. \tag{2.51}$$

Substituting this result in Equation (2.50) and recalling that $B_z \approx B$, we eventually arrive at

$$\frac{\partial \rho}{\partial t} + \frac{1}{R^2}\frac{\partial(\rho R^2 U)}{\partial z} = 0. \tag{2.52}$$

This equation is valid in the core of the tube. Since $\boldsymbol{B} \parallel \boldsymbol{U}$, $BR^2 = \text{const}$ and ρ, U are independent of r in the leading order approximation then it follows from Equations (2.6) and (2.49) that Equation (2.52) is also valid outside the transitional layer.

Using the new stretched variables we transform Equation (2.38)–(2.42) to

$$P = -\frac{1}{\mu_0}\left(rB^2\frac{\partial w}{\partial \psi} + \frac{B^2}{r}\frac{\partial \xi_\phi}{\partial \phi} - \epsilon^2 \widetilde{B}_r \frac{\partial w}{\partial Z} + B_z \frac{w}{r}\right), \tag{2.53}$$

$$u_\perp = \frac{\epsilon}{B}\frac{\partial w}{\partial T} + \frac{\epsilon U_z}{rB}\frac{\partial (rw)}{\partial Z}, \tag{2.54}$$

$$u_\phi = \epsilon \frac{\partial \xi_\phi}{\partial T} + \epsilon r U_z \frac{\partial}{\partial Z}\left(\frac{\xi_\phi}{r}\right), \tag{2.55}$$

$$\begin{aligned}\epsilon\frac{\partial u_\perp}{\partial T} + \epsilon r U B_z \frac{\partial}{\partial Z}\left(\frac{u_\perp}{rB}\right) &= \epsilon^2 \frac{rBB_z}{\mu_0 \rho}\frac{\partial}{\partial Z}\left(\frac{B_z}{r^2B^2}\frac{\partial (rw)}{\partial Z}\right) \\ &+ \frac{B^2}{\rho}\left[\epsilon^2 \tilde{b}_{0r}\frac{\partial}{\partial Z}\left(\frac{P}{B^2}\right) - rB\frac{\partial}{\partial \psi}\left(\frac{P}{B^2}\right)\right],\end{aligned} \tag{2.56}$$

$$\epsilon\frac{\partial u_\phi}{\partial T} + \epsilon\frac{U_z}{r}\frac{\partial (ru_\phi)}{\partial Z} = \frac{\epsilon^2 B_z}{\mu_0 \rho r}\frac{\partial}{\partial Z}\left[r^2 B_z \frac{\partial}{\partial Z}\left(\frac{\xi_\phi}{r}\right)\right] - \frac{1}{\rho r}\frac{\partial P}{\partial \phi}, \tag{2.57}$$

where $\tilde{b}_{0r} = \epsilon^{-1} b_{0r}$. Below, we consider $\xi_\perp$ and ξ_ϕ as quantities of the order of unity. Then, it follows from Equations (2.54) and (2.55) that $u_\perp = \mathcal{O}(\epsilon)$ and $u_\phi = \mathcal{O}(\epsilon)$. With the aid of these estimates, we obtain from Equations (2.56) and (2.57) that $P = \mathcal{O}(\epsilon^2)$. In accordance with these estimates, we put $u_\perp = \epsilon \tilde{u}_\perp$, $u_\phi = \epsilon \tilde{u}_\phi$, and $P = \epsilon^2 B^2 Q$. Further, assuming that perturbations of all quantities are proportional to $e^{i\phi}$, we reduce the system of Equations (2.53)–(2.57) to

$$rB^2\frac{\partial w}{\partial \psi} + \frac{iB^2 \xi_\phi}{r} + B_z \frac{w}{r} = \mathcal{O}(\epsilon^2), \tag{2.58}$$

$$\tilde{u}_\perp = \frac{1}{B}\frac{\partial w}{\partial T} + \frac{U_z}{rB}\frac{\partial (rw)}{\partial Z}, \tag{2.59}$$

$$\tilde{u}_\phi = \frac{\partial \xi_\phi}{\partial T} + r U_z \frac{\partial}{\partial Z}\left(\frac{\xi_\phi}{r}\right), \tag{2.60}$$

$$\begin{aligned}\frac{\partial \tilde{u}_\perp}{\partial T} + rUB_z\frac{\partial}{\partial Z}\left(\frac{\tilde{u}_\perp}{rB}\right) &= \frac{rBB_z}{\mu_0\rho}\frac{\partial}{\partial Z}\left(\frac{B_z}{r^2B^2}\frac{\partial (rw)}{\partial Z}\right) \\ &- \frac{rB^3}{\rho}\frac{\partial Q}{\partial \psi} + \mathcal{O}(\epsilon^2),\end{aligned} \tag{2.61}$$

$$\frac{\partial \tilde{u}_\phi}{\partial T} + \frac{U_z}{r}\frac{\partial (r\tilde{u}_\phi)}{\partial Z} = \frac{B_z}{\mu_0 \rho r}\frac{\partial}{\partial Z}\left[r^2 B_z \frac{\partial}{\partial Z}\left(\frac{\xi_\phi}{r}\right)\right] - \frac{iB^2 Q}{\rho r}. \tag{2.62}$$

Eliminating $\tilde{u}_\perp$, $\tilde{u}_\phi$, and ξ_ϕ and only keeping the leading terms with respect to ϵ, we now obtain the system of equations for w and Q in the leading order approximation:

$$\begin{aligned} Q = {} & \frac{1}{\mu_0 B}\frac{\partial}{\partial Z}\left(r^2 B \frac{\partial^2 W}{\partial \psi \partial Z}\right) \\ & - \frac{\rho}{B^2}\left(r^2\frac{\partial}{\partial T} + U\frac{\partial}{\partial Z}r^2\right)\left(\frac{\partial^2 W}{\partial T \partial \psi} + U\frac{\partial^2 W}{\partial \psi \partial Z}\right), \end{aligned} \tag{2.63}$$

$$\begin{aligned} & \left(\frac{\partial}{\partial T} + r^2 U B^2 \frac{\partial}{\partial Z}\frac{1}{r^2 B^2}\right)\left(\frac{\partial W}{\partial T} + U\frac{\partial W}{\partial Z}\right) \\ & \qquad = \frac{r^2 B^3}{\mu_0 \rho}\frac{\partial}{\partial Z}\left(\frac{1}{r^2 B}\frac{\partial W}{\partial Z}\right) - \frac{r^2 B^4}{\rho}\frac{\partial Q}{\partial \psi}, \end{aligned} \tag{2.64}$$

where $W = rw = rB\xi_\perp$. Using Equation (2.43) and recalling that, outside of the transitional layer, we can consider ρ, B, and U as quantities independent of r, we reduce Equations (2.63) and (2.64) to

$$\begin{aligned} Q = {} & \frac{2\psi}{h}\frac{\partial}{\partial \psi}\left[\frac{1}{\mu_0}\frac{\partial^2 W}{\partial Z^2}\right. \\ & \left. - \frac{\rho}{h^2}\left(\frac{\partial}{\partial T} + hU\frac{\partial}{\partial Z}\frac{1}{h}\right)\left(\frac{\partial W}{\partial T} + U\frac{\partial W}{\partial Z}\right)\right], \end{aligned} \tag{2.65}$$

$$\left(\frac{\partial}{\partial T} + hU\frac{\partial}{\partial Z}\frac{1}{h}\right)\left(\frac{\partial W}{\partial T} + U\frac{\partial W}{\partial Z}\right) = \frac{h^2}{\mu_0 \rho}\frac{\partial^2 W}{\partial Z^2} - \frac{2\psi h^3}{\rho}\frac{\partial Q}{\partial \psi}. \tag{2.66}$$

We differentiate Equation (2.66) with respect to ψ and then eliminate W from the obtained equation and Equation (2.65), to obtain

$$4\psi\frac{\partial}{\partial \psi}\left(\psi\frac{\partial Q}{\partial \psi}\right) - Q = 0. \tag{2.67}$$

The solution to this equation must be regular at $\psi = 0$ and decays as $\psi \to \infty$. Hence, we obtain

$$Q = \begin{cases} Q_i(T,Z)\psi^{1/2}, & 0 \le \psi \le \psi_i, \\ Q_e(T,Z)\psi^{-1/2}, & \psi \ge \psi_e, \end{cases} \tag{2.68}$$

where $Q_i(T,Z)$ and $Q_e(T,Z)$ are arbitrary functions. Recall that $\psi = \psi_i$ and $\psi = \psi_e$, where ψ_i and ψ_e are constants, are the equations of the boundaries of the transitional layer. It follows from Equation (2.43) that

$$\psi_i = \frac{C}{2}\left(1 - \frac{l}{2}\right)^2, \quad \psi_e = \frac{C}{2}\left(1 + \frac{l}{2}\right)^2. \tag{2.69}$$

Equations (2.66) and (2.68) imply that $W = \psi^{1/2}\widetilde{W}(T, Z)$ inside the tube core region. Then, recalling the definition of W and using Equation (2.43) we conclude that $\xi_\perp$ is independent of r inside the tube core region, which implies that, in the thin tube approximation, the tube oscillates as a solid.

Substituting Equation (2.68) in Equation (2.66) we arrive at

$$\left(\frac{\partial}{\partial T} + hU_i\frac{\partial}{\partial Z}\frac{1}{h}\right)\left(\frac{\partial W_i}{\partial T} + U_i\frac{\partial W_i}{\partial Z}\right) - \frac{h^2}{\mu_0\rho_i}\frac{\partial^2 W_i}{\partial Z^2} = -\frac{\psi_i^{1/2}h^3 Q_i}{\rho_i}, \tag{2.70}$$

$$\left(\frac{\partial}{\partial T} + hU_e\frac{\partial}{\partial Z}\frac{1}{h}\right)\left(\frac{\partial W_e}{\partial T} + U_e\frac{\partial W_e}{\partial Z}\right) - \frac{h^2}{\mu_0\rho_e}\frac{\partial^2 W_e}{\partial Z^2} = \frac{h^3 Q_e}{\rho_e\psi_e^{1/2}}, \tag{2.71}$$

where W_i and W_e are calculated at $\psi = \psi_i$ and $\psi = \psi_e$, respectively. Let us now introduce the new variable

$$\eta = \frac{1}{R(z)}\xi_\perp\big|_{\psi=\psi_i}. \tag{2.72}$$

Let us also introduce the jumps of this new variable and the magnetic pressure perturbation across the transitional layer,

$$\delta\eta = \frac{1}{R(z)}\left(\xi_\perp\big|_{\psi=\psi_e} - \xi_\perp\big|_{\psi=\psi_i}\right), \quad \delta P = P\big|_{\psi=\psi_e} - P\big|_{\psi=\psi_i}. \tag{2.73}$$

We have the estimates $\delta\eta = \mathcal{O}(l)$, $\delta P = \mathcal{O}(l)$. Then, with the aid of Equation (2.68), we obtain

$$\begin{gathered} W_i = C(1 - l/2)\eta, \quad W_e = C[(1 + l/2)\eta + \delta\eta], \\ \psi_i^{1/2}h^3 Q_i = \frac{\epsilon^{-2}C}{R^2}P\big|_{\psi=\psi_i}, \psi_e^{-1/2}h^3 Q_e = \frac{\epsilon^{-2}C}{R^2}P\big|_{\psi=\psi_e}. \end{gathered} \tag{2.74}$$

Now, we multiply Equation (2.70) by ρ_i, Equation (2.71) by ρ_e, add the results, use Equations (2.46), Equation (2.73), and Equation (2.74), and return to the original non-scaled independent variables. As a result, we arrive at

$$\begin{aligned} &\rho_i\left(\frac{\partial}{\partial t} + \frac{U_i}{R^2}\frac{\partial}{\partial z}R^2\right)\left(\frac{\partial\eta}{\partial t} + U_i\frac{\partial\eta}{\partial z}\right) \\ &+ \rho_e\left(\frac{\partial}{\partial t} + \frac{U_e}{R^2}\frac{\partial}{\partial z}R^2\right)\left(\frac{\partial\eta}{\partial t} + U_e\frac{\partial\eta}{\partial z}\right) - \frac{2B^2}{\mu_0}\frac{\partial^2\eta}{\partial z^2} = \mathcal{L}, \end{aligned} \tag{2.75}$$

$$\begin{aligned} \mathcal{L} = &\frac{\delta P}{R^2} + \frac{B^2}{\mu_0}\frac{\partial^2(l\eta + \delta\eta)}{\partial z^2} \\ &- \rho_e\left(\frac{\partial}{\partial t} + \frac{U_e}{R^2}\frac{\partial}{\partial z}R^2\right)\left(\frac{\partial}{\partial t} + U_e\frac{\partial}{\partial z}\right)(l\eta + \delta\eta). \end{aligned} \tag{2.76}$$

§ 2.4 Summary

We now summarise Chapter 2. First of all we considered linear MHD equations. Then by the means of perturbation method we rearranged the system in terms of parallel and perpendicular components. Under the thin tube thin boundary approximation we obtained governing equation for kink oscillations. This equation will be used in following chapters to study the effect of background flow and resonant absorption on kink oscillations of coronal loops. We notice that in the absence of the transitional layer, $l = 0$, we have $\mathcal{L} = 0$. Then Equation (2.75) governs the kink oscillations of a thin expanding magnetic flux tube with a background field-aligned flow. Such configuration will be studied in Chapter 3 in more details. However, in the presence of transitional layer the system of Equations (2.75) and (2.76) is not closed. To close this system we need to express jumps across transitional layer of the plasma displacement across transitional layer divided by the tube radius, $\delta\eta$, and the plasma pressure across the transitional layer, δP, in terms of the plasma displacement of the magnetic flux tube boundary divided by its radius, η. These jumps will be obtained in case of the absence of a background field-aligned flow in Chapter 4 and in case of the presence of a background field-aligned flow in Chapter 5. The resulting governing equations will be investigated analytically and numerically to study the effects of a magnetic flux tube expansion, a background field-aligned flow and a resonant absorption on kink oscillations of coronal loops.

Chapter 3

Kink Oscillations in the Absence of Transitional Layer

§ 3.1 Equilibrium configuration

In this chapter we assume that kink oscillation of magnetic tube has sharp boundaries. That means that $l = 0$. The sketch of such equilibrium configuration is given by Figure 3.1.

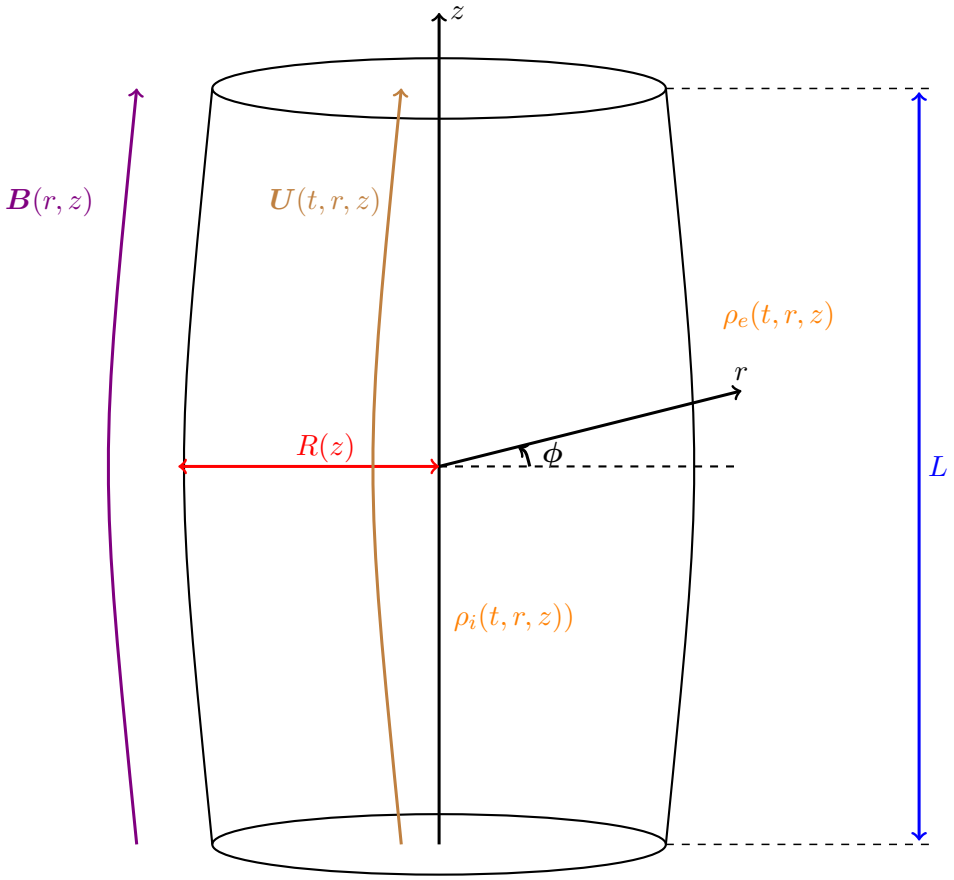

Figure 3.1: Equilibrium configuration of the straight expanding magnetic flux tube in the presence of the background flow

Since transitional layer is absent under the current equilibrium configuration in this chapter, we will use Equation (2.75), with the right-hand side of it equal to 0, since $l = 0$. Hence, we rewrite Equation (2.75) as

$$\rho_i\left(\frac{\partial}{\partial t}+\frac{U_i}{R^2}\frac{\partial}{\partial z}R^2\right)\left(\frac{\partial \eta}{\partial t}+U_i\frac{\partial \eta}{\partial z}\right)+ \rho_e\left(\frac{\partial}{\partial t}+\frac{U_e}{R^2}\frac{\partial}{\partial z}R^2\right)\left(\frac{\partial \eta}{\partial t}+U_e\frac{\partial \eta}{\partial z}\right)-\frac{2B^2}{\mu_0}\frac{\partial^2 \eta}{\partial z^2}=0. \tag{3.1}$$

§ 3.2 Eigenvalue problem in the presence of stationary flow: General analysis

In this section we assume that both the density and flow velocity are independent of time and the external plasma is at rest, $U_e = 0$. Since we assume that the characteristic scale of variation of the equilibrium quantities in the radial direction is the same as in the axial direction, we can neglect their radial variation inside the tube in the thin tube approximation. Then, it follows from mass conservation Equation (2.6) that the density and flow speed are related by

$$\rho_i U R^2 = \text{const}, \tag{3.2}$$

where we have dropped the subscript "i" at the internal flow speed U. It follows from the magnetic flux conservation that

$$BR^2 = \text{const}. \tag{3.3}$$

Below, we study standing waves and assume that magnetic flux tube ends are fixed at the dense photosphere. Thus we impose the boundary conditions

$$\eta = 0 \quad \text{at} \quad z = \pm L/2, \tag{3.4}$$

where L is the tube length. We look for stationary solutions, so we take $\eta \propto e^{-i\omega t}$. Then, Equation (3.2) reduces to

$$\left(\frac{2B^2}{\mu_0} - \rho_i U^2\right)\frac{d^2\eta}{dz^2} + \left(2i\omega\rho_i U - \frac{\rho_i U}{R^2}\frac{d(UR^2)}{dz}\right)\frac{d\eta}{dz} + \left(\frac{2i\omega\rho_i U}{R}\frac{dR}{dz} + \omega^2(\rho_i + \rho_e)\right)\eta = 0. \tag{3.5}$$

This equation, together with the boundary conditions Equation (3.4), constitute an eigenvalue problem. The aim of this section is to study general properties of this problem. We are interested in condition for which the tube will be stable with respect to long kink perturbations. Thus, we assume that $\mu_0\rho_i U^2 < 2B^2$, that is $U^2 < 2V_{Ai}^2 \equiv 2B^2/\mu_0\rho_i$, and this condition is satisfied for all $z \in [-L/2, L/2]$. Then, we make the variable substitution

$$\eta = q\exp(-i\omega\sigma(z)), \quad \sigma = \int_{-L/2}^{z} \frac{\mu_0\rho_i U\, dz'}{2B^2 - \mu_0\rho_i U^2}. \tag{3.6}$$

Now, multiplying the obtained equation by R^4, we reduce Equation (3.5) to

$$\frac{d}{dz}\left[R^4\left(\frac{2B^2}{\mu_0} - \rho_i U^2\right)\frac{dq}{dz}\right] + \omega^2 W(z) q = 0, \tag{3.7}$$

where

$$W(z) = R^4\frac{2(\rho_i + \rho_e)B^2 - \mu_0\rho_i\rho_e U^2}{2B^2 - \mu_0\rho_i U^2}. \tag{3.8}$$

Equation (3.7) with the boundary conditions Equation (3.4) constitute the classical Sturm-Liouville problem with the eigenvalue ω^2. It follows from the general theory of the Sturm-Liouville problem (e.g. Coddington and Levinson, 1955) that the eigenvalues are real and constitute a monotonically increasing unbounded sequence. The first eigenvalue is the square of the fundamental frequency, and the corresponding eigenfunction has no nodes in $(-L/2, L/2)$. All other eigenvalues are the squares of frequencies of corresponding overtones. The eigenfunction corresponding to the n^{th} overtone has $n-1$ nodes in $(-L/2, L/2)$.

It is obvious that we can always take q to be real. Multiplying Equation(3.7) by q, integrating the obtained equation, and using Equation (3.12) we obtain

$$\omega^2 \int_{-L/2}^{L/2} W(z) q^2 \, dz = \int_{-L/2}^{L/2} R^4 \left(\frac{2B^2}{\mu_0} - \rho_i U^2 \right) \left(\frac{dq}{dz} \right)^2 dz. \tag{3.9}$$

Since $W(z) > 0$, it follows from this equation that $\omega^2 > 0$, that all the eigenfrequencies are real. This implies that the inequality $U^2 < 2V_{Ai}^2$ is a sufficient condition for stability of the tube with respect to long kink perturbations. We emphasize that this condition is sufficient but not necessary. On the other hand, this analysis does not prove that the tube is stable if the condition $U^2 < 2V_{Ai}^2$ is satisfied. While it guaranties that the tube is stable with respect to long kink perturbations, it can be unstable with respect to other types of perturbations.

§ 3.3 Eigenmodes of kink oscillations of expanding coronal loops with siphon flow

3.3.1 Unperturbed state

We consider now a loop of a semicircle shape with the variable cross-section of radius $R(z)$. Below, we neglect the effect of the loop curvature on kink oscillations. Hence, the loop shape only determines the density variation along the loop. There is the plasma flow inside the loop, while the external plasma is at rest ($U_e = 0$). The flow velocity at one of the loop foot points is fixed and equal to U_f. We assume that the plasma temperature is constant and it is the same inside the loop and in the external plasma. Then, the plasma density in the external plasma is given by barometric formula

$$\rho_e(z) = \frac{\rho_f}{\zeta} \exp\left(-\frac{L}{\pi H} \cos\frac{\pi z}{L} \right), \quad H = \frac{k_B T}{m g}, \tag{3.10}$$

where H is the atmospheric scale height, k_B is the Boltzmann constant, T is the plasma temperature, m the mean mass per particle (approximately equal to $0.6 m_p$ in the solar corona with m_p being the proton mass), $g \approx 274 \ \mathrm{m\,s^{-2}}$ the gravity acceleration, ρ_f the density inside the loop at the foot point, and $\zeta > 1$ is the ratio of densities inside and outside the loop at the foot point. The plasma density, radius of the flux tube and the flow bulk velocity are all related by the mass conservation Equation (3.2) that now takes the form

$$\rho_i(z) U(z) R^2(z) = \rho_f U_f R_f^2, \tag{3.11}$$

where R_f is the radius of the tube at the footpoint. For the isothermal motion the equilibrium flow velocity is defined by the following momentum equation:

$$U\frac{dU}{dz} = -g\left(\frac{H}{\rho_i}\frac{d\rho_i}{dz} - \sin\frac{\pi z}{L}\right). \tag{3.12}$$

Integrating this equation, we obtain

$$\frac{U^2}{2} + gH\ln\frac{\rho_i}{\rho_f} = \frac{U_f^2}{2} - \frac{gL}{\pi}\cos\frac{\pi z}{L}. \tag{3.13}$$

Using Equation (3.11) we transform Equation (3.13) to

$$\chi\left[\frac{1}{\kappa^2}\left(\frac{R_f}{R}\right)^4 - 1\right] + 2\ln\kappa = -\frac{2L}{\pi H}\cos\frac{\pi z}{L}, \tag{3.14}$$

where

$$\chi = \frac{U_f^2}{gH}, \qquad \kappa = \frac{\rho_i}{\rho_f}. \tag{3.15}$$

Now, we take $R(z)$ the same as in Ruderman et al. (2008),

$$R(z) = R_f\vartheta\sqrt{\frac{\cosh(L/2L_c) - 1}{\cosh(L/2L_c) - \vartheta^2 + (\vartheta^2 - 1)\cosh(z/L_c)}}, \tag{3.16}$$

where L_c is an arbitrary positive constant with the dimension of length and $\vartheta = R(0)/R_f$ is the expansion factor. It is shown in Ruderman et al. (2008) that, to have the z-component of the magnetic field positive everywhere in the region $|z| \le L/2$, the expansion factor must satisfy the inequality $\vartheta < \vartheta_m$, where

$$\vartheta_m^2 \approx \frac{1.4\cosh(L/2L_c)}{1 + 0.4\cosh(L/2L_c)}. \tag{3.17}$$

The parameter ϑ_m is a monotonically increasing function of L/L_c, $\vartheta_m \to 1$ as $L/L_c \to 0$, and $\vartheta_m \to 1.87$ as $L/L_c \to \infty$. Substituting Equation (3.16) in Equation (3.14) we obtain the equation determining the dependence of κ on z,

$$\begin{aligned} f(\kappa, z) \equiv \chi\left(\frac{\cosh(L/2L_c) - \vartheta^2 + (\vartheta^2 - 1)\cosh(z/L_c)}{\kappa\vartheta^2[\cosh(L/2L_c) - 1]}\right)^2 \\ - \chi + 2\ln\kappa + \frac{2L}{\pi H}\cos\frac{\pi z}{L} = 0. \end{aligned} \tag{3.18}$$

The solution describing the plasma flow only exists when Equation (3.18), considered as an equation determining κ, has a positive solution for any $z \in [-L/2, L/2]$. At fixed z the function $f(\kappa, z)$ takes its minimum equal to

$$\begin{aligned} f_m(z) = 1 - \chi + \ln\chi + \frac{2L}{\pi H}\cos\frac{\pi z}{L} \\ + 2\ln\frac{\cosh(L/2L_c) - \vartheta^2 + (\vartheta^2 - 1)\cosh(z/L_c)}{\vartheta^2[\cosh(L/2L_c) - 1]} \end{aligned} \tag{3.19}$$

at

$$\kappa = \kappa_z \equiv \sqrt{\chi}\,\frac{\cosh(L/2L_c) - \vartheta^2 + (\vartheta^2 - 1)\cosh(z/L_c)}{\vartheta^2[\cosh(L/2L_c) - 1]}. \tag{3.20}$$

It is straightforward to see that $\kappa_z > 0$ and $\kappa_z = \sqrt{\chi}$ when $z = \pm L/2$. The condition that Equation (3.18) has a positive solution reduces to $f_m(z) < 0$ for $z \in [-L/2, L/2]$. It is easy to show that the last term on the left-hand side of Equation (3.19) is negative when $\vartheta > 1$ and it is zero when $\vartheta = 1$. This implies that the condition that $f_m(z) < 0$ for $z \in [-L/2, L/2]$ is satisfied for any $\vartheta > 1$ if it is satisfied for $\vartheta = 1$. When $\vartheta = 1$ this condition reduces to (see Ruderman, 2010)

$$\frac{L}{\pi H} < \frac{L_M}{\pi H} = \frac{1}{2}\left(\chi - \ln\chi - 1\right). \tag{3.21}$$

The dependence of $L_M/\pi H$ on χ is shown in Figure 3.2. Below, we assume that the condition Equation (3.21) is satisfied.

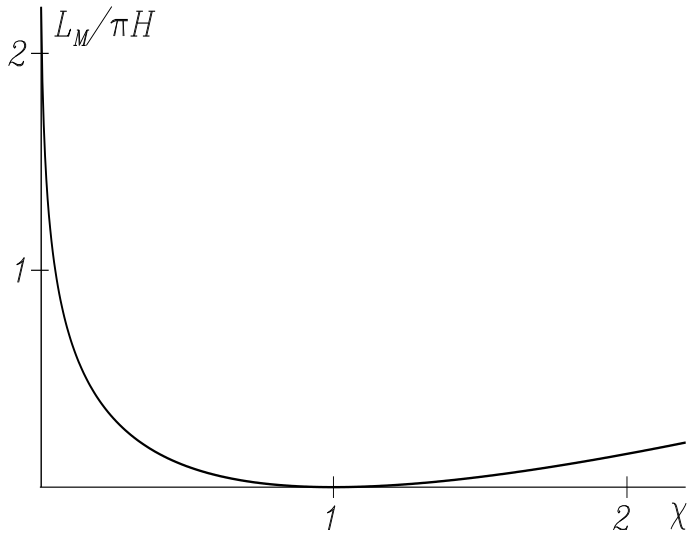

Figure 3.2: The dependence of the maximum possible ratio of the coronal loop height to the atmospheric scale height, $L_M/\pi H$, on χ.

At any fixed z function $f(\kappa, z)$ tends to infinity as either $\kappa \to 0$ or $\kappa \to \infty$. It monotonically decreases for $\kappa \in (0, \kappa_z)$, monotonically increases for $\kappa \in (\kappa_z, \infty)$, and $f(\kappa_z, z) < 0$. This implies that Equation (3.18) defines two functions of z: $\kappa_1(z) < \kappa_z$ and $\kappa_2(z) > \kappa_z$. In the solar atmosphere $g \approx 274\ \mathrm{m\,s^{-2}}$. The observed flow velocities in coronal loops do not exceed $100\ \mathrm{km\,s^{-1}}$ (see Schrijver, 2001), so that we can take $U_f \lesssim 100\ \mathrm{km\,s^{-1}}$. Then, taking $H \sim 60$ Mm, we obtain $\chi \lesssim 0.61 < 1$. Since $\kappa(-L/2) = 1$ and $\kappa_z = \sqrt{\chi}$ when $z = \pm L/2$, this result implies that we have to choose the solution $\kappa_2(z)$. In what follows we will drop the subscript 2.

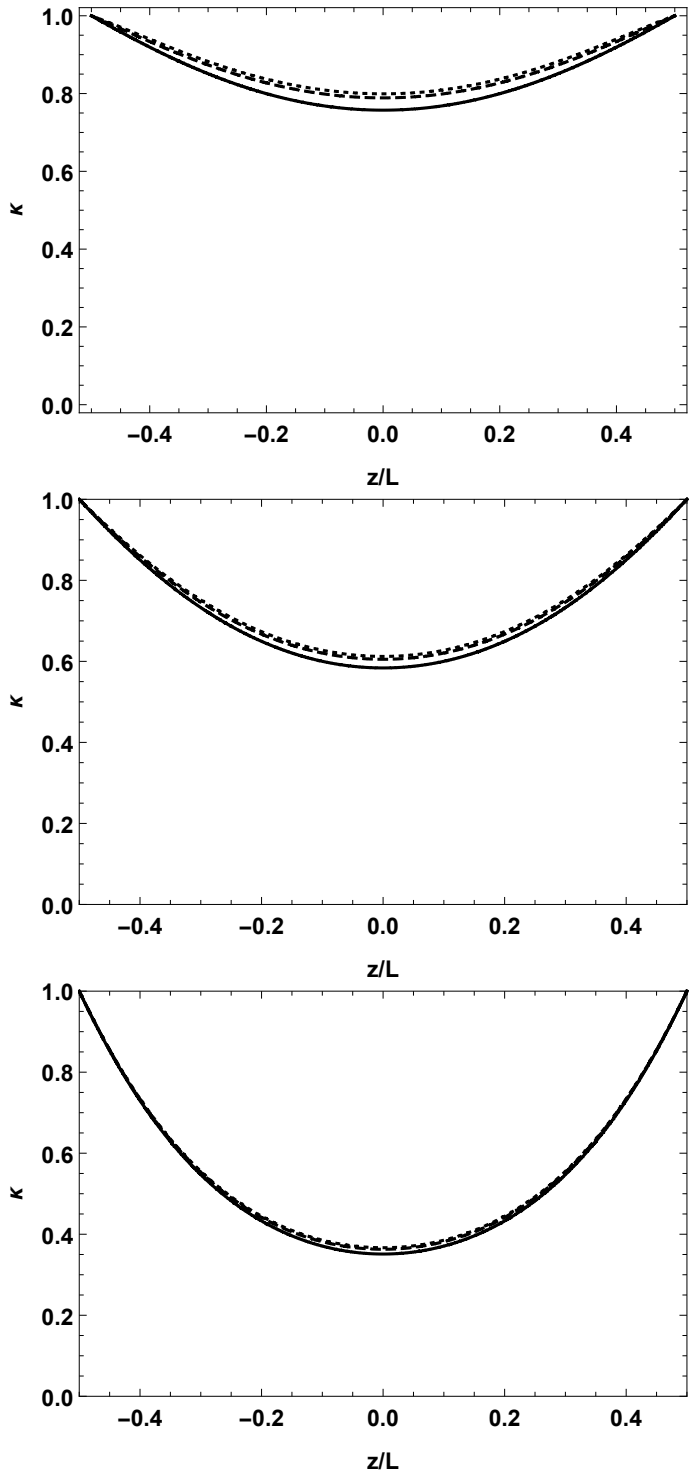

Figure 3.3: The dependence of the density κ on the length along the loop z at $\chi = 0.25\chi_M$. The upper, middle, and lower panels correspond to $L/\pi H = 0.25$, $L/\pi H = 0.5$, and $L/\pi H = 1$. In all panels the solid, dashed, and dotted lines correspond to $\vartheta = 1$, $\vartheta = 1.25$, and $\vartheta = 1.5$.

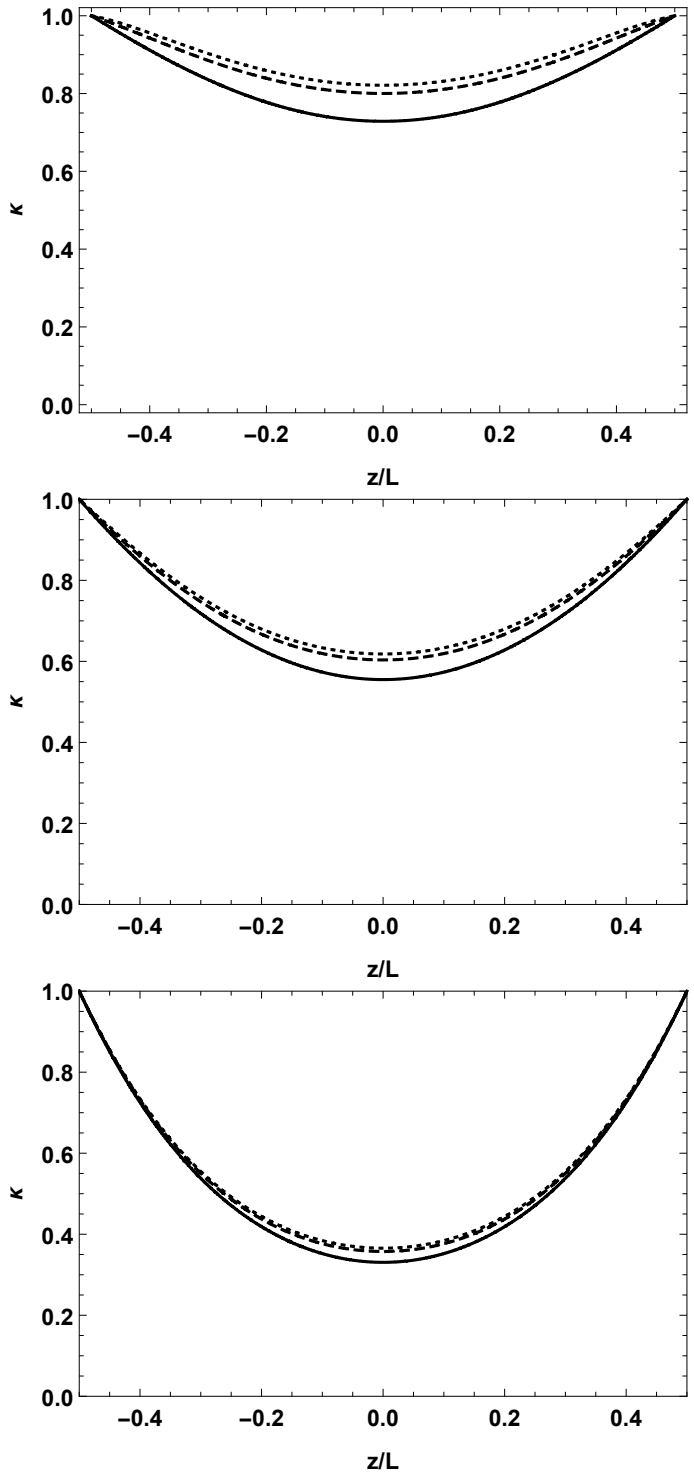

Figure 3.4: The dependence of the density κ on the length along the loop z at $\chi = 0.5\chi_M$. The upper, middle, and lower panels correspond to $L/\pi H = 0.25$, $L/\pi H = 0.5$, and $L/\pi H = 1$. In all panels the solid, dashed, and dotted lines correspond to $\vartheta = 1$, $\vartheta = 1.25$, and $\vartheta = 1.5$.

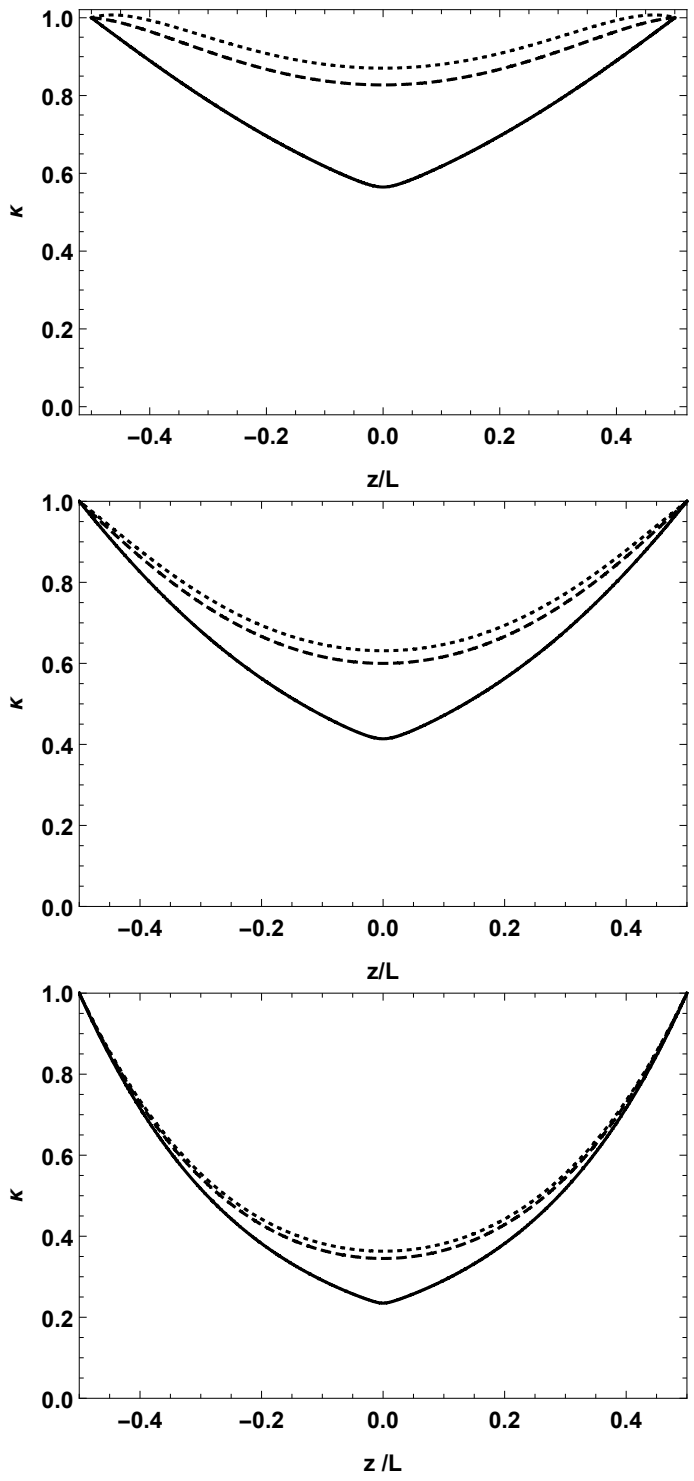

Figure 3.5: The dependence of the density κ on the length along the loop z at $\chi = \chi_M$. The upper, middle, and lower panels correspond to $L/\pi H = 0.25$, $L/\pi H = 0.5$, and $L/\pi H = 1$. In all panels the solid, dashed, and dotted lines correspond to $\vartheta = 1$, $\vartheta = 1.25$, and $\vartheta = 1.5$.

Below, we assume that $\chi < 1$. Then, we can see from Figure 3.2 that, when $L/\pi H$ is fixed, there is a value of χ, denoted as χ_M, such that the inequality Equation (3.21) is only satisfied when $\chi < \chi_M$. In particular, $\chi_M \approx 0.301$ when $L/\pi H = 0.25$, $\chi_M \approx 0.158$ when $L/\pi H = 0.5$, and $\chi_M \approx 0.0524$ when $L/\pi H = 1$. These estimates yield the maximum values of U_f equal to 87 km/s, 63 km/s, and 36.6 km/s, respectively. Note that $\kappa(0) = \sqrt{\chi_M}$ when $\vartheta = 1$ and $\chi = \chi_M$.

In our calculations we have taken $L_c = L/6$, which is the same as that used by Ruderman et al. (2008) (note that these authors considered the loop length equal to $2L$, while it is L in the present study).

In Figures 3.3 – 3.5, we display the dependence of κ on z for various values of χ, ϑ, and $L/\pi H$.

We can see that the effect of the siphon flow on the density inside tube, $\rho_i = \rho_f \kappa$, decreases with the increase of the relative loop height, $L/\pi H$, and with the loop expansion ϑ. We also can see that the increase of flow speed amplifies the difference of density profiles inside the tube for various expansion ϑ.

3.3.2 The effect of flow on the eigenmode frequencies

We now study the effect of bulk flows on the frequencies of eigenmodes of kink oscillations using the model described in the previous subsection. To determine the eigenfrequencies, we solve Equations (3.5) with the boundary conditions Equation (3.4) numerically. In addition to the dimensionless parameters ϑ, χ, and $L/\pi H$, and function $\kappa(z)$ we introduce the dimensionless quantities

$$\begin{gathered} s = \frac{z}{L}, \quad M_A = \frac{U_f \sqrt{\mu_0 \rho_f}}{B_f}, \quad \Omega = \frac{\omega}{\omega_f}, \\ \Lambda = \frac{R(s)}{R_f}, \quad \hat{\rho}_e = \frac{\zeta \rho_e}{\rho_f} \equiv \exp\left(-\frac{L}{\pi H}\cos(\pi s)\right), \end{gathered} \tag{3.22}$$

where B_f is the magnetic field magnitude at the footpoint, and ω_f is the fundamental frequency of oscillations of a homogeneous tube with the internal density ρ_f, external density ρ_f/ζ, and constant cross-section with radius equal to R_f, defined by

$$\omega_f = \frac{\pi C_f}{L}, \quad C_f^2 = \frac{2\zeta B_f^2}{\mu_0 \rho_f (1+\zeta)}. \tag{3.23}$$

Now, using Equation (3.11) and the relation $BR^2 = B_f R_f^2$ we rewrite Equation (3.7) and the boundary condition Equation (3.12) in the dimensionless form as

$$\frac{d}{ds}\left[\left(2 - \frac{M_A^2}{\kappa}\right)\frac{dq}{ds}\right] + \frac{\pi^2 \Lambda^4 \Omega^2}{\zeta + 1}\,\frac{2\kappa^2\zeta - (M_A^2 - 2)\hat{\rho}_e}{2\kappa - M_A^2}\, q = 0, \tag{3.24}$$

$$q = 0 \quad \text{at} \quad s = \pm 1/2. \tag{3.25}$$

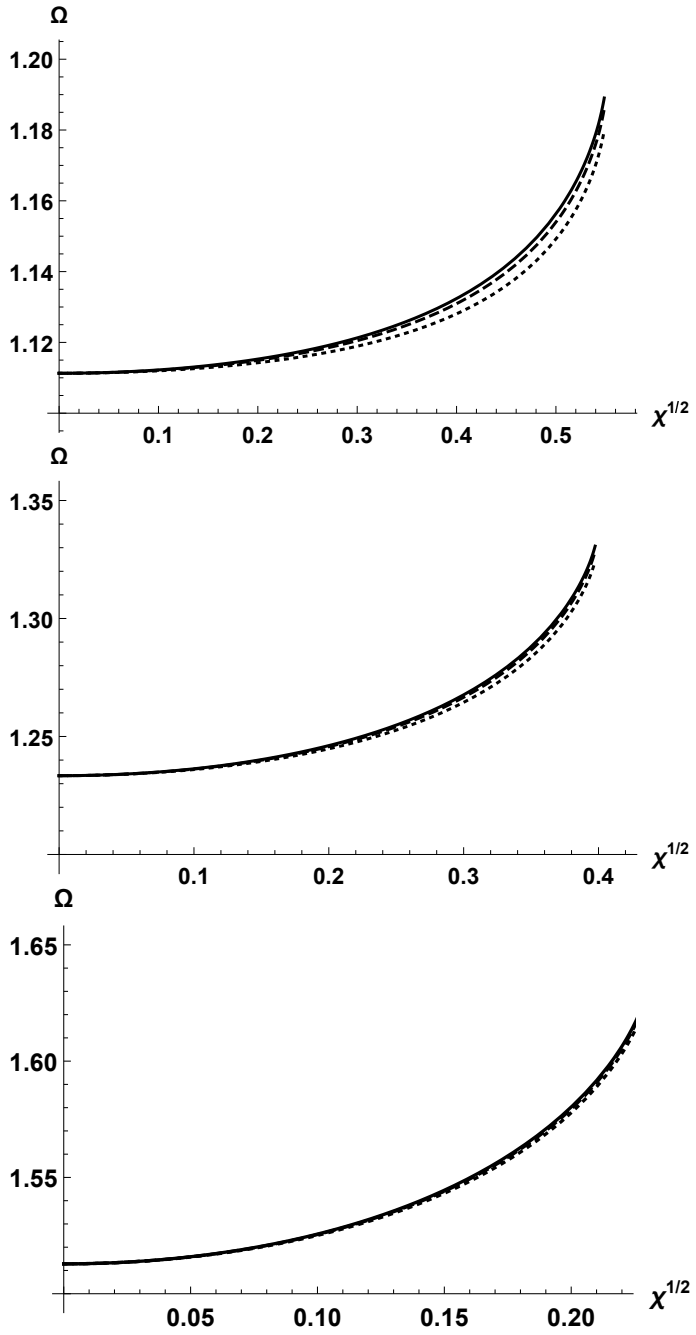

Figure 3.6: The dependence of scaled frequency Ω on χ at $\vartheta = 1$. The upper, middle, and lower panels correspond to $L/\pi H = 0.25$, $L/\pi H = 0.5$, and $L/\pi H = 1$. In all panels the solid, dashed, and dotted lines correspond to $gH/C_f^2 = 0.02,\ 0.03$, and 0.05, respectively.

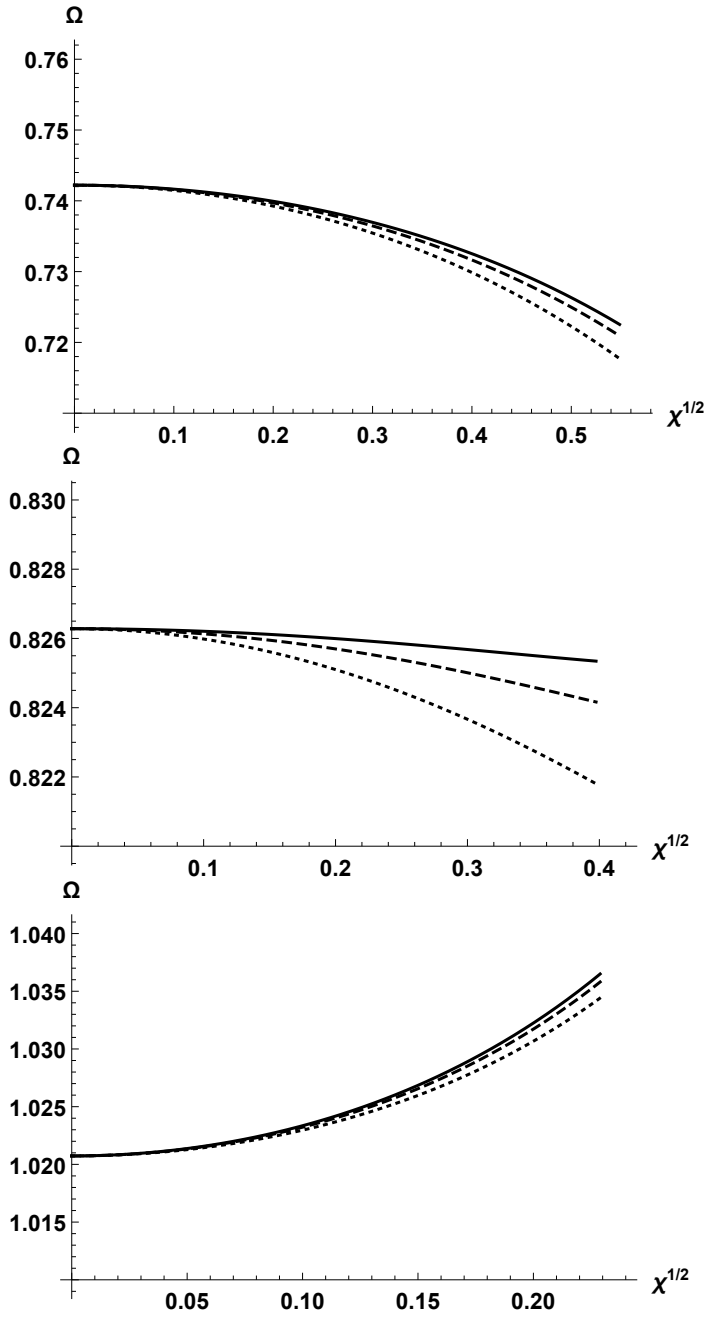

Figure 3.7: The dependence of scaled frequency Ω on χ at $\vartheta = 1.25$. The upper, middle, and lower panels correspond to $L/\pi H = 0.25$, $L/\pi H = 0.5$, and $L/\pi H = 1$. In all panels the solid, dashed, and dotted lines correspond to $gH/C_f^2 = 0.02,\ 0.03$, and 0.05, respectively.

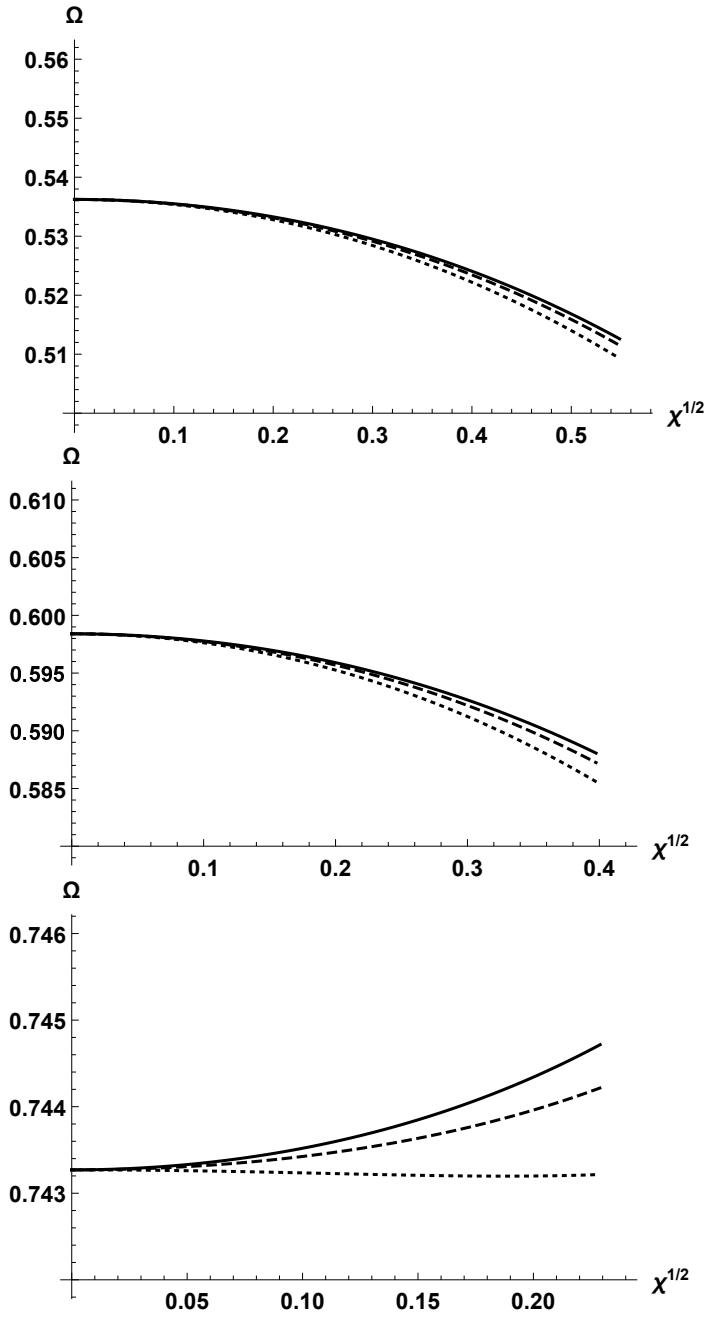

Figure 3.8: The dependence of scaled frequency Ω on χ at $\vartheta = 1.5$. The upper, middle, and lower panels correspond to $L/\pi H = 0.25$, $L/\pi H = 0.5$, and $L/\pi H = 1$. In all panels the solid, dashed, and dotted lines correspond to $gH/C_f^2 = 0.02,\ 0.03$, and 0.05, respectively.

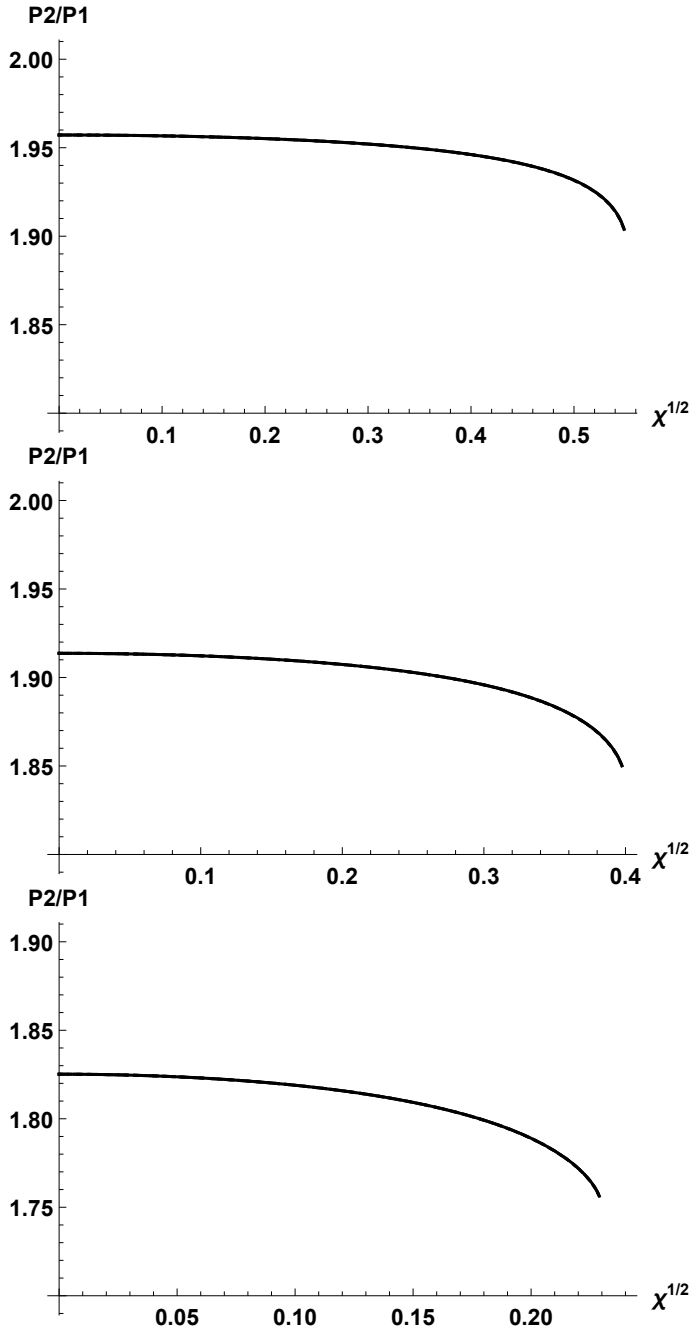

Figure 3.9: The dependence of the period ratio, P_1/P_2, on χ at $\vartheta = 1$. The upper, middle, and lower panels correspond to $L/\pi H = 0.25$, $L/\pi H = 0.5$, and $L/\pi H = 1$. In all panels the solid, dashed, and dotted lines correspond to $gH/C_f^2 = 0.02,\ 0.03$, and 0.05, respectively. Note that in the upper and middle, and lower panels, the three curves are practically indistinguishable for realistic values of gH/C_f^2.

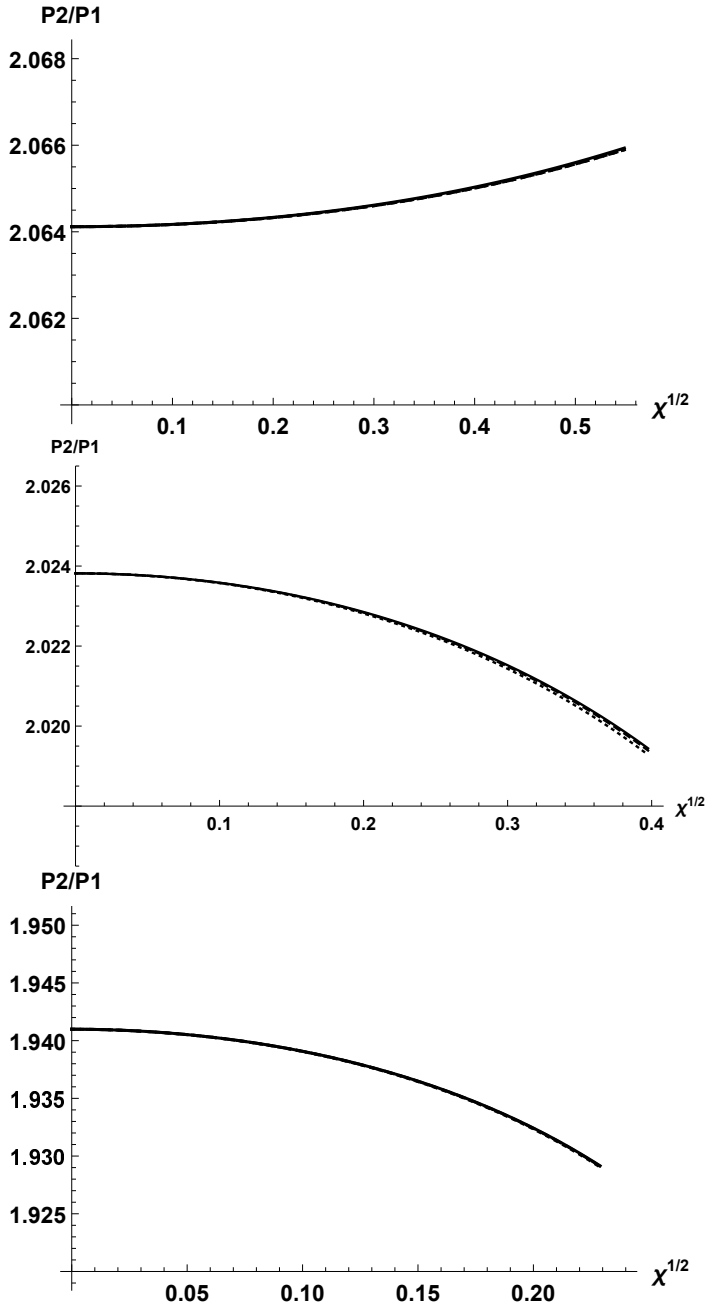

Figure 3.10: The dependence of the period ratio, P_1/P_2, on χ at $\vartheta = 1.25$. The upper, middle, and lower panels correspond to $L/\pi H = 0.25$, $L/\pi H = 0.5$, and $L/\pi H = 1$. In all panels the solid, dashed, and dotted lines correspond to $gH/C_f^2 = 0.02,\ 0.03$, and 0.05, respectively. Note that in the upper and middle, and lower panels, the three curves are practically indistinguishable for realistic values of gH/C_f^2.

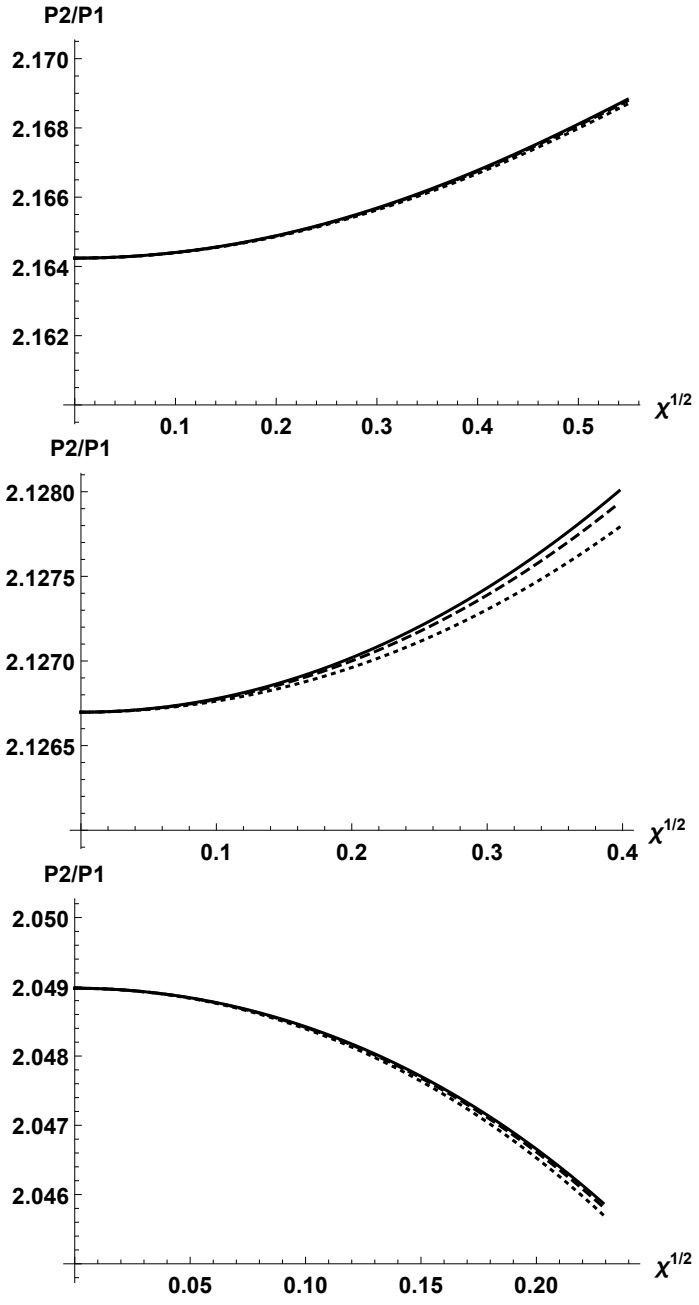

Figure 3.11: The dependence of the period ratio, P_1/P_2, on χ at $\vartheta = 1.5$. The upper, middle, and lower panels correspond to $L/\pi H = 0.25$, $L/\pi H = 0.5$, and $L/\pi H = 1$. In all panels the solid, dashed, and dotted lines correspond to $gH/C_f^2 = 0.02,\ 0.03$, and 0.05, respectively.

The eigenvalue Ω of the boundary value problem defined by Equations (3.24) and (3.25) depends on five dimensionless parameters: ζ, $L/\pi H$, ϑ, χ, and M_A. We aim to study the dependence of the kink oscillation eigenfrequencies on the magnitude U_f of the siphon flow. Then it is not convenient to use these five dimensionless parameters because both χ and M_A^2 are proportional to U_f^2. Therefore we use the dimensionless parameter gH/C_f^2 that was also introduced by Ruderman (2010). Note that M_A is expressed in terms of other parameters by

$$M_A^2 = \frac{2\zeta\chi}{\zeta+1}\,\frac{gH}{C_f^2}. \tag{3.26}$$

Below, we take $\zeta = 3$ same as proposed by Ruderman (2010). Ruderman et al. (2008) showed, employing the observations made by Verwichte et al. (2004) and Van Doorsselaere et al. (2007), that scale height may vary between 38 and 109 Mm. If we take $H = 60$ Mm, then, for realistic values of C_f, say, for $C_f = 600$ km s^{-1}, we obtain $gH/C_f^2 = 0.05$. In Figures 3.6 – 3.8 the dependence of Ω on χ is shown for the fundamental harmonic for various values of $L/\pi H$, ϑ, and gH/C_f^2. We also calculated the dependence of the ratio of periods of the fundamental harmonic and first overtone P_1/P_2, on χ for various values of $L/\pi H$, ϑ, and gH/C_f^2. This dependence is shown in Figures 3.9 – 3.11. After analysing the numerical results we first of all note that the effect of realistic flow values on the fundamental frequency of kink oscillations is fairly weak. When the flow velocity increases from zero to its maximum value the fundamental frequency varies by less than 10%. Another interesting property is that, depending on the other parameters, the flow can result either in the increase or decrease of the fundamental frequency.

The effect of background flow on the ratio of frequencies of the first overtone and fundamental mode also only weakly depends on the magnitude of the flow velocity. Again, depending on the other parameters, the flow can result either in the increase or decrease of this ratio frequency. The frequency ratio is less than two at Figure 3.9 and lower panel of Figure 3.10, and exceeds two on five other panels of Figures 3.10 and 3.11. In the absence of flow this behaviour is in a complete agreement with the theorem proved by Ruderman et al. (2016). Indeed, it can be shown that, when $\chi = 0$, the kink speed increases from the foot point to the loop apex for the parameters corresponding to the Figure 3.9 and the lower panel of Figure 3.10, and decreases for the parameters corresponding to five other panels of Figures 3.10 and 3.11 .

§ 3.4 Kink oscillations of coronal loops with slowly varying density

The analysis in this section is motivated by observations of kink oscillation of coronal loops (e.g. Aschwanden and Terradas, 2008; Aschwanden and Schrijver, 2011). Below we consider kink oscillations of a magnetic tube with slowly varying density. We assume that magnetic flux tube is fixed at the dense photosphere, which means that the boundary condition Equation (3.5) is satisfied. In addition, we also assume that the characteristic time of density variation, t_{ch}, is much greater than the characteristic time of oscillations. We note that this is not very restrictive assumption. It is

usually believed that the characteristic time of oscillations is the oscillation period. However, in fact it is $1/\omega$, where ω is the oscillation frequency. This time is about 6 times smaller than the oscillation period. Hence, the condition that t_{ch} should be much larger than the characteristic time of oscillations is satisfied even when t_{ch} is of the order of oscillation period.

3.4.1 Derivation of adiabatic invariant

We denote the ratio of t_{ch} to the characteristic time of oscillations as ν^{-1}, where $\nu \ll 1$. Hence, the characteristic time of oscillations is νt_{ch}. On the other hand, it is also of the order of the loop length divided by the characteristic kink speed, which is equal to $L/(B/\sqrt{\mu_0\rho_{ch}})$, where ρ_{ch} is the characteristic density. As a result, we have

$$B \sim \nu^{-1}\sqrt{\mu_0\rho_{ch}}\frac{L}{t_{ch}}. \tag{3.27}$$

Following this estimate we introduce the scaled magnetic field $\widetilde{B} = \nu B$. Then we rewrite Equation (3.1) as

$$\rho_i\left(\frac{\partial}{\partial t} + \frac{U_i}{R^2}\frac{\partial}{\partial z}R^2\right)\left(\frac{\partial \eta}{\partial t} + U_i\frac{\partial \eta}{\partial z}\right) + \rho_e\left(\frac{\partial}{\partial t} + \frac{U_e}{R^2}\frac{\partial}{\partial z}R^2\right)\left(\frac{\partial \eta}{\partial t} + U_e\frac{\partial \eta}{\partial z}\right) - \frac{2\nu^{-2}\widetilde{B}^2}{\mu_0}\frac{\partial^2\eta}{\partial z^2} = 0. \tag{3.28}$$

Now, we use the Wentzel-Kramer-Brillouin (WKB) method (e.g. (Bender and Orszag, 1978)) and look for solution to this equation in the form

$$\eta = S(t,z)\exp[\nu^{-1}\Theta(t)]. \tag{3.29}$$

Then we expand S in the series

$$S = S_0 + \nu S_1 + \ldots \tag{3.30}$$

We substitute Equation (3.29) in Equation (3.28) (for more details see Appendix B). Then, using equation (3.30) and collecting terms of order ν^{-2}, we obtain

$$\frac{\partial^2 S_0}{\partial z^2} + \frac{\Omega^2}{\widetilde{C}_k^2}S_0 = 0, \tag{3.31}$$

where

$$\Omega = \frac{d\Theta}{t}, \quad \widetilde{C}_k^2 = \frac{2\widetilde{B}^2}{\mu_0(\rho_i + \rho_e)}. \tag{3.32}$$

Finally, taking into account boundary condition Equation (3.4), yields

$$S_0 = 0 \quad \text{at} \quad z = \pm L/2. \tag{3.33}$$

As a result, Equations (3.31) and (3.33) constitute the classical Sturm-Liouville problem. An approximation of such order is called the approximation of geometrical optics (e.g. Bender and Orszag (1978)). The Sturm-Liouville problem Equations (3.31) and (3.33) coincides with a problem obtained by Dymova and Ruderman (2005) to describe oscillations of magnetic flux tubes whose density varies along the tube, and by Ruderman et al. (2008) to describe kink oscillation of magnetic tubes whose density and cross-section radius vary along the tube. Below, we assume that Ω^2 is an eigenvalue and S_0 the corresponding eigenfunction. In accordance with the general theory (e.g. Coddington and Levinson (1955)), Ω^2 is real. It is easy to prove that $\Omega^2 > 0$ by multiplying equation (3.31) by S_0, then integrating by parts with respect to z from $-L/2$ to $L/2$ and using the boundary condition (3.33). Obviously, we can always assume that S_0 is real function.

Now, we collect terms of the order ν^{-1} to obtain

$$\frac{\partial^2 S_1}{\partial z^2} + \frac{\Omega^2}{\widetilde{C}_k^2} S_1 = \frac{2i\Omega}{\widetilde{C}_k^2}\left(\frac{\partial S_0}{\partial t} + \frac{S_0}{2\Omega}\frac{\partial \Omega}{\partial t} + \frac{\rho_i U_i + \rho_e U_e}{R(\rho_i + \rho_e)}\frac{\partial R S_0}{\partial z}\right). \tag{3.34}$$

This order of approximation is the approximation of the physical optics. S_1 must satisfy the boundary conditions

$$S_1 = 0 \quad z = \pm L/2. \tag{3.35}$$

The homogeneous counterpart of the boundary value problem constituted by Equation (3.34) and the boundary condition Equation (3.35) has non-trivial solution $S_1 = S_0$. This implies that the boundary value problem determining S_1 has a solution only if the right-hand side of Equation (3.34) satisfies the compatibility condition, which is the condition that it should be orthogonal to S_0. To obtain this condition we multiply Equation (3.34) by S_0 and then integrate with respect to z from $-L/2$ to $L/2$. After some algebra (for more details please see Appendix C) we obtain

$$\int_{-L/2}^{L/2} \frac{1}{\widetilde{C}_k^2}\frac{\partial \Omega S_0^2}{\partial t} dz = -\frac{\mu_0 \Omega}{2}\int_{-L/2}^{L/2} \frac{\rho_i U_i + \rho_e U_e}{R^2 \widetilde{B}^2}\frac{\partial (S_0^2 R^2)}{\partial z} dz. \tag{3.36}$$

Using integration by parts, Equation (2.52) and the relation $R^2\widetilde{B} = \text{const}$, yields

$$\int_{-L/2}^{L/2} \frac{\rho_i U_i + \rho_e U_e}{R^2 \widetilde{B}^2}\frac{\partial S_0^2 R^2}{\partial z} dz = \int_{-L/2}^{L/2} \frac{S_0^2}{\widetilde{B}^2}\frac{\partial (\rho_i + \rho_e)}{\partial t} dz. \tag{3.37}$$

Substituting Equation (3.37) in Equation (3.36) and using Equation (3.32) we eventually obtain

$$\omega \int_{-L/2}^{L/2} \frac{S_0^2}{C_k^2} dz = \text{const}, \tag{3.38}$$

where

$$\omega = \nu^{-1}\Omega, \quad C_k^2 = \nu^{-2}\widetilde{C}_k^2 = \frac{2B^2}{\mu_0(\rho_i + \rho_e)}. \tag{3.39}$$

The left-hand side of Equation (3.38) is an adiabatic invariant. Equation (3.38) states that this invariant is conserved. It is worth noting that the adiabatic invariant is the same as that obtained by Ruderman (2011b) for oscillations of magnetic tubes with constant cross-section radius. Hence, the tube expansion only affects the time evolution of kink oscillations of magnetic flux tubes with the varying density through C_k and S_0 that both depend on $R(z)$.

3.4.2 Effect of cooling on the kink oscillations of coronal magnetic loops

In this subsection, we consider the kink oscillations of cooling coronal loops. The main cause of the loop cooling is radiation. The coronal loop is an object, which is assumed to consist of optically thin confined plasma. Then, its intensity is proportional to the plasma density squared. This implies that the energy deposition that is sufficient to cover the energy losses in the rarefied plasma outside the loop may be too small to cover the energy losses inside the loop. Hence, it seems to be viable assumption that, while the plasma inside the loop is cooling, the temperature of the plasma outside the loop remains constant. Following Aschwanden and Terradas (2008) and Morton and Erdélyi (2010), we approximate the temperature evolution inside the loop by an exponentially decaying function, e.g.,

$$T(t) = T_0 \exp(-t/t_{cool}), \tag{3.40}$$

where we have assumed that the cooling starts at the initial time $t = 0$, implying that the temperature of external plasma remains equal to T_0. Below, we again consider the loop with a half-circle shape and neglect the effect of the loop curvature. Hence, the loop shape only determines the density variation along the loop. In the external plasma it is given by the barometric formulae

$$\rho_e(z) = \frac{\rho_f}{\zeta} \exp\left(- \frac{L}{\pi H_0} \cos\frac{\pi z}{L}\right), \tag{3.41}$$

where ζ is ratio of the densities inside and outside the loop at $t = 0$,

$$H_0 = \frac{k_b T_0}{mg}, \tag{3.42}$$

The cooling causes the plasma flow inside the loop. This flow affects the plasma density meaning that it is not described by the barometric formulae. However, Ruderman (2011b) showed that for typical coronal conditions and observed cooling times the effect of this flow on the plasma is fairly weak. Hence, the barometric formula provides a sufficiently good approximation for the plasma density inside the loop. Thus we have

$$\rho_i(z) = \rho_f \exp\left(- \frac{L}{\pi H(t)} \cos\frac{\pi z}{L}\right), \tag{3.43}$$

where

$$H(t) = \frac{k_B T(t)}{mg}. \tag{3.44}$$

To describe the cross-section radius variation along the loop follow Ruderman et al. (2008), Equation (3.16). Here, analysis is analogous to section 3.3, and holds for ϑ. Recalling that loop expansion factor ϑ typically does not exceed 1.5. By properly choosing L/L_c, we can cover the entire range of expansion factor variations. Similarly to section 3.3, we introduce dimensionless variables and parameters

$$Z = \frac{2z}{L},\ \tau = \frac{t}{t_{cool}},\ \varpi = \frac{\omega L}{C_f},\ \kappa = \frac{L}{\pi H_0}. \tag{3.45}$$

Then, using Equations (3.22) and (3.23) Equation (3.31) reduces to

$$\frac{\partial^2 S_0}{\partial Z^2} + \frac{\varpi^2 \Lambda^4(Z) S_0}{4(\zeta+1)}[\zeta \exp\left(-\kappa e^{\tau} \cos(\pi Z/2)\right) + \exp\left(-\kappa \cos(\pi Z/2)\right)] = 0. \tag{3.46}$$

When deriving this equation we dropped the prime at S_0 and used the relation $B\Lambda^2 = B_f$. The function $\Lambda(Z)$ is defined by Equations (3.16) and (3.22). The eigenfunction corresponding to the fundamental mode is even, while the eigenfunction corresponding to first overtone is odd. This enables us to solve Equation (3.46) not on the interval $[-1, 1]$, but on the interval $[0, 1]$. The solution corresponding to the fundamental mode must satisfy the boundary condition.

$$\frac{\partial S_0}{\partial Z} = 0 \quad \text{at} \quad Z = 0, \quad S_0 = 0 \quad \text{at} \quad Z = 1, \tag{3.47}$$

and the solution corresponding to first overtone must satisfy the boundary conditions

$$S_0 = 0 \quad \text{at} \quad Z = 0, 1. \tag{3.48}$$

Since the eigenfunction S_0 is determined with the accuracy up to the multiplication by an arbitrary function τ, we can always fix its value at one particular point. Let $X(\tau, Z)$ be an eigenfunction corresponding to the fundamental mode that satisfies the condition $X(\tau, 0) = 1$. Then the general solution corresponding to the fundamental mode is $S_0(\tau, Z) = A(\tau)X(\tau, Z)$, where $A(\tau)$ is the oscillation amplitude at $Z = 0$. Then Equation (3.38) reduces to

$$\varpi A^2 \int_{-1}^{1} X^2 \Lambda^4 [\zeta \exp(-\kappa e^{\tau} \cos(\pi Z/2)) + \exp(-\kappa \cos(\pi Z/2))] dZ = \text{const}. \tag{3.49}$$

Equations (3.46) and (3.49) have been solved numerically for $\zeta = 3$, similarly to Ruderman (2011b), and $L_c = L/6$ enables to cover the full range of expansion factors. In this case $\vartheta \approx 1.67$. In Figures 3.12 – 3.14 the dependence of the dimensionless fundamental mode frequency, the ratio of frequencies of the first overtone and fundamental mode, and oscillation amplitude at $Z = 0$ on τ are shown for various values of κ and ϑ.

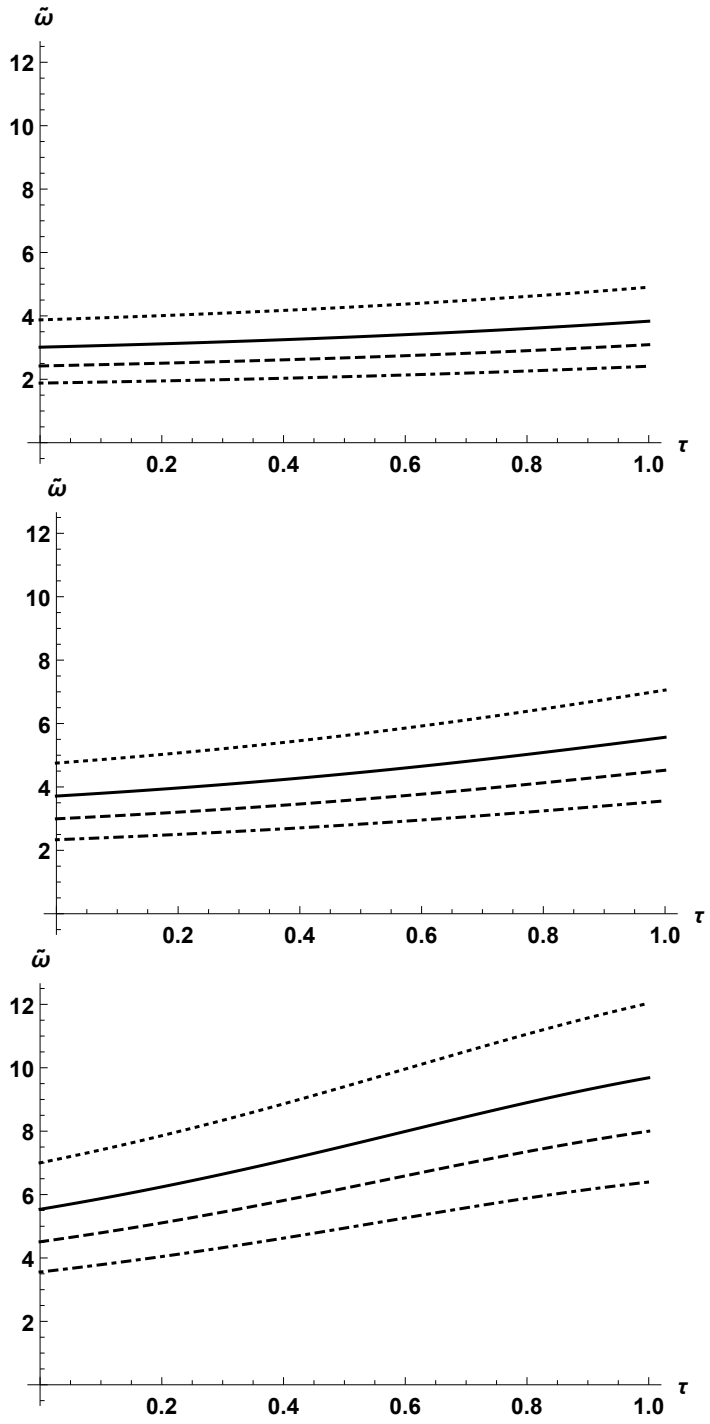

Figure 3.12: The dependence of the dimensionless fundamental mode frequency on dimensionless time τ. The upper, middle, and lower panel correspond to values of relative lengths $\kappa = 0.5$, $\kappa = 1$, and $\kappa = 2$. The dotted, solid, dashed, and dashed dotted lines correspond to expansion factors $\vartheta = 1$, 1.15, 1.3 and 1.5, respectively.

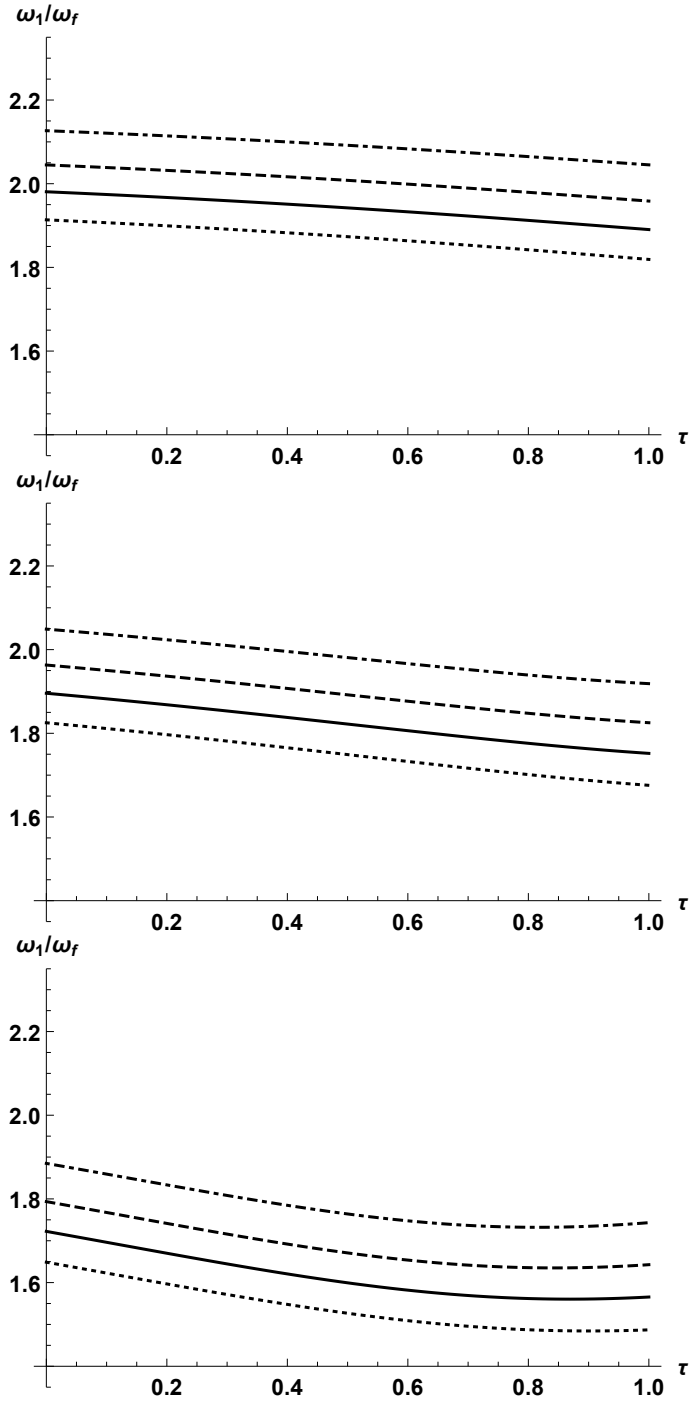

Figure 3.13: The dependence of the ratio frequencies of the first overtone and fundamental mode on dimensionless time τ. The upper, middle, and lower panel correspond to values of relative loop length $\kappa = 0.5$, $\kappa = 1$, and $\kappa = 2$. The dotted, solid, dashed, and dashed dotted lines correspond to expansion factors $\vartheta = 1$, 1.15, 1.3 and 1.5, respectively.

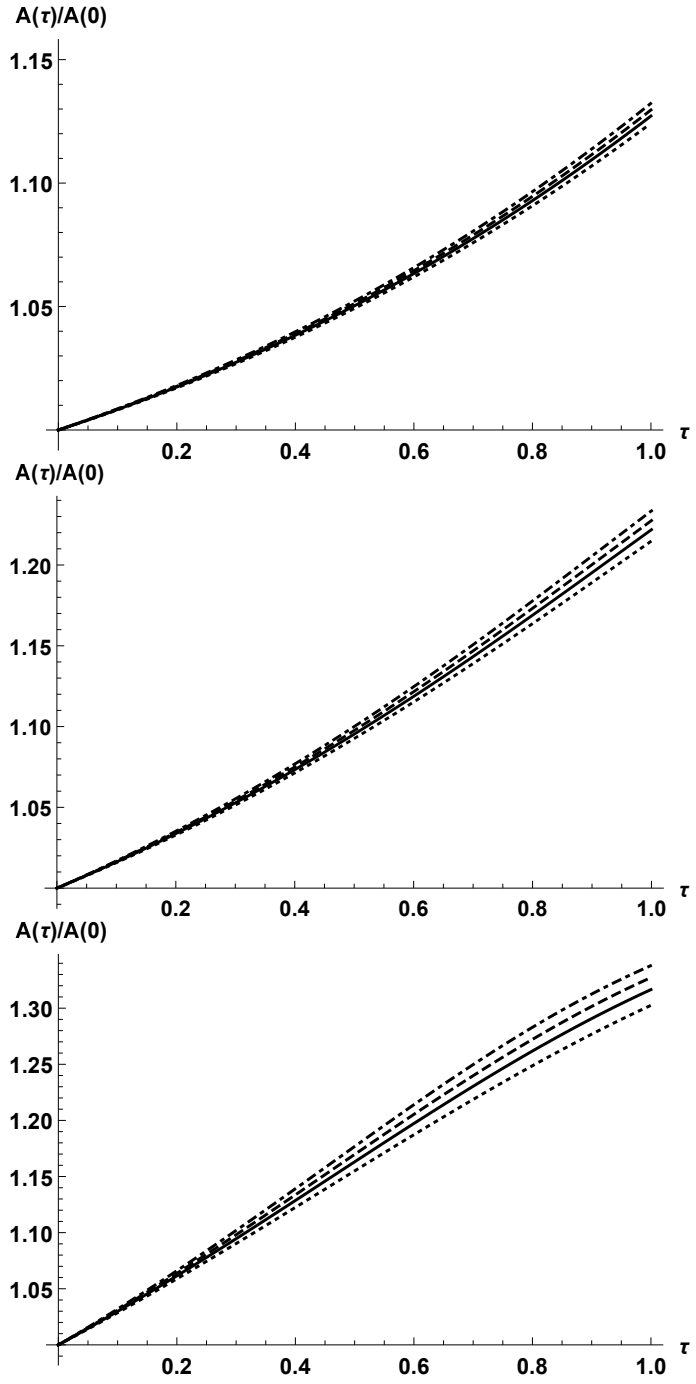

Figure 3.14: The dependence of the dimensionless amplitude of the fundamental mode at $Z = 0$ on dimensionless time τ. The upper, middle, and lower panel correspond to values of relative loop length $\kappa = 0.5$, $\kappa = 1$, and $\kappa = 2$. The dotted, solid, dashed, and dashed dotted lines correspond to expansion factors $\vartheta = 1$, 1.15, 1.3 and 1.5, respectively.

We conclude from Figure 3.12 that the oscillation frequency grows for all parameters of the expansion factor and for all values of the loop. A similar result was obtained by Morton and Erdélyi (2009), Morton and Erdélyi (2010) and Ruderman (2011b) for non-expanding magnetic loops. This result has a simple physical explanation. When the loop is cooling the plasma starts to flow with the velocity directed to the loop footpoints. The plasma is evacuated from the loop meaning that the mass of the loop decreases. At the same time the restoring force created by magnetic tension remains the same. As a result the oscillation frequency increases.

Figure 3.13 shows that the ratio frequencies of the first overtone and fundamental harmonic decreases with time. Again analogous results were obtained by Morton and Erdélyi (2009), Morton and Erdélyi (2010) and Ruderman (2011b) for non-expanding loops. As a result of cooling, the plasma density at the loop decreases everywhere except for the loop footpoints. In particular, the density decreases at the loop apex. Therefore, the kink speed at the loop apex increases, while it remains the same at the loop footpoints. Ruderman et al. (2016) showed that the frequency ratio is a monotonically decreasing function of the ratio of the kink speed at the loop apex and footpoints.

The most interesting result of this section is shown in Figure 3.14. We see that cooling enhances the oscillation amplitude. Previously, a similar result was obtained by Ruderman (2011b) for non-expanding loops. We also see that the loop expansion makes the oscillation amplification stronger. This effect becomes more pronounced when the loop height increases. However, even for loops whose height is equal to two times the initial atmospheric scale height, the effect is fairly weak.

§ 3.5 Summary

We now summarise Chapter 3. First of all we assumed that transitional layer is absent and considered the density and flow velocity independent of time. We also assumed that footpoints are fixed. Then by using the model for coronal loop cross-section expansion proposed by Ruderman et al. (2008), we obtained equation describing kink oscillation. We then studied numerically the dependence of density along the loop for various expansion factors. We found out that, for typical parameters of coronal loops, the increase in the relative loop height and the loop expansion causes the decrease in density inside the tube. We then numerically studied the effect of background flow on kink oscillation. We found out that the expansion effect on kink oscillations of coronal loops is fairly weak, the difference for frequency evolution of non-expanding tube to the frequency evolution of expanding cases is less than 10%. We also found out that the presence of relatively slow bulk flow with flow speed less than double of Alfvén has negligible effect on dimensionless fundamental frequency and ratio of first overtone period on fundamental period. This result is particularly important for coronal seismology as it allows to neglect the presence of a relatively slow background flow even in an expanding coronal loop.

In the next subsection we considered the case of slowly varying density. We assumed that there is no heat transfer between the coronal loop and surroundings. By the means

of WKB approximation we obtained the equation describing kink oscillations. From that equation we obtained the adiabatic invariant. We numerically studied the effect of cooling on kink oscillation. We concluded that oscillation frequency grows with time for all parameters of the expansion factor and for all values of the relative loop length. We also noticed that the increase in expansion factor decreases both the dimensionless fundamental frequency as well as the ratio of the first overtone on the fundamental mode. In addition, we found out that the ratio of the first overtone on fundamental mode decreases with time for all the parameters of the expansion factor and for all values of the relative loop length. Finally, we conclude that the expansion factor effect on the amplitude is fairly weak, even for high values of the relative loop length. These results have a particularly high value for the coronal seismology as it presents the significant importance of expansion factor on the evolution of frequency with time for cooling coronal loops. In addition to that by obtaining the values of observable expansion factor, frequency profile and length of a coronal loop these results create a possibility to estimate the kink speed at the footpoints of the loop.

Chapter 4

Resonant Damping of Kink Oscillation in Absence of Background Flow

§ 4.1 Equilibrium configuration and governing equations

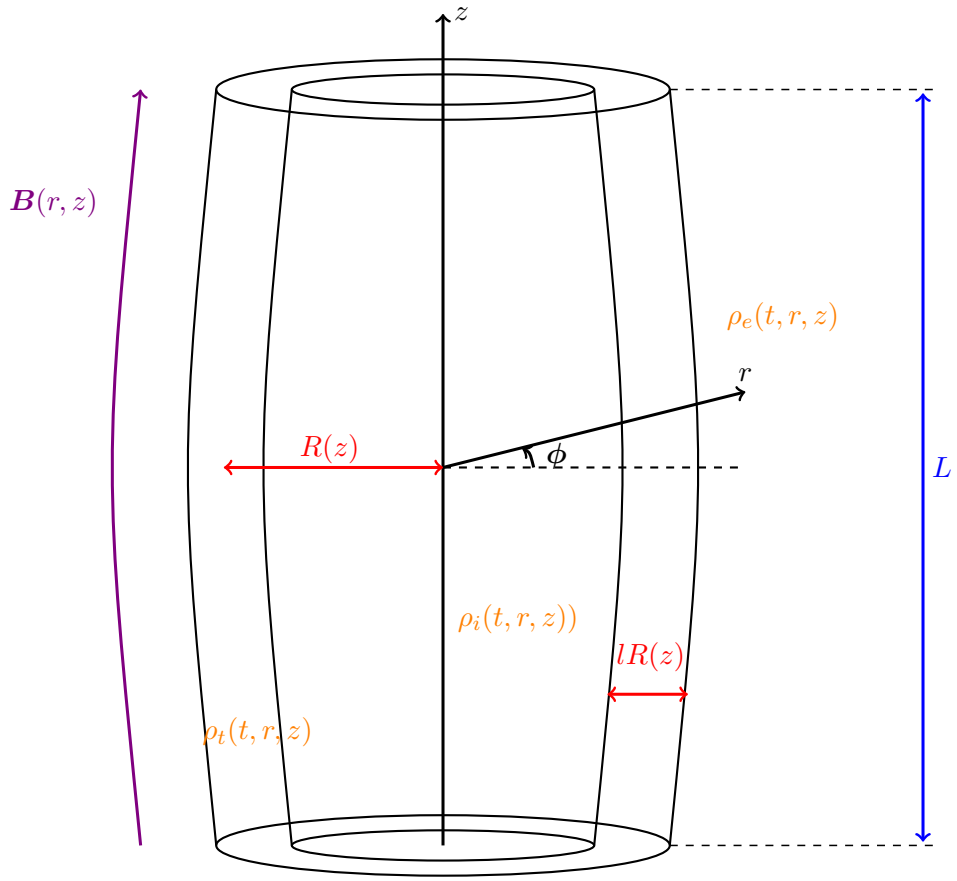

Figure 4.1: Equilibrium configuration of the straight expanding two layered magnetic flux tube

In this chapter, we consider an amended version of model of the one proposed in Chapter 2. Here, we assume that there is no background flow $\boldsymbol{U}$. Thus, we consider coronal loops as straight, thin, and expanding magnetic tubes with a circular cross-section. The tube consists of a core and a transition region where the density decreases from a higher value inside the tube to the lower value representing the surrounding plasma. Figure 4.1 shows such an equilibrium configuration, in cylindrical coordinates r, ϕ, z with the z-axis coinciding with the tube axis. We recall that the plasma density is defined by Equation 2.1 in Chapter 2.

Once again, assume that the boundaries of the transitional layer are magnetic surfaces. We use the cold plasma approximation and thin tube and thin boundary (TTTB) approximation and assume that $R(z) \ll L$ and $l \ll 1$, where L is the tube length. This assumption slightly differs to that in Chapter 2 as L may be also wavelength for propagating waves. We also assume that the characteristic scale of variation of $\rho_i(r, z)$,

$\rho_e(r,z)$, and $\boldsymbol{B}$ in the radial direction is R_*. On the other hand, the characteristic scale of variation of $\rho_t(r,z)$ in the radial direction is lR_*, where R_* is a typical value of $R(z)$. Below, we use the notation $R_*/L = \epsilon \ll 0$. The tube ends are assumed to be frozen in the dense plasma at $z = \pm L/2$. In Chaper 2 we derived the system of two equations that describe kink oscillations of expanding magnetic flux tubes in the presence of siphon flow and the equilibrium quantities varying in time using the cold plasma and TTTB approximation. In the case of a static equilibrium, i.e. when there is no background flow and the equilibrium quantities are time-independent, these system of equations reduces to

$$\frac{\partial^2 \eta}{\partial t^2} - C_k^2 \frac{\partial^2 \eta}{\partial z^2} = \widetilde{\mathcal{L}}, \tag{4.1}$$

$$\widetilde{\mathcal{L}} = \frac{1}{\rho_i + \rho_e} \left(\frac{\delta P}{R^2} + \frac{B^2}{\mu_0} \frac{\partial^2 (l\eta + \delta\eta)}{\partial z^2} - \rho_e \frac{\partial^2 (l\eta + \delta\eta)}{\partial t^2} \right). \tag{4.2}$$

We recall that in these equations $\eta = \xi_\perp / R(z)$, where $\xi_\perp$ is the plasma displacement in the direction perpendicular to $\boldsymbol{B}$ and in the plane $\phi = \text{const}$, P is the perturbation of the magnetic pressure, μ_0 is magnetic permeability of free space, C_k , δP and $\delta\eta$ are defined by Equations (3.39) and (2.73) respectively where $\psi = \psi_e$ and $\psi = \psi_i$ are the equations of the external and internal boundaries of the transitional layer, respectively.

It follows from analysis in Chapter 2 that, in the thin tube approximation, the dependence of B, ρ_i, and ρ_e on r is neglected, and these quantities are only considered as functions of z. In Equation (4.1) η is calculated in the core of the tube where it is independent of r in the thin tube approximation. It follows from the magnetic flux conservation that B and R are related by

$$BR^2 = \text{const}. \tag{4.3}$$

The system of Equations (4.1) and (4.2) is not closed. To close it we need to express δP and $\delta\eta$ in terms of η. This will be done in the next section.

§ 4.2 Derivation of expressions for δP and $\delta\eta$

4.2.1 Transformation of linearised MHD equations

To derive the expressions for δP and $\delta\eta$ we solve the linearised MHD equations using the approximation of low beta. To remove the singularity at the Alfvén resonant position we take viscosity into account. In the solar corona, viscosity is strongly anisotropic. The full Braginkii's expression for the viscosity tensor contains five terms (Braginskii, 1965). For typical coronal conditions the coefficient at the first term describing the compressional viscosity is at least ten orders of magnitude larger than the coefficients at the fourth and fifth term describing the shear viscosity (see e.g. Ofman et al. (1994)). However in weakly dissipative plasmas like the coronal plasma the viscosity is only important in the vicinity of the ideal resonant position. In this vicinity only the shear viscosity works (e.g. Ofman et al., 1994; Erdélyi and Goossens, 1995). Hence, we can only keep the terms describing shear viscosity. As a result, the term describing

the viscous force on the right-hand side of the momentum equation is given by $\rho\iota\nabla^2\boldsymbol{u}$, where ι is the coefficient of shear viscosity and $\boldsymbol{u} = (u_r, u_\phi, u_z)$ is the velocity. Then the linearised set of MHD equations in the cold plasma approximation is

$$\frac{\partial\rho}{\partial t} + \nabla\cdot(\rho\boldsymbol{u}) = 0, \tag{4.4}$$

$$\rho\frac{\partial\boldsymbol{u}}{\partial t} = \frac{1}{\mu_0}(\nabla\times\boldsymbol{b})\times\boldsymbol{B} + \rho\iota\nabla^2\boldsymbol{u}, \tag{4.5}$$

$$\frac{\partial\boldsymbol{b}}{\partial t} = \nabla\times(\boldsymbol{u}\times\boldsymbol{B}). \tag{4.6}$$

Similarly to Chapter 2, we introduce the plasma displacement $\boldsymbol{\xi} = (\xi_r, \xi_\phi, \xi_z)$ related to the velocity by $\boldsymbol{u} = \partial\boldsymbol{\xi}/\partial t$. Below, we again use the components of the velocity and plasma displacement that are perpendicular to the equilibrium magnetic field and are in the $\phi = \text{const}$ plane,

$$\xi_\perp = \frac{\xi_r B_z - \xi_z B_r}{B}, \quad u_\perp = \frac{u_r B_z - u_z B_r}{B}. \tag{4.7}$$

We also use the magnetic pressure perturbation $P = \boldsymbol{b}\cdot\boldsymbol{B}/\mu_0$.

Below, we need the expression for the viscous force in terms of $\xi_\perp$ and ξ_ϕ. We use the identity (Korn and Korn, 1961)

$$\nabla^2\boldsymbol{u} = \nabla(\nabla\cdot\boldsymbol{u}) - \nabla\times\nabla\times\boldsymbol{u}. \tag{4.8}$$

Applying the expressions for the gradient, divergence, and curl in cylindrical coordinates and taking into account that in the cold plasma approximation the velocity perturbation is orthogonal to the equilibrium magnetic field, $\xi_r B_r + \xi_z B_z = 0$, we obtain

$$\left(\nabla^2\boldsymbol{u}\right)_r = \frac{\partial}{\partial r}\frac{1}{r}\frac{\partial}{\partial r}\left(\frac{rB_z u_\perp}{B}\right) + \frac{\partial^2}{\partial z^2}\left(\frac{B_z u_\perp}{B}\right) + \frac{B_z}{r^2 B}\frac{\partial^2 u_\perp}{\partial\phi^2} - \frac{2}{r^2}\frac{\partial u_\phi}{\partial\phi}, \tag{4.9}$$

$$\left(\nabla^2\boldsymbol{u}\right)_\phi = \frac{\partial}{\partial r}\frac{1}{r}\frac{\partial(ru_\phi)}{\partial r} + \frac{1}{r^2}\frac{\partial^2 u_\phi}{\partial\phi^2} + \frac{\partial^2 u_\phi}{\partial z^2} + \frac{2B_z}{r^2 B}\frac{\partial u_\perp}{\partial\phi}, \tag{4.10}$$

$$\left(\nabla^2\boldsymbol{u}\right)_z = -\frac{1}{r}\frac{\partial}{\partial r}r\frac{\partial}{\partial r}\left(\frac{B_r u_\perp}{B}\right) - \frac{B_r}{r^2 B}\frac{\partial^2 u_\perp}{\partial\phi^2} - \frac{\partial^2}{\partial z^2}\left(\frac{B_r u_\perp}{B}\right). \tag{4.11}$$

Now, we note that in the thin tube approximation $B_r = \mathcal{O}(\epsilon B)$, $B_z = B[1 + \mathcal{O}(\epsilon)]$, and the derivative with respect to z is of the order of ϵ times the derivative either with respect to r or ϕ. In addition, viscosity is only important in the vicinity of the ideal resonant position where the gradients of perturbations strongly dominate the gradients of equilibrium quantities (see e.g. Goossens et al. (2011)), which implies that the second derivatives with respect to r and ϕ of $u_\perp$ and u_ϕ strongly dominate all other terms in Equations (4.9)–(4.11). Then, using the relation between $\boldsymbol{u}$ and $\boldsymbol{\xi}$ we obtain the approximate expressions

$$\left(\nabla^2\boldsymbol{u}\right)_\perp = \frac{\partial}{\partial t}\left(\frac{\partial^2\xi_\perp}{\partial r^2} + \frac{1}{r^2}\frac{\partial^2\xi_\perp}{\partial\phi^2}\right), \tag{4.12}$$

$$\left(\nabla^2 \boldsymbol{u}\right)_\phi = \frac{\partial}{\partial t}\left(\frac{\partial^2 \xi_\phi}{\partial r^2} + \frac{1}{r^2}\frac{\partial^2 \xi_\phi}{\partial \phi^2}\right). \tag{4.13}$$

We have already derived the system of equations describing the kink oscillations in a thin non-stationary expanding tube in the approximation of ideal MHD in the presence of flow in Chapter 2 (see Equations (2.73), (2.75) and (2.76)). To obtain the system of equations describing the kink oscillations in thin static expanding tube, assuming the approximation of a viscous MHD, we take all equilibrium quantities in equations derived in Chapter 2 independent of time, the background velocity equal to zero, eliminate the velocity perturbation, and add the terms describing the viscosity force in the momentum equation. Then, we obtain

$$P = -\frac{1}{\mu_0}\left(\frac{B_z}{r}\frac{\partial (rw)}{\partial r} + \frac{B^2}{r}\frac{\partial \xi_\phi}{\partial \phi} - B_r \frac{\partial w}{\partial z}\right), \tag{4.14}$$

$$\frac{\partial^2 w}{\partial t^2} = \frac{B^2}{\rho}\left[B_r \frac{\partial}{\partial z}\left(\frac{P}{B^2}\right) - B_z \frac{\partial}{\partial r}\left(\frac{P}{B^2}\right)\right] + \frac{B}{\mu_0 \rho}\left(rB_r \frac{\partial}{\partial r}\frac{1}{r} + B_z \frac{\partial}{\partial z}\right)$$
$$\left(\frac{B_r}{rB}\frac{\partial (rw)}{\partial r} + \frac{B_z}{B}\frac{\partial w}{\partial z}\right) + \iota \frac{\partial}{\partial t}\left(\frac{\partial^2 w}{\partial r^2} + \frac{1}{r^2}\frac{\partial^2 w}{\partial \phi^2}\right), \tag{4.15}$$

$$\frac{\partial^2 \xi_\phi}{\partial t^2} + \frac{1}{r\rho}\frac{\partial P}{\partial \phi} = \frac{1}{\mu_0 \rho}\left(\frac{B_r}{r}\frac{\partial}{\partial r} r + B_z \frac{\partial}{\partial z}\right)\left(rB_r \frac{\partial}{\partial r}\left(\frac{\xi_\phi}{r}\right) + B_z \frac{\partial \xi_\phi}{\partial z}\right)$$
$$+ \iota \frac{\partial}{\partial t}\left(\frac{\partial^2 \xi_\phi}{\partial r^2} + \frac{1}{r^2}\frac{\partial^2 \xi_\phi}{\partial \phi^2}\right). \tag{4.16}$$

We recall that $w = B\xi_\perp$. We also recall that, since $\nabla \cdot \boldsymbol{B} = 0$, we can express $\boldsymbol{B}$ in terms of the flux function ψ. Similar to Chapter 2 we use ψ as an independent variable instead of r. Then, using the following relations obtained in Chapter 2

$$\frac{\partial f}{\partial r} = rB_z \frac{\partial f}{\partial \psi}, \quad \left.\frac{\partial f}{\partial z}\right|_r = \left.\frac{\partial f}{\partial z}\right|_\psi - rB_r \frac{\partial f}{\partial \psi}, \tag{4.17}$$

where f is any function, and the subscripts r and ψ indicate that a derivative is taken at constant r and ψ, respectively, and assuming that P, $\xi_\perp$, and ξ_ϕ are proportional to $\exp(i\phi - i\omega t)$, we reduce Equations (4.14)–(4.16) to

$$P = -\frac{1}{\mu_0}\left(rB^2 \frac{\partial w}{\partial \psi} + iB^2 \frac{\xi_\phi}{r} - B_r \frac{\partial w}{\partial z} + B_z \frac{w}{r}\right), \tag{4.18}$$

$$\begin{aligned} \omega^2 w &= -\frac{rB^2 B_z}{\mu_0 \rho}\frac{\partial}{\partial z}\left(\frac{B_z}{r^2 B^2}\frac{\partial (rw)}{\partial z}\right) - \frac{B^2}{\rho}\left[B_r \frac{\partial}{\partial z}\left(\frac{P}{B^2}\right)\right. \\ &- \left. rB^2 \frac{\partial}{\partial \psi}\left(\frac{P}{B^2}\right)\right] + i\iota\omega\left(r^2 B_z^2 \frac{\partial^2 w}{\partial \psi^2} - \frac{w}{r^2}\right), \end{aligned} \tag{4.19}$$

$$\omega^2\xi_\phi = \frac{iP}{\rho r} - \frac{B_z}{\mu_0\rho r}\frac{\partial}{\partial z}\left[r^2 B_z \frac{\partial}{\partial z}\left(\frac{\xi_\phi}{r}\right)\right] + i\iota\omega\left(r^2 B_z^2 \frac{\partial^2\xi_\phi}{\partial\psi^2} - \frac{\xi_\phi}{r^2}\right). \tag{4.20}$$

We now consider the terms on the right-hand sides of Equations (4.19) and (4.20) that are proportional to ι. The second term in the brackets is of the order of ξ_ϕ/R_*^2 while the first term is of the order of ξ_ϕ divided by the characteristic spatial scale in the vicinity of the ideal resonant position squared. Since this characteristic spatial scale is much smaller than R_* we can neglect the second term in these brackets. Taking into account that the characteristic scale in the z-direction is $R_* = \epsilon L$ similarly to Chapter 2 we introduce the stretching variable $Z = \epsilon z$. We also introduce the scaled frequency $\Omega = \epsilon^{-1}\omega$, scaled magnetic pressure perturbation $Q = \epsilon^{-2}P/B^2$, and scaled viscosity $\bar{\iota} = \epsilon^{-1}\iota$. Then we use the scaled variables to transform Equations (4.18)–(4.20) and only keep leading terms with respect to ϵ. As a result we obtain

$$\xi_\phi = ir^2\frac{\partial w}{\partial\psi} + \frac{iw}{B}, \tag{4.21}$$

$$\Omega^2 w = \frac{rB^4}{\rho}\frac{\partial Q}{\partial\psi} - \frac{rB^3}{\mu_0\rho}\frac{\partial}{\partial Z}\left(\frac{1}{r^2B}\frac{\partial(rw)}{\partial Z}\right) + i\bar{\iota}\Omega r^2 B^2\frac{\partial^2 w}{\partial\psi^2}, \tag{4.22}$$

$$\Omega^2\xi_\phi = \frac{iB^2Q}{\rho r} - \frac{B}{\mu_0\rho r}\frac{\partial}{\partial Z}\left[r^2 B\frac{\partial}{\partial Z}\left(\frac{\xi_\phi}{r}\right)\right] + i\bar{\iota}\Omega r^2 B^2\frac{\partial^2\xi_\phi}{\partial\psi^2}. \tag{4.23}$$

Substituting r for f in the first relation in Equation (4.17) we obtain

$$rB\frac{\partial r}{\partial\psi} = 1, \tag{4.24}$$

where we substituted B for B_z. Using this result we transform Equation (4.21) to

$$\xi_\phi = ir\frac{\partial(rw)}{\partial\psi}. \tag{4.25}$$

4.2.2 Solution outside the dissipative layer

Since the Alfvén speed in the core region is almost independent of the radial direction, the magnetic field lines frozen in the dense plasma at $z = \pm L/2$ oscillate with the same frequency. The same is true for the magnetic field lines outside the magnetic tube. However there is strong density variation in the transition layer, which implies that there is also strong variation of the Alvén speed. This means that the oscillation frequency of magnetic field lines in the transitional layer depends on ψ. If this oscillation frequency coincides with the frequency of a kink oscillation at a particular magnetic surface then at this surface there is resonance between the global kink oscillation and the local Alfvén oscillations of magnetic field lines. In a weakly dissipative plasma there are large gradients of perturbations in the vicinity of the resonant surface, and the size of this vicinity is much smaller than lR_*. Dissipation is only important in a thin dissipative layer surrounding the resonant position. This observation suggests a method of solving problems involving resonant interaction of MHD waves. In this method the

wave motion is described by the dissipative MHD equations in the dissipative layer and by the ideal MHD equations at the two sides of this layer. Then the solutions are matched in the two overlap regions.

We calculate δP and $\delta\eta$ in the leading order approximation with respect to l. In accordance with this, we substitute Q_i for Q in Equation (4.23), where Q_i is the value of Q calculated at $\psi = \psi_i$. Now substituting Equation (4.25) in Equation (4.23) and taking into account that $BR^2 = \text{const}$ we obtain

$$V_A^2 \frac{\partial^2 W}{\partial Z^2} + \Omega^2 W - i\bar{\imath}\Omega R^2 B^2 \frac{\partial^2 W}{\partial \psi^2} = \frac{\mu_0 V_A^2 Q_i}{R^2}, \tag{4.26}$$

where

$$W = \frac{\partial (rw)}{\partial \psi}, \quad V_A^2 = \frac{B^2}{\mu_0 \rho}. \tag{4.27}$$

We then consider the Sturm-Liouville problem

$$V_A^2 \frac{\partial^2 Y}{\partial Z^2} = -\lambda Y, \quad Y(\pm \widetilde{L}/2) = 0, \tag{4.28}$$

where $\widetilde{L} = \epsilon L$. The eigenvalues of this problem are real and constitute a monotonically increasing sequence $\{\lambda_n\}$, $\lambda_n \to \infty$ as $n \to \infty$ (Coddington and Levinson, 1955). It is straightforward to show that all eigenvalues are positive. Any integrable by quadrature in the interval $[-\widetilde{L}/2, \widetilde{L}/2]$ function $f(z)$ can be expanded in the generalised Fourier series

$$f(Z) = \sum_{n=1}^{\infty} f_n Y_n(Z), \tag{4.29}$$

where $Y_n(z)$ is the eigenfunction corresponding to the eigenvalue λ_n. Obviously, we can choose all eigenfunctions to be real. If $f(z)$ has the continuous second derivative and satisfies the boundary condition $f(\pm\widetilde{L}/2) = 0$, then the series in Equation (4.29) convergences uniformly and can be differentiated twice. The eigenfunctions satisfy the orthogonality condition

$$\int_{-L/2}^{L/2} V_A^{-2}(Z) Y_n(Z) Y_m(Z)\, dZ = 0 \quad \text{for} \quad m \neq n. \tag{4.30}$$

Dymova and Ruderman (2006a) assumed that the density is factorised and equal to a product of two functions, one depending on r and the other on z. They called this the condition of homogeneous stratification. We, similarly, assume that the density in the transitional layer can be factorised and expressed as a product of two functions, one depending on z and the other on ψ. Since we neglect the radial dependence of $\boldsymbol{B}$ this implies that the Alfvén speed can be written as

$$V_A^2(\psi, Z) = V_{Ai}^2(Z) g(\psi), \quad g(\psi_i) = 1, \quad g(\psi_e) = \frac{V_{Ae}^2}{V_{Ai}^2}, \tag{4.31}$$

where $g(\psi) = \text{const}$ for $\psi \leq \psi_i$ and $\psi \geq \psi_e$, while $g(\psi)$ is a monotonically increasing function in $\psi \in (\psi_i, \psi_e)$, V_{Ai} and V_{Ae} are the values of the Alfvén speed at $\psi = \psi_i$

and $\psi = \psi_e$, respectively, and $\psi = \psi_e$ is the equation of the external boundary of the transitional layer. Then we can rewrite Equations (4.28) as

$$V_{Ai}^2 \frac{\partial^2 Y}{\partial Z^2} = -\frac{\lambda}{g(\psi)} Y, \quad Y(\pm \widetilde{L}/2) = 0. \tag{4.32}$$

It follows from this equation that

$$\lambda_n(\psi) = g(\psi)\lambda_n(\psi_i). \tag{4.33}$$

We normalise the eigenfunctions by the condition

$$\int_{-\widetilde{L}/2}^{\widetilde{L}/2} V_{Ai}^{-2} Y_n^2(Z)\, dZ = 1. \tag{4.34}$$

Then the Fourier coefficients in Equation (4.29) are given by

$$f_n = \int_{-L/2}^{L/2} V_{Ai}^{-2}(Z) f(Z) Y_n(Z)\, dZ. \tag{4.35}$$

Below, we will see that the ratio of the imaginary and real part of Ω is of the order of $l \ll 1$. This enables us to look for Ω in the form $\Omega_0 + l\Omega_1$, where Ω_0 and Ω_1 are of the same order. In Equation (4.26) we keep terms of the order of one and l, while we neglect smaller terms. Hence, we write $\Omega^2 \approx \Omega_0^2 + 2l\Omega_0\Omega_1$. The last term on the left-hand side of Equation (4.26) is calculated in the leading order approximation. Next, we take $\bar{\iota}\Omega_0 r^2 B^2 \approx \bar{\iota}\Omega_0 R^2 B^2$. Since the viscosity is only used to remove the singularity at the ideal resonant surface, we can choose the z-dependence of ι arbitrarily. It is convenient to assume that ιB is independent of z. Then it follows from Equation (4.3) that the coefficient at the second derivative with respect to ψ in Equation (4.26) is independent of Z. Now, substituting the expansions

$$W(\psi, Z) = \sum_{n=1}^{\infty} W_n(\psi) Y_n(Z), \quad \frac{V_{Ai}^2 Q_i}{R^2} = \sum_{n=1}^{\infty} \Phi_n Y_n(Z) \tag{4.36}$$

in (4.26) yields

$$[\Omega_0^2 + 2l\Omega_0\Omega_1 - \lambda_n(\psi)] W_n - i\bar{\iota}\Omega_0 B^2 R^2 \frac{d^2 W_n}{d\psi^2} = \mu_0 \Phi_n g(\psi). \tag{4.37}$$

The resonant surfaces are defined by the equation

$$\lambda_n(\psi) = \Omega_0^2. \tag{4.38}$$

There is the Alfvén resonance at any surface defined by this equation. Below, we assume that the intervals $(\lambda_n(\psi_i), \lambda_n(\psi_e))$ do not overlap and Ω_0^2 is in one of these intervals. Let it be in the interval with $n = N$. Then there is exactly one value of ψ satisfying Equation (4.38) which we denote as ψ_A. The last term on the left-hand side

of Equation (4.37) is only important in a dissipative layer surrounding the resonant magnetic surface. The thickness of this layer is much smaller than lR_*. Outside of this layer we can neglect the last term on the left-hand side of Equation (4.37). We also can neglect $2l\Omega_0\Omega_1$ in comparison with Ω_0^2. Then we obtain

$$W_n = \frac{\mu_0 \Phi_n g(\psi)}{\Omega_0^2 - \lambda_n(\psi)}. \tag{4.39}$$

Since there is no Alfvén resonance when $n \neq N$ this equation is valid in the entire transition layer when $n \neq N$. Then using Eq. (4.27) and substituting $R(z)$ for r yields

$$(Rw)_n = \begin{cases} (Rw)_{ni} + \mu_0 \Phi_n \displaystyle\int_{\psi_i}^{\psi} \frac{g(\psi')\, d\psi'}{\Omega_0^2 - \lambda_n(\psi')}, & \psi < \psi_A, \\ (Rw)_{ne} - \mu_0 \Phi_n \displaystyle\int_{\psi}^{\psi_e} \frac{g(\psi')\, d\psi'}{\Omega_0^2 - \lambda_n(\psi')}, & \psi > \psi_A. \end{cases} \tag{4.40}$$

We see that there is a non-integrable singularity in the integrals when at $\psi = \psi_A$ when $n = N$. Substituting $R(z)$ for r in Equation (4.22), and using Equations (4.3) and (4.28) we obtain

$$\frac{\partial Q}{\partial \psi} = \frac{\rho}{R^2 B^4} \sum_{n=1}^{\infty} [\Omega_0^2 - \lambda_n(\psi)](Rw)_n. \tag{4.41}$$

We see that, in contrast to w, Q does not have a singularity at $\psi = \psi_A$.

4.2.3 Connection formulae

As we have seen, the solution to the ideal linear MHD equations has a singularity at $\psi = \psi_A$. Near this surface there are large gradients, which implies that the viscosity becomes important in a thin dissipative layer embracing the magnetic surface $\psi = \psi_A$. If we are not interested in the motion in the dissipative layer, then all what we need from the dissipative solution are the jumps of the total pressure and the normal component of the plasma displacement across this dissipative layer. Sakurai et al. (1991) suggested to call the expressions giving these jumps the connection formulae. They found, for a static system, the solution of the dissipative MHD equations in terms of Bessel functions and obtained the connection formulae for driven problem where the system oscillations are driven by an external source and the system oscillates with the constant amplitude. Later, Goossens et al. (1995) obtained the solution in the dissipative layer in terms of so-called F and G functions. Erdélyi et al. (2001) generalised the connection formulae for steady dissipative systems. Goossens et al. (1992) used the connection formulae to study the damping of magnetic tube kink oscillations. In this study it was assumed that the viscosity is not very weak in the sense that the last term on the left-hand side of Equation (4.37) dominates the term proportional to Ω_1, so the latter can be neglected. Ruderman et al. (1995) showed that when this is not the case the type of solution in the dissipative layer changes substantially and it becomes strongly oscillatory. Ruderman et al. (1995) studied a planar problem. Tirry and Goossens (1996) generalised this

study to the cylindrical geometry. Since the thickness of the dissipative layer is much smaller than that of the transitional layer, the variation of $\lambda_N(\psi)$ in the dissipative layer is small and it can be approximated by the first two terms of the Taylor expansion:

$$\lambda_N(\psi) \approx \Omega_0^2 - \Delta(\psi - \psi_A), \quad \Delta = -\left.\frac{d\lambda_N}{d\psi}\right|_{\psi=\psi_A}. \tag{4.42}$$

Using this equation and introducing the dimensionless quantities τ and Λ defined by

$$\tau = \frac{\psi - \psi_A}{\delta_A}, \quad \Lambda = \frac{2il\Omega_0\Omega_1}{\delta_A}, \quad \delta_A = \left(\frac{\bar{\iota}\Omega_0 B^2 R^2}{|\Delta|}\right)^{1/3}, \tag{4.43}$$

we reduce Equation (4.37) with $n = N$ to

$$\frac{d^2 W_N}{d\tau^2} + [i\,\mathrm{sign}(\Delta) + \Lambda] W_N = \frac{i\mu_0 \Phi_N g(\psi_A)}{\delta_A |\Delta|}. \tag{4.44}$$

This equation can be obtained from Equation (A1) in Tirry and Goossens (1996) by substituting W_N for Ψ, $-\Lambda$ for Λ, and $-\mu_0\Phi_N/\delta_A|\Delta|$ for right hand side in the latter. Then we obtain the solution to Equation (4.44) making the same substitution in Equation (A4) in Tirry and Goossens (1996). This yields

$$W_N = -\frac{i\mu_0 \Phi_N g(\psi_A)}{\delta_A |\Delta|}\, F_\Lambda(\tau), \tag{4.45}$$

where

$$F_\Lambda(\tau) = \int_0^\infty \exp\left(i\sigma\tau\,\mathrm{sign}(\Delta) - \tfrac{1}{3}\sigma^3 + \Lambda\sigma\right) d\sigma. \tag{4.46}$$

Further, using Equations (4.27), (4.45), and (4.46), the relations $\eta = \xi_\perp/R$ and $w = B\xi_\perp$, and substituting R for r we obtain

$$\frac{d\eta_N}{d\tau} = -\frac{i\mu_0 \Phi_N g(\psi_A)}{|\Delta| B R^2}\, F_\Lambda(\tau). \tag{4.47}$$

Integrating this equation yields

$$\eta_N = -\frac{\mu_0 \Phi_N g(\psi_A)}{\Delta B R^2}\, G_\Lambda(\tau) + C, \tag{4.48}$$

where C is an arbitrary constant and

$$G_\Lambda(\tau) = \int_0^\infty \frac{e^{-\sigma^3/3}}{\sigma} \left[\exp(i\sigma\tau\,\mathrm{sign}(\Delta) + \Lambda\sigma) - 1\right] d\sigma. \tag{4.49}$$

The function F_Λ and G_Λ were introduced by Goossens et al. (2011). When $\Lambda = 0$ they coincide with the F and G functions, respectively. We defined the jump of function $f(\tau)$ through the dissipative layer as

$$[f(\tau)] = \lim_{\tau\to\infty} [f(\tau) - f(-\tau)]. \tag{4.50}$$

Using the substitution $\sigma\tau = \varsigma$, we obtain

$$\begin{aligned}[G_\Lambda(\tau)] &= 2i\,\mathrm{sign}(\Delta)\lim_{\tau\to\infty}\int_0^\infty \exp\left(\frac{\Lambda\varsigma}{\tau} - \frac{\varsigma^3}{3\tau^3}\right)\frac{\sin\varsigma}{\varsigma}\,d\varsigma \\ &= 2i\,\mathrm{sign}(\Delta)\int_0^\infty \frac{\sin\varsigma}{\varsigma}\,d\varsigma = \pi i\,\mathrm{sign}(\Delta). \end{aligned} \tag{4.51}$$

Then using the expansion of η in the Fourier series and Equation (4.48), and taking into account that $[\eta_n] = 0$ for $n \neq N$, we finally arrive at

$$[\eta(\tau)] = -\frac{\pi i\mu_0\Phi_N g(\psi_A)}{|\Delta|BR^2}\,Y_N(Z). \tag{4.52}$$

It follows from Equation (4.41) that $[Q] = 0$.

4.2.4 Matching solutions

To calculate $\delta\eta$ and δP we need to match the internal solution, which is the solution in the dissipative layer, and the external solution, which is the solution outside the dissipative layer, in two overlap regions at the left and right of the dissipative layer. In these overlap regions both solutions are valid. In accordance with the method of matched asymptotic expansions (e.g. Bender and Orszag, 1978) the jump of function $f(\psi)$ across the dissipative layer can be calculated using the external solution as

$$[f(\psi)] = \lim_{\varepsilon\to+0}[f(\psi_A+\varepsilon) - f(\psi_A-\varepsilon)]. \tag{4.53}$$

Using the relation $Rw = BR^2\eta$ and recalling that $BR^2 = \mathrm{const}$, we obtain $(Rw)_n = BR^2\eta_n$. Then it follows from Equations (4.40) and (4.53) that

$$[\eta] = \delta\eta - \frac{\mu_0}{BR^2}\,\mathcal{P}\int_{\psi_i}^{\psi_e}\sum_{n=1}^{\infty}\frac{\Phi_n g(\psi)Y_n(Z)}{\Omega_0^2 - \lambda_n(\psi)}\,d\psi, \tag{4.54}$$

where $\mathcal{P}$ indicates the Cauchy principal part of the integral. Comparing Equations (4.52) and (4.54) yields

$$\delta\eta = \frac{\mu_0}{BR^2}\,\mathcal{P}\int_{\psi_i}^{\psi_e}\sum_{n=1}^{\infty}\frac{\Phi_n g(\psi)Y_n(Z)}{\Omega_0^2 - \lambda_n(\psi)}\,d\psi - \frac{\pi i\mu_0\Phi_N g(\psi_A)}{|\Delta|BR^2}Y_N(Z). \tag{4.55}$$

To calculate δQ we use Equation (4.22). In the transitional layer we can take $r \approx R(z)$. We also can neglect the derivative of r with respect to ψ because the ratio its characteristic variation scale with respect to ψ to the characteristic scale of variation of w, P, and ξ_ϕ with respect to ψ is R_*/l. Then, using Equation (4.3) we obtain from Equation (4.22)

$$\frac{\partial Q}{\partial\psi} = \mathcal{M}[Rw], \tag{4.56}$$

where

$$\mathcal{M}[Rw] = \left(\frac{\rho\Omega^2}{R^2B^4} + \frac{1}{\mu_0 R^2 B^2}\frac{\partial^2}{\partial Z^2} - \frac{i\rho\bar{\iota}\Omega}{B^2}\frac{\partial^2}{\partial\psi^2} \right) Rw. \tag{4.57}$$

We can use the expansion $Rw = \sum_{n=1}^{\infty}(Rw)_n Y_n$. Since the variation of w in the transitional layer is of the order of lw, it follows that $(Rw)_n = (Rw)_{ni}[1+\mathcal{O}(l)]$. It also immediately follows from this relation that $\mathcal{M}[(Rw)_n Y_n] = \mathcal{M}[(Rw)_{ni}Y_n][1+\mathcal{O}(l)]$ for all n except $n = N$. The problem is that, although the expression for $(Rw)_N$ obtained in the approximation of ideal MHD has only a logarithmic singularity at $\psi = \psi_A$, the second derivative of $(Rw)_n$ with respect to ψ has a singularity of the form $(\psi = \psi_A)^{-2}$. Hence, in principle, $\mathcal{M}[Rw]$ can be significantly different from $\mathcal{M}[(Rw)_i]$. However, in fact, this is not the case. The straightforward calculation using Equations (4.28), (4.43), (4.48) and (4.49) shows that $\mathcal{M}[Rw] = 0$ in the dissipative layer. As a result, we can now write that $\mathcal{M}[Rw] = \mathcal{M}[(Rw)_i][1+\mathcal{O}(l)]$.

In Chapter 2 we showed that P/ψ is independent of ψ in the core region of the tube defined by the inequality $r \le R(1-l/2)$. It follows from this result that in the core region $Q = Q_i(\psi/\psi_i)$. Using this expression we obtain from Equation (4.22) that $(\mathcal{M}[Rw])_i = Q_i/\psi_i$, and consequently

$$\mathcal{M}[Rw] = \left(\frac{Q_i}{\psi_i} - \frac{(\rho_i-\rho)\Omega^2 w_i}{RB^4} \right)[1+\mathcal{O}(l)]. \tag{4.58}$$

Substituting this result in Equation (4.56), integrating the obtained equation, and using the relation $w = BR\eta$ yields in the leading order approximation with respect to l

$$\delta Q = \int_{\psi_i}^{\psi_e} \left(\frac{Q_i}{\psi_i} - \frac{(\rho_i-\rho)\Omega^2\eta}{B^3} \right) d\psi. \tag{4.59}$$

Equations (4.55) and (4.59) enable us to calculate jumps $\delta\eta$ and δQ in terms of η. Thus, we finally closed the system of governing equations (4.1) and (4.2) and are able to proceed with theoretical analysis.

§ 4.3 Calculation of the eigenmode decrement

Taking η, $\delta\eta$, and δP proportional to $e^{-i\omega t}$ and only keeping terms of the order of unity and l we transform Equations (4.1) and (2.73) to

$$C_k^2\frac{d^2\eta}{dZ^2} + \Omega^2\eta = -\mathcal{L}, \tag{4.60}$$

$$\mathcal{L} = \frac{1}{\rho_i+\rho_e}\left(\frac{B^2}{R^2}\delta Q + \frac{B^2}{\mu_0}\frac{d^2(l\eta+\delta\eta)}{dZ^2} + \rho_e\Omega_0^2(l\eta+\delta\eta) \right). \tag{4.61}$$

Recall that in these equations η calculated in the tube core region where it is independent of ψ. Using Equations (3.39), (4.28), (4.55), and (4.59) we obtain

$$\mathcal{L} = \mathcal{L}_1 + \frac{\pi i\mu_0(\rho_i-\rho_e)\Omega_0^2\Phi_N g(\psi_A)Y_N(Z)}{|\Delta|BR^2(\rho_i+\rho_e)}, \tag{4.62}$$

where

$$\begin{aligned}\mathcal{L}_1 &= \frac{\mu_0\rho_e}{BR^2(\rho_i+\rho_e)}\mathcal{P}\int_{\psi_i}^{\psi_e} g(\psi)\sum_{n=1}^{\infty}\frac{[\Omega_0^2-\lambda_n(\psi_e)]\Phi_n Y_n(Z)}{\Omega_0^2-\lambda_n(\psi)}\,d\psi \\ &+ \frac{2lB^2Q_i}{R^2(\rho_i+\rho_e)}+\frac{\Omega_0^2\eta}{\rho_i+\rho_e}\left(\frac{1}{BR^2}\int_{\psi_i}^{\psi_e}\rho\,d\psi - l(3\rho_i-\rho_e)\right). \qquad (4.63)\end{aligned}$$

Now, we substitute $\Omega = \Omega_0 + l\Omega_1$ in Equation (4.60) and then look for a solution to Equations (4.60) and (4.61) in the form

$$\eta = \eta_0 + l\eta_1 + \ldots \qquad (4.64)$$

Taking into account that $\mathcal{L} = \mathcal{O}(l)$ we obtain in the leading order approximation

$$C_k^2\frac{d^2\eta_0}{dZ^2}+\Omega_0^2\eta_0 = 0, \quad \eta_0 = 0 \ \text{ at } \ Z = \pm\widetilde{L}/2. \qquad (4.65)$$

We see that η must be an eigenfunction of the boundary value problem Equation (4.65) and Ω_0^2 the corresponding eigenvalue. Obviously, we can take η_0 to be real.

In the next order approximation we obtain

$$\begin{aligned}\frac{d^2\eta_1}{dZ^2} &+ \frac{\Omega_0^2}{C_k^2}\eta_1 = -\frac{\pi i\mu_0^2(\rho_i-\rho_e)\Omega_0^2\Phi_N g(\psi_A)Y_N(Z)}{2|\Delta|B^3R^2} \\ &- \frac{\mathcal{L}_1+2\Omega_0\Omega_1\eta_0}{C_k^2}, \quad \eta_1 = 0 \ \text{ at } \ Z = \pm\widetilde{L}/2. \qquad (4.66)\end{aligned}$$

This boundary layer problem only has solutions if its right-hand side satisfies the compatibility condition. To obtain this condition, we multiply Equation (4.66) by η_0, integrate the obtained equation, use the integration by parts, and use the boundary conditions. As a result, we obtain

$$\begin{aligned}\Omega_0\Omega_1 &\int_{-\widetilde{L}/2}^{\widetilde{L}/2}\frac{\eta_0^2}{C_k^2}\,dZ = -\frac{1}{l}\int_{-\widetilde{L}/2}^{\widetilde{L}/2}\frac{\mathcal{L}_1\eta_0}{2C_k^2}\,dZ \\ &- \frac{\pi i\mu_0^2\Omega_0^2\Phi_N g(\psi_A)}{4l|\Delta|BR^2}\int_{-\widetilde{L}/2}^{\widetilde{L}/2}\frac{(\rho_i-\rho_e)Y_N\eta_0}{B^2}\,dZ\,. \qquad (4.67)\end{aligned}$$

We write $\Omega_1 = \Omega_{1r} - i\Gamma$, where both Ω_{1r} and Γ are real quantities. Ω_{1r} only gives a small correction to the oscillation frequency Ω_0, while Γ determines the oscillation damping rate. Below, we mainly are interested in Γ, which is defined by

$$\Gamma = \frac{\pi\mu_0^2\Omega_0\Phi_N g(\psi_A)}{4l|\Delta|BR^2}\left(\int_{-\widetilde{L}/2}^{\widetilde{L}/2}\frac{\eta_0^2}{C_k^2}\,dZ\right)^{-1}\int_{-\widetilde{L}/2}^{\widetilde{L}/2}\frac{(\rho_i-\rho_e)Y_N\eta_0}{B^2}\,dZ\,. \qquad (4.68)$$

We note that Γ is the scaled decrement, while non-scaled decrement is $\gamma = \epsilon l\Gamma$.

Using Equation (4.31) we transform Equation (4.65) to

$$V_{Ai}^2 \frac{d^2\eta_0}{dZ^2} = -\chi^{-1}\Omega_0^2\eta_0, \quad \chi = \frac{2g(\psi_e)}{1+g(\psi_e)}. \tag{4.69}$$

Comparing Equations (4.32) and (4.69) we conclude that $\chi^{-1}\Omega_0^2 = \lambda_n(\psi_i)$ and η_0 is proportional to $Y_n(Z)$ for some n. To have the proper dimension of η we take $\eta_0 = \widetilde{L}^{-1/2}\Omega_0^{-1}Y_n(Z)$. Since $1 < \chi < g(\psi_e)$, it follows that $\Omega_0^2 \in (\lambda_n(\psi_i), \lambda_n(\psi_e))$. Then the condition that $\Omega_0^2 \in (\lambda_N(\psi_i), \lambda_N(\psi_e))$ implies that $n = N$ and we obtain $\Omega_0^2 = \chi\lambda_N(\psi_i)$ and $\eta_0 = \widetilde{L}^{-1/2}\Omega_0^{-1}Y_N(Z)$. Using this result and Equations (3.39), (4.31), and (4.34) we obtain

$$\begin{aligned} \int_{-\widetilde{L}/2}^{\widetilde{L}/2} \frac{\eta_0^2}{C_k^2}\, dZ &= \frac{1}{\chi\widetilde{L}\Omega_0^2}, \\ \mu_0 \int_{-\widetilde{L}/2}^{\widetilde{L}/2} \frac{(\rho_i-\rho_e)Y_N\eta_0}{B^2}\, dZ &= \frac{2(\chi-1)}{\chi\Omega_0\widetilde{L}^{1/2}}. \end{aligned} \tag{4.70}$$

Using Equations (4.57) and (4.58) and the relation $Rw_i = BR^2\eta_0$ we obtain in the leading order approximation

$$Q_i = \frac{\rho_i\psi_i}{B^3}\big[\Omega_0^2 - \lambda_N(\psi_i)\big]\eta_0. \tag{4.71}$$

Then we obtain with the aid of Equations (4.34)–(4.36)

$$\begin{aligned} \Phi_N = \int_{-\widetilde{L}/2}^{\widetilde{L}/2} \frac{Q_iY_N}{R^2}\, dZ &= \frac{\psi_i\big[\Omega_0^2 - \lambda_N(\psi_i)\big]}{\mu_0\Omega_0\widetilde{L}^{1/2}BR^2} \int_{-\widetilde{L}/2}^{\widetilde{L}/2} \frac{Y_N^2}{V_{Ai}^2}\, dZ \\ &= \frac{\psi_i\big[\Omega_0^2 - \lambda_N(\psi_i)\big]}{\mu_0\Omega_0\widetilde{L}^{1/2}BR^2}. \end{aligned} \tag{4.72}$$

Substituting Equations (4.70) and (4.72) in Equation (4.68) and recalling that $\gamma = \epsilon l\Gamma$ and $\omega_0 = \epsilon\Omega_0$ we reduce this equation to

$$\frac{\gamma}{\omega_0} = \frac{\pi\psi_i\lambda_N(\psi_i)g(\psi_A)(\chi-1)[g(\psi_A)-1]}{2|\Delta|B^2R^4}. \tag{4.73}$$

In Chapter 2 we have shown that in the approximation of thin tube $\psi = \frac{1}{2}r^2B$. It follows from this relation that $\psi_i \approx \frac{1}{2}R^2B$. In addition, it follows from Equations (4.31), (4.33), and (4.42) that $\Delta = -\lambda_N(\psi_i)g'(\psi_A)$, where the prime indicates the derivative. It follows from Equations (4.33) and (4.38), and from the relation $\Omega_0^2 = \chi\lambda_N(\psi_i)$ that ψ_A is defined by

$$g(\psi_A) = \chi. \tag{4.74}$$

Then we can simplify Equation (4.73) to

$$\frac{\gamma}{\omega_0} = \frac{\pi\chi(\chi-1)^2}{4g'(\psi_A)BR^2}. \tag{4.75}$$

It is straightforward to verify that this expression coincides with the corresponding expression in Dymova and Ruderman (2006a) (see their Equation (83)).

Now, we can notice that, while to calculate ω_0 and γ we need to define $V_{Ai}(z)$, the ratio γ/ω_0 is independent of a particular form of this function. The ratio γ/ω_0 is also independent of the number of mode N. We recall that this result was obtained under the assumption of homogeneous stratification. It is a generalisation of a similar result previously obtained by Dymova and Ruderman (2006a) for non-expanding magnetic tubes.

As a example, we consider the linear density variation in the transitional layer and take

$$\rho_t(r,z) = \frac{\rho_i + \rho_e}{2} + (\rho_i - \rho_e)\frac{R-r}{lR}. \tag{4.76}$$

Using the relation $\psi = \frac{1}{2}Br^2$, we obtain

$$r = R\left(1 - \frac{l}{2}\right) + \frac{\psi - \psi_i}{lBR} + \mathcal{O}\big(l^2\big). \tag{4.77}$$

It follows from Equations (4.31), (4.76), and (4.77) that

$$\frac{1}{g(\psi)} = 1 - \frac{(\rho_i - \rho_e)(\psi - \psi_i)}{\rho_i(\psi_e - \psi_i)} + \mathcal{O}(l). \tag{4.78}$$

Using this equation and Equation (4.69), we obtain

$$\chi = \frac{2\rho_i}{\rho_i + \rho_e} + \mathcal{O}(l). \tag{4.79}$$

Then it follows from Equation (4.74) that

$$\psi_A = \frac{\psi_i + \psi_e}{2} + \mathcal{O}(l). \tag{4.80}$$

Using Equations (4.78) and (4.80), we obtain in the leading order approximation with respect to l

$$g'(\psi_A) = \frac{4\rho_i(\rho_i - \rho_e)}{(\rho_i + \rho_e)^2(\psi_e - \psi_i)} = \frac{4\rho_i(\rho_i - \rho_e)}{lBR^2(\rho_i + \rho_e)^2}. \tag{4.81}$$

When deriving this expression we used the relation $\psi = \frac{1}{2}r^2B$. Substituting this expression in Equation (4.75) and using Equation (4.79) yields

$$\frac{\gamma}{\omega_0} = \frac{\pi l(\zeta - 1)}{8(\zeta + 1)}, \tag{4.82}$$

where $\zeta = \rho_i/\rho_e$. This expression coincides with that obtained for a non-expanding tube with the density non-varying along the tube (e.g. Goossens et al., 2002). We repeat that, in accordance with the homogeneous stratification assumption $\rho_i/\rho_e = \text{const}$, the ratio of the decrement to the frequency is independent of a particular law of the density variation along the tube.

§ 4.4 Summary

We summarise results of Chapter 4 in what follows. First of all we slightly amended the equilibrium configuration proposed in Chapter 2, by neglecting a field-aligned background flow. Thus we modified the governing equations. Then we assumed approximation of a viscous MHD in the transitional layer. Using it we derived set of equations describing kink oscillations. Then, by the means of general Fourier series, and in accordance with homogeneous stratification assumption $\rho_i/\rho_e = \text{const}$ we obtained the connection formulae and jumps of δP and $\delta\eta$. As a result, we closed the system of governing equations. Thus, we gained ability to proceed with theoretical results.

Further, employing the closed system of governing equations we obtained the decrement of kink oscillations. We concluded that the ratio of the decrement γ on the oscillation frequency ω_0 is independent of number of mode N. We also obtained that the ratio of the kink oscillation decrement to the oscillation frequency is independent of a particular law of the density variation along the tube as well as the tube cross-section variation along the tube. This conclusion is particularly important for coronal seismology observations. Since this result allows us to neglect coronal loops expansions and density variation along the loops to get information about the radial structure of the loops, by observing damping of kink oscillations.

Chapter 5

Resonant Damping of Kink Oscillation in the Presence of Background Flow

§ 5.1 Equilibrium Configuration

In this chapter we use the equilibrium configuration proposed in Chapter 2. We recall that we consider kink oscillations of a thin straight magnetic flux tube with circular cross-section. The cross-section radius varies along the tube. The tube consists of a core region where the plasma density only weakly varies in the radial direction, and the transitional region where the density quickly decreases from its value in the core region to that in the external plasma. The sketch of unperturbed configuration is shown in Figure 2.1.

§ 5.2 Kink oscillations of coronal loops with slowly varying density

5.2.1 The WKB approximation

In this section we study kink oscillations of a magnetic flux tube with the variable cross-section and slowly varying density. Similarly to Chapters 3 and 4 we assume that the resonant damping is weak and the damping time is much larger than the oscillation period. Since the ratio of the oscillation period to the damping time is of the order of l (e.g. Hollweg and Yang, 1988; Goossens et al., 1992; Ruderman and Roberts, 2002; Shukhobodskiy and Ruderman, 2018) we assume that $l \ll 1$.

We aim to study the competition between the oscillation amplification due to cooling and damping due to resonant absorption. The oscillation amplification occurs on the time-scale comparable to the characteristic time $t_{\rm ch}$ of the density variation (Ruderman, 2011a; Ruderman et al., 2017). We assume that the characteristic time of the amplitude variation is comparable to the damping time and take $t_{\rm ch}$ equal to l^{-1} times the characteristic wave period. In accordance with this estimate we introduce the "slow" time $t_1 = lt$.

Now, we follow Chapter 3 and use the WKB method to seek the solution to the problem. In accordance with this method we write

$$\eta = S(t_1, z)\exp[il^{-1}\Theta(t_1)]. \tag{5.1}$$

Then we expand S in the series

$$S = S_0 + lS_1 + \ldots \tag{5.2}$$

We have the estimate $\delta P \sim lP$. In accordance with these estimates we introduce the scaled jump of the magnetic pressure perturbation $\widetilde{\delta P} = l^{-1}\,\delta P$. We also have the estimate $\delta\eta \sim l\eta$. Since $\delta\eta = \delta S e^{il^{-1}\Theta}$, this estimate inspires us to introduce $\widetilde{\delta S} = l^{-1}\delta S$. Finally, it follows from Equation (2.50) that $U \sim l$, so we introduce the scaled velocity $\tilde{U} = l^{-1}U$. Now, substituting Equation (5.1) in Equations (2.75) and (2.76) we obtain

$$\begin{aligned}&(\rho_i+\rho_e)\left[S\omega^2 - il\left(2\omega\frac{\partial S}{\partial t_1} + S\frac{\partial \Omega}{\partial t_1}\right)\right]\\ &-\frac{2il\omega}{R}(\rho_i\tilde{U}_i+\rho_e\tilde{U}_e)\frac{\partial (RS)}{\partial z} + \frac{2\tilde{B}^2}{\mu_0}\frac{\partial^2 S}{\partial z^2} = -l\widetilde{\mathcal{L}} + \mathcal{O}\big(l^2\big),\end{aligned} \tag{5.3}$$

$$\widetilde{\mathcal{L}} = \left(\rho_e\omega^2 + \frac{B^2}{\mu_0}\frac{\partial^2}{\partial z^2}\right)\left(S + \widetilde{\delta S}\right) + \frac{\widetilde{\delta P}}{R^2}e^{-il^{-1}\Theta}, \tag{5.4}$$

where $\omega = d\Theta/dt_1$.

Substituting Equation (5.2) in Equation (5.3) and collecting terms of order of unity (for more details see Appendix B) yields

$$\frac{\partial^2 S_0}{\partial z^2} + \frac{\omega^2}{C_k^2}S_0 = 0, \quad C_k^2 = \frac{2B^2}{\mu_0(\rho_i + \rho_e)}. \tag{5.5}$$

This approximation is called the approximation of geometric optics. The same approximation was also used in Chapters 3 and 4. Since we assume that the tube ends are frozen in the dense photosphere, we impose the boundary conditions $\eta = 0$ at $z = \pm L/2$. Then we obtain

$$S_0 = 0 \quad \text{at} \quad z = \pm L/2.. \tag{5.6}$$

Equations (5.5) and (5.6) constitute the Sturm-Liouville problem for function S_0. This problem coincides with the boundary value problem obtained by Dymova and Ruderman (2005) for kink oscillations of a magnetic tube with the density varying along the tube that is in a static equilibrium. This particular Sturm-Liouville problem also coincides with the boundary value problem obtained by Shukhobodskiy and Ruderman (2018) and described in Chapter 4 for kink oscillations of an expanding magnetic tube with the density varying along the tube that is in a static equilibrium. We assume that ω^2 is the eigenvalue and S_0 is the corresponding eigenfunction. In accordance with the Sturm-Liouville theory, eigenvalues are real and constitute monotonically increasing sequence. Multiplying Equation (5.6) by S_0 and integrating it over z we have

$$\omega^2 \int_{-L/2}^{L/2} \frac{S_0^2}{C_k^2}\, dz = \int_{-L/2}^{L/2} \left(\frac{\partial S_0}{\partial z}\right)^2 dz. \tag{5.7}$$

This result implies that $\omega^2 > 0$.

Proceeding to the next order approximation, we collect terms of the order of l in Equation (5.3) (for more details see Appendix B). This yields

$$\begin{aligned}\frac{\partial^2 S_1}{\partial z^2} + \frac{\omega^2}{C_k^2}S_1 = \frac{i}{C_k^2}\Bigg(&2\omega\frac{\partial S_0}{\partial t_1} + S_0\frac{\partial \omega}{\partial t_1} \\ &+ \frac{2\omega(\rho_i\tilde{U}_i + \rho_e\tilde{U}_e)}{R(\rho_i + \rho_e)}\frac{\partial(RS_0)}{\partial z}\Bigg) - \frac{\widetilde{\mathcal{L}}}{C_k^2(\rho_i + \rho_e)}.\end{aligned} \tag{5.8}$$

The function S_1 must satisfy the boundary conditions

$$S_1 = 0 \quad \text{at} \quad z = \pm L/2. \tag{5.9}$$

The homogeneous counterpart of Equation (5.8) with the boundary conditions given by Equation (5.9) has a non-trivial solution $S_1 = S_0$. This implies that the boundary

value problem determining S_1 has solutions only if the right-hand side of Equation (5.8) satisfies the compatibility condition, which is the condition that it must be orthogonal to S_0. To obtain this condition, we multiply Equation (5.8) by S_0, integrate the obtained equation with respect to z, and use the integration by parts and the boundary conditions given by Equations (5.6) and (5.9). As a result, we obtain

$$\int_{-L/2}^{L/2}\left(\frac{\partial(\omega S_0^2)}{\partial t_1}+\frac{\omega(\rho_i\tilde{U}_i+\rho_e\tilde{U}_e)}{R^2(\rho_i+\rho_e)}\frac{\partial(R^2S_0^2)}{\partial z}\right)\frac{dz}{C_k^2} = -i\int_{-L/2}^{L/2}\frac{\widetilde{\mathcal{L}}\,dz}{C_k^2(\rho_i+\rho_e)}. \tag{5.10}$$

Using integration by parts and Equations (2.50), (2.46), and (5.6) we obtain the identity

$$\begin{aligned}&\int_{-L/2}^{L/2}\frac{(\rho_i\tilde{U}_i+\rho_e\tilde{U}_e)}{R^2C_k^2(\rho_i+\rho_e)}\frac{\partial(R^2S_0^2)}{\partial z}dz\\ &=\frac{\mu_0}{2R^4B^2}\int_{-L/2}^{L/2}R^2(\rho_i\tilde{U}_i+\rho_e\tilde{U}_e)\frac{\partial(R^2S_0^2)}{\partial z}dz\\ &=-\frac{\mu_0}{2}\int_{-L/2}^{L/2}\frac{S_0^2}{R^2B^2}\frac{\partial}{\partial z}\left[R^2(\rho_i\tilde{U}_i+\rho_e\tilde{U}_e)\right]dz\\ &=\frac{\mu_0}{2}\int_{-L/2}^{L/2}\frac{S_0^2}{B^2}\frac{\partial(\rho_i+\rho_e)}{\partial t_1}dz=\int_{-L/2}^{L/2}S_0^2\frac{\partial C_k^{-2}}{\partial t_1}dz.\end{aligned} \tag{5.11}$$

Using this identity and returning to the non-scaled time we transform Equation (5.10) to

$$\frac{d}{dt}\left(\omega\int_{-L/2}^{L/2}\frac{S_0^2}{C_k^2}\,dz\right)=-il\int_{-L/2}^{L/2}\frac{S_0\widetilde{\mathcal{L}}\,dz}{C_k^2(\rho_i+\rho_e)}. \tag{5.12}$$

The quantity in the brackets on the left-hand side of this equation is called adiabatic invariant. This quantity can be interpreted as the wave action. When $l=0$ the right-hand side is zero and the adiabatic invariant is conserved. This result was previously obtained by Ruderman et al. (2017) and presented in Chapter 3. It is worth noting that the oscillation energy is not conserved because, in general, there is the plasma flow through the loop footpoints. Even if we impose the condition that there is no plasma flow through the footpoints, there is the plasma redistribution in the loop caused by cooling. As a result, there is the exchange of energy between the oscillation and the gravitational field.

5.2.2 Calculation of $\widetilde{\mathcal{L}}$

Equation (5.12) describes the evolution of S_0 and, consequently, the oscillation amplitude. This equation is not closed because the expression for $\widetilde{\mathcal{L}}$ contains $\widetilde{\delta S}$ and $\widetilde{\delta P}$. To close it we need to express $\widetilde{\delta S}$ and $\widetilde{\delta P}$ in terms of S_0. Since we only need to calculate the right-hand side of Equation (5.12) in the leading order approximation with respect

to l, it follows that we need to calculate $\widetilde{\delta S}$ and $\widetilde{\delta P}$ also only in the leading order approximation. Using Equation (2.50), we obtain the estimate that $U_{i,e} \sim lC_k$. It also follows that $\partial S_0/\partial t \sim l\omega S_0$. These estimates imply that the account of the flow in the transitional layer and the time derivative of S can only give corrections of order l to $\widetilde{\delta S}$ and $\widetilde{\delta P}$. Hence, we can neglect the flow and the time derivative of S when calculating these quantities. Then we can use the same equations as in Chapter 4 to calculate $\widetilde{\delta S}$ and $\widetilde{\delta P}$. However, we cannot directly use the results obtained in Chapter 4. The reason is that it was assumed in Chapter 4 that the unperturbed density is equal to the product of two functions, one depending on ψ, and the other on z. Here we cannot make this assumption because even if it is satisfied at the initial time, in general, later it will be not valid because of the density variation with time. Hence, we need to modify the analysis given by Chapter 4. Below, we briefly describe this analysis and the modification that we make.

Following Chapters 2 and 4, we use the variable ψ instead of r. Then we consider Alfvén oscillations of individual magnetic filed lines, which are described by the eigenvalue problem

$$V_A^2 \frac{\partial^2 Y}{\partial z^2} = -\lambda Y, \quad Y = 0 \ \text{ at } \ z = \pm L/2, \tag{5.13}$$

where Alfvén speed V_A is defined by Equation (4.5). Here Y and V_A depend on t, ψ, and z, and λ on t and ψ. The eigenvalues of this problem are real and constitute a monotonically increasing sequence λ_n, where $\lambda_n \to \infty$ as $n \to \infty$ (e.g. Coddington and Levinson, 1955). It is easy to show that all eigenvalues are positive. Any integrable by quadrature in the interval $[-L/2, L/2]$ function $f(z)$ can be expanded in a generalised Fourier series

$$f(t,\psi,z) = \sum_{n=1}^{\infty} f_n(t,\psi) Y_n(t,\psi,z), \tag{5.14}$$

where $Y_n(t,\psi,z)$ is an eigenfunction of the boundary value problem (5.13). Obviously, all Y_n can be chosen to be real. According to the classical Sturm-Liouville theory, the eigenfunctions corresponding to different eigenvalues are orthogonal with the weight $V_A^{-2}(t,\psi,z)$. In addition, we can normalise them in such a way that they satisfy the relation

$$\int_{-L/2}^{L/2} V_A^{-2}(z) Y_m(z) Y_n(z)\, dz = \delta_{mn}, \tag{5.15}$$

where δ_{mn} is the Kronecker delta-symbol. If $f(z)$ has a continuous second derivative and satisfies the boundary condition $f(\pm L/2) = 0$, then the sum in (5.14) is uniformly convergent and can be differentiated twice (see, e.g. Naimark, 1967). The Fourier coefficients in the Fourier series (5.14) are given by

$$f_n = \int_{-L/2}^{L/2} V_A^{-2}(z) f(z) Y_n(z)\, dz. \tag{5.16}$$

The resonance of a global kink oscillation with the n^{th} harmonic of local Alfvén oscillations occurs at the resonant magnetic surface defined by the equation $\psi = \psi_n$ if the

relation $\lambda_n(\psi_n) = \omega^2$ is satisfied. Since $\lambda_n \to \infty$ as $n \to \infty$, it follows that only a finite number of Alfvén resonances exist.

Observations show that, in most cases, the fundamental harmonic of kink oscillations is dominant, so the oscillation amplitude is determined by the fundamental harmonic. In accordance with this, below, we restrict our analysis to the fundamental harmonic. We assume that $\rho(t, \psi, z)$ is a monotonically decreasing function of ψ for all $z \in [-L/2, L/2]$ and at any time. Then $V_{Ai}(z) < C_k(z) < V_{Ae}(z)$ for all $z \in [-L/2, L/2]$. Using the comparison theorem for ordinary differential equations (e.g. Coddington and Levinson, 1955) it is straightforward to show that $\lambda_1(\psi_i) < \omega^2 < \lambda_1(\psi_e)$. This implies that there is $\psi_1 \in [\psi_i, \psi_e]$ such that $\lambda_1(\psi_1) = \omega^2$. Hence, there is always at least one resonant surface in the transitional layer. Below, we assume that $\lambda_2(\psi_i) > \lambda_1(\psi_e)$. Then it follows that there is exactly one resonant surface.

Now, the derivation of expressions for δP and $\delta\eta$ are analogous to the derivations of expressions for these quantities given already in Chapter 4. The only difference is the following. In accordance with the assumption about the density made in Chapter 4 $V_A^2 = V_{Ai}^2 g(\psi)$, where $g(\psi)$ is a monotonically increasing function and $g(\psi_i) = 1$. Then in Chapter 4 we used Equation (4.36). Since in this chapter V_A^2 cannot be factorised we use, instead, the expansion

$$\frac{V_A^2 Q}{R^2} = \sum_{n=1}^{\infty} \Phi_n(\psi) Y_n(\psi, z). \tag{5.17}$$

After that, we obtain the expressions for δQ and $\delta\eta$ substituting $\Phi_n(\psi)$ for $\Phi_n g(\psi)$ in all equations from (4.37) to (4.52) in Chapter 4. They read

$$\delta Q = \int_{\psi_i}^{\psi_e} \left(\frac{Q_i}{\psi_i} - \frac{(\rho_i - \rho)\omega^2 \eta}{B^3} \right) d\psi, \tag{5.18}$$

$$\begin{aligned} \delta\eta \;\; = \;\; & \frac{\mu_0}{BR^2} \mathcal{P} \int_{\psi_i}^{\psi_e} \sum_{n=1}^{\infty} \frac{\Phi_n(t,\psi) Y_n(t,\psi,z)}{\omega^2(t) - \lambda_n(t,\psi)} \, d\psi \\ & - \frac{\pi i \mu_0 \Phi_1(t,\psi_1) Y_1(t,\psi_1,z)}{|\Delta(t)| BR^2}, \end{aligned} \tag{5.19}$$

where $\mathcal{P}$ indicates the principal Cauchy part of the integral and

$$\Delta = -\left. \frac{d\lambda_1}{d\psi} \right|_{\psi=\psi_1}. \tag{5.20}$$

When deriving Equation (5.19), we took into account that $BR^2 = \text{const}$. Now, we use the Equation (4.26) from Chapter 4 where we substitute ω for Ω, ι for $\bar{\iota}$, and z for Z because in this chapter we do not use the scaled frequency, kinematic viscosity, and the coordinate along the tube. Then we obtain

$$V_A^2 \frac{\partial^2 W}{\partial z^2} + \omega^2 W - i\iota\omega R^2 B^2 \frac{\partial^2 W}{\partial \psi^2} = \frac{\mu_0 V_A^2 Q_i}{R^2}, \tag{5.21}$$

where

$$W = \frac{\partial(rB\xi_\perp)}{\partial\psi}. \tag{5.22}$$

The last term on the left-hand side of Equation (5.21) describing the effect of viscosity is only important in the thin dissipative layer embracing the resonant surface. Below we use Equation (5.21) outside of the dissipative layer and thus can neglect this term. In Chapter 2 we showed that in the thin tube approximation B and $\xi_\perp$ are independent of ψ and $\psi = \frac{1}{2}r^2B$. Then we obtain $W = \eta$. As a result, Equation (5.21) reduces to

$$V_A^2\frac{\partial^2\eta}{\partial z^2} + \omega^2\eta = \frac{\mu_0 V_A^2 Q_i}{R^2}. \tag{5.23}$$

We take this equation at $\psi = \psi_i$. Then, using Equation (5.5), we obtain in the leading order approximation with respect to l

$$Q_i = \frac{\omega^2 R^2 S_0(\rho_i - \rho_e)}{2B^2} e^{il^{-1}\Theta}. \tag{5.24}$$

Substituting this result in Equation (5.18), noticing that $\psi_i = \frac{1}{2}BR^2[1 + \mathcal{O}(l)]$, and using the relation $\widetilde{\delta P} = l^{-1}B^2\delta Q$ yields

$$\widetilde{\delta P} = \frac{\omega^2 l^{-1} S_0}{B}\, e^{il^{-1}\Theta}\int_{\psi_i}^{\psi_e}(\rho - \rho_e)\, d\psi. \tag{5.25}$$

Now, we need to express $\widetilde{\delta S}$ in terms of S_0. We have $\widetilde{\delta S} = l^{-1}\delta\eta\, e^{-il^{-1}\Theta}$, where $\delta\eta$ is given by Equation (5.19). This equation contains the functions $\Phi_n(t,\psi)$, thus we need to express these functions in terms of S_0. To achieve this we use Equation (5.17). Since we only need to calculate $\Phi_n(t,\psi)$ in the leading order approximation with respect to l, we can substitute Q_i for Q in this equation. Then, using Equations (5.16) and (5.24) we obtain

$$\Phi_n = \omega^2 e^{il^{-1}\Theta}\int_{-L/2}^{L/2}\frac{S_0 Y_n(\rho_i - \rho_e)}{2B^2} dz. \tag{5.26}$$

Substituting this expression in Equation (5.19) and using the relation between $\widetilde{\delta S}$ and $\delta\eta$ yields

$$\begin{aligned}
\widetilde{\delta S} \;=\; & \frac{l^{-1}\pi i\mu_0\omega^2 Y_1(\psi_1, z)}{|\Delta|BR^2}\int_{-L/2}^{L/2}\frac{S_0(\tilde z)Y_1(\psi_1,\tilde z)[\rho_e(\tilde z) - \rho_i(\tilde z)]}{2B^2(\tilde z)}\, d\tilde z \\
+ \; & \frac{l^{-1}\mu_0\omega^2}{BR^2}\,\mathcal{P}\int_{\psi_i}^{\psi_e}\left(\sum_{n=1}^{\infty}\frac{Y_n(z)}{\omega^2 - \lambda_n}\right. \\
\times \; & \left.\int_{-L/2}^{L/2}\frac{S_0(\tilde z)Y_n(\tilde z)[\rho_i(\tilde z) - \rho_e(\tilde z)]}{2B^2(\tilde z)}\, d\tilde z\right) d\psi,
\end{aligned} \tag{5.27}$$

where we only showed the dependence on z, but we did not show the dependence on t and ψ. Finally, using Equations (5.4), (5.5), (5.25), and (5.27) we obtain

$$\begin{aligned}
\widetilde{\mathcal{L}} &= l^{-1}\omega^2 S_0(z)\left(\int_{\psi_i}^{\psi_e}\frac{\rho(z)-\rho_i(z)}{B(z)R^2(z)}\,d\psi - \frac{\rho_i(z)-\rho_e(z)}{2}\right)\\
&+ \frac{\mu_0\omega^2}{BR^2}\,\mathcal{P}\int_{\psi_i}^{\psi_e}\left(\sum_{n=1}^{\infty}\frac{Y_n(z)[\omega^2\rho_e(z)-\lambda_n\rho(z)]}{\omega^2-\lambda_n}\right.\\
&\times \left.\int_{-L/2}^{L/2}\frac{S_0(\tilde{z})Y_n(\tilde{z})[\rho_i(\tilde{z})-\rho_e(\tilde{z})]}{2B^2(\tilde{z})}\,d\tilde{z}\right)d\psi\\
&+ \frac{l^{-1}\pi i\mu_0\omega^4 Y_1(\psi_1,z)[\rho(\psi_1,z)-\rho_e(z)]}{|\Delta|BR^2}\\
&\times \int_{-L/2}^{L/2}\frac{S_0(\tilde{z})Y_1(\psi_1,\tilde{z})[\rho_i(\tilde{z})-\rho_e(\tilde{z})]}{2B^2(\tilde{z})}\,d\tilde{z}. \qquad (5.28)
\end{aligned}$$

5.2.3 Amplitude variation

We consider an eigenfunction $X(t,z)$ of the boundary value problem constituted by Equations (5.5) and (5.6) that is real-valued, corresponds to the fundamental mode, and satisfies the condition $\max_z X(t,z)=1$. Since S_0 is also an eigenvalue of the same boundary value problem, it must be proportional to $X(t,z)$ with the proportionality coefficient depending on time. Hence, we can write

$$S_0(t,z) = A(t)\,e^{iF(t)}X(t,z), \qquad (5.29)$$

where $A(t)$ and $F(t)$ are real-valued functions, and $A(t)>0$. Since $\max_z|S(t,z)| = A(t)$, the function $A(t)$ can be considered as the oscillation amplitude. Using Equation (5.29), we obtain

$$\begin{aligned}
\frac{d}{dt}\left(\omega\int_{-L/2}^{L/2}\frac{S_0^2}{C_k^2}\,dz\right) &= e^{2iF(t)}\frac{d}{dt}\left(\omega A^2\int_{-L/2}^{L/2}\frac{X^2}{C_k^2}\,dz\right)\\
&+ 2i\omega A^2 e^{2iF(t)}\frac{dF}{dt}\int_{-L/2}^{L/2}\frac{X^2}{C_k^2}\,dz. \qquad (5.30)
\end{aligned}$$

With the aid of Equation (5.28) we calculate the right-hand side of Equation (5.12),

$$-il\int_{-L/2}^{L/2}\frac{S_0\widetilde{\mathcal{L}}\,dz}{C_k^2(\rho_i+\rho_e)} = A^2e^{2iF(t)}\left(\Gamma+i\omega\Upsilon\right), \qquad (5.31)$$

where

$$\begin{aligned}
\Gamma &= \frac{\pi\mu_0^2\omega^4}{|\Delta|BR^2}\int_{-L/2}^{L/2}\frac{XY_1(\psi_1)}{2B^2}[\rho(\psi_1)-\rho_e]\,dz\\
&\times \int_{-L/2}^{L/2}\frac{XY_1(\psi_1)(\rho_i-\rho_e)}{2B^2}\,dz, \qquad (5.32)
\end{aligned}$$

$$\begin{aligned}\Upsilon &= \omega e^{2iF(t)}\left[\int_{-L/2}^{L/2}\frac{X^2}{2C_k^2}\left(\frac{\rho_i-\rho_e}{\rho_i+\rho_e}-2\int_{\psi_i}^{\psi_e}\frac{(\rho-\rho_i)\,d\psi}{BR^2(\rho_i+\rho_e)}\right)dz\right.\\ &- \frac{\mu_0}{BR^2}\mathcal{P}\int_{\psi_i}^{\psi_e}\left(\sum_{n=1}^{\infty}\int_{-L/2}^{L/2}\frac{XY_n(\omega^2\rho_e-\lambda_n\rho)}{C_k^2(\rho_i+\rho_e)(\omega^2-\lambda_n)}\right.\\ &\times \left.\left.\int_{-L/2}^{L/2}\frac{XY_n(\rho_i-\rho_e)}{2B^2}\,dz\right)d\psi\right]. \qquad (5.33)\end{aligned}$$

Substituting Equations (5.30) and (5.31) in Equation (5.12), we eventually arrive at

$$\frac{d}{dt}\left(\omega A^2\int_{-L/2}^{L/2}\frac{X^2}{C_k^2}\,dz\right)=-\Gamma A^2, \qquad (5.34)$$

$$\frac{dF}{dt}\int_{-L/2}^{L/2}\frac{X^2}{C_k^2}\,dz=\Upsilon. \qquad (5.35)$$

Equation (5.34) describes the evolution of the oscillation amplitude with time. The function $F(t)$ determines the phase shift related to the presence of the transitional layer.

§ 5.3 Kink oscillations of coronal loops with barometric density distribution

5.3.1 Kink oscillations of static coronal loops

We now verify that equation (5.34) correctly describes the damping of kink oscillations of static coronal loops. In the case of a static loop Equation (5.34) becomes

$$\frac{dA}{dt}=\gamma A,\quad \gamma=\frac{\Gamma}{2\omega I}, \qquad (5.36)$$

where

$$I=\int_{-L/2}^{L/2}\frac{X^2}{C_k^2}\,dz. \qquad (5.37)$$

It follows form equation (5.36) that oscillation amplitude decreases exponentially with the decrement γ. Let $\zeta=\rho_i(L/2)/\rho_e(L/2)$. Similarly to Chapter 4, we assume, that $\rho_i(z)/\rho_e(z)=\zeta$ and $\rho_t(\psi,z)=\rho_i(z)/g(\psi)$, where $g(\psi)$ is a monotonically increasing function satisfying $g(\psi_i)=1$ and $g(\psi_e)=V_{Ae}^2/V_{Ai}^2$. As a result, following the analysis in Chapter 4, we can write λ_1 as

$$\lambda_1(\psi)=\lambda_1(\psi_i)g(\psi). \qquad (5.38)$$

We recall that we assume that there is only one resonant surface $\psi=\psi_1$. Now, we can rewrite Equation (5.5) as

$$\frac{B^2}{\mu_0\rho_e(z)}\frac{\partial^2 S_0}{\partial z^2}=-\frac{\omega^2(\zeta+1)}{2}S_0. \qquad (5.39)$$

For fundamental mode at $\psi = \psi_1$ Equation (5.13) can be rewritten as

$$\frac{B^2}{\mu_0 \rho_e(z)} \frac{\partial^2 Y_1(\psi_1)}{\partial z^2} = -\frac{\zeta \lambda_1(\psi_1)}{g(\psi_1)} Y_1(\psi_1). \tag{5.40}$$

We see that both S_0 and Y_1 are eigenfunctions of the same differential operator corresponding to the fundamental mode. Therefore, the coefficients on the right-hand sides of Equations (5.39) and (5.40) must be equal. Then it follows from the resonant condition, $\lambda_1 = \omega^2$, that

$$g(\psi_1) = \frac{2\zeta}{\zeta + 1}. \tag{5.41}$$

Substituting Equations (5.38) and (5.41) in Equation (5.20) yields

$$\Delta = -\omega^2 g'(\psi_1) \tag{5.42}$$

Using Equations (5.41) we obtain

$$\rho_e(z) = \frac{2\rho(\psi_1)}{\zeta + 1}. \tag{5.43}$$

The functions $X(z)$ and $Y_1(\psi_1, z)$ are the eigenfunctions of the same eigenvalue problem corresponding to the same eigenvalue. Therefore, we have $X = \varsigma Y_1(\psi_1)$, where ς is a constant. Using this result and Equations (5.15), (5.42), and (5.43) we transform equation (5.32) to

$$\Gamma = \frac{\pi \varsigma^2 \omega^2 \zeta (\zeta - 1)^2}{B R^2 g'(\psi_1)(\zeta + 1)^3}. \tag{5.44}$$

Again, using the relation $X = \varsigma Y_1(\psi_1)$, and also Equations (5.15) and (5.43) we obtain $I = \varsigma^2$. Using this result and Equation (5.44) yields

$$\gamma = \frac{\pi \omega \zeta (\zeta - 1)^2}{2 B R^2 g'(\psi_1)(\zeta + 1)^3}, \tag{5.45}$$

Following the analysis in Chapter 4 we consider the linear density profile in transitional layer and assume that ρ_t is defined by Equation (4.76). Then, using Equation (5.41) and the relation $\psi = \frac{1}{2} B r^2$, we obtain in the leading order approximation

$$g'(\psi_1) = \frac{4\zeta(\zeta - 1)}{l B R^2 (\zeta + 1)^2}. \tag{5.46}$$

Substituting this expression in Equation (5.45) yields

$$\frac{\gamma}{\omega} = \frac{\pi l (\zeta - 1)}{8(\zeta + 1)}. \tag{5.47}$$

This expression coincides with expression obtained by Goossens et al. (2002) for a tube with the density not varying along the tube and in Chapter 4.

Next, we consider sinusoidal profile determined by

$$\rho_t(r,z) = \frac{\rho_i + \rho_e}{2} - \frac{\rho_i - \rho_e}{2} \sin\left(\frac{\pi(r-R)}{lR}\right). \tag{5.48}$$

Using the relation $\psi = \frac{1}{2}Br^2$, we obtain

$$r = R\left(1 - \frac{l}{2}\right) + \frac{\psi - \psi_i}{BR} + \mathcal{O}(l^2). \tag{5.49}$$

It follows from Equations (5.48) and (5.49) that

$$\frac{1}{g(\psi)} = \frac{\zeta+1}{2\zeta} + \frac{\zeta-1}{2\zeta}\cos\frac{\pi(\psi-\psi_i)}{lBR^2}. \tag{5.50}$$

With the aid of Equations (5.41) and (5.50) we obtain

$$\psi_1 = \psi_i + \frac{1}{2}lBR^2. \tag{5.51}$$

Then, using Equations (5.41), (5.50) and (5.51) yields

$$g'(\psi_1) = \frac{2\pi\zeta(\zeta-1)}{lBR^2(\zeta+1)^2}. \tag{5.52}$$

Substituting this result in Equation (5.45) we arrive at

$$\frac{\gamma}{\omega} = \frac{l(\zeta-1)}{4(\zeta+1)}. \tag{5.53}$$

This expression coincides with one obtained by Ruderman and Roberts (2002) who considered damping of kink oscillations of a magnetic tube with the constant cross-section and density invariant along the tube. This result, again, confirms the conclusion made in Chapter 3 that the ratio γ/ω is not affected by the density and cross-section radius variation along the tube if $\rho_t(\psi,z) = \rho_i(z)/g(\psi)$.

5.3.2 Kink oscillations of cooling coronal loops

In this section, we again assume that there is only one resonant position $\psi = \psi_1$. Also, similarly to Ruderman (2011b) we assume that the temperature of plasma outside the loop does not change with time and is T_0, while inside the loop it decreases with time due to the effect of radiative cooling. Similar to Aschwanden and Terradas (2008), Morton and Erdélyi (2010), Ruderman (2011a), Ruderman et al. (2017) and Chapter 3 we approximate the temperature evolution inside the loop by the exponentially decaying function by Equation (4.36). Following Ruderman et al. (2008, 2017) and Chapter 3 we describe $R(z)$ by Equation (3.16). Then the same analysis hold for expansion factor ϑ as in Chapter 3.

Typical coronal loop expansion factor does not exceed 1.5 (see e.g. Klimchuk, 2000; Watko and Klimchuk, 2000), thus by varying L/L_c we can cover the whole range of

values of the expansion factor. In what follows, we consider a loop with a half-circle shape. We neglect the effect of the loop shape on oscillations because, as it was shown by Van Doorsselaere et al. (2004) and Terradas et al. (2006), it is very weak. As a result, the loop shape only determines the density variation along the loop. Hence, we describe internal and external densities by equations proposed in Chapter 3. We also assume that the density profile in transitional layer is linear, therefore

$$\rho_t(t,r,z) = \frac{1}{2}[\rho_i(t,z) + \rho_e(z)] + [\rho_i(t,z) - \rho_e(z)]\frac{R-r}{lR}. \tag{5.54}$$

It follows that $\rho_t = (\rho_i + \rho_e)/2$ at $r = R$. It is straightforward to see that $V_A = C_k$ when $r = R$, the boundary value problems for S_0 and Y are the same and, consequently, $\lambda_1 = \omega^2$ and $r = R$ is the resonant surface. Then, using the relation $\psi = \frac{1}{2}Br^2$, we obtain that $\psi_1 = \frac{1}{2}BR^2$.

The functions X and $Y_1(\psi_1)$ are defined by the same boundary value problem which implies that $Y_1(\psi_1)$ is proportional to X and $Y_1(\psi_1)$. Since the equilibrium is symmetric with respect to the apex point, it follows that that $X(z)$ describing the fundamental mode is an even function. Hence, it takes maximum at $z = 0$, and thus the condition $\max_z(X) = 1$ reduces to $X(0) = 1$. Summarising, we obtain

$$Y_1(\psi_1, z) = Y_1(\psi_1, 0)X(z). \tag{5.55}$$

Then, it follows from Equation (5.15) and the relation $V_A(\psi_1) = C_k$, that

$$Y_1^2(\psi, 0) = \frac{1}{I}. \tag{5.56}$$

We substitute Y_1 for Y in Equation (5.13), differentiate the obtained equation with respect to ψ, take $\psi = \psi_1$, and use $\lambda_1(\psi_1) = \omega^2$ and $V_A(\psi_1) = C_k$. As a result we obtain

$$\frac{\partial^3 Y_1}{\partial z^2 \partial \psi} + \frac{\omega^2}{C_k^2}\frac{\partial Y_1}{\partial \psi} = -\frac{1}{C_k^2}\frac{\partial V_A^2}{\partial \psi}\frac{\partial^2 Y_1}{\partial z^2} - \frac{d\lambda_1}{d\psi}\frac{Y_1}{C_k^2}, \tag{5.57}$$

where $\psi = \psi_1$. Using Equation (5.54) yields

$$\left.\frac{\partial V_A^2}{\partial \psi}\right|_{\psi=\psi_1} = \frac{2C_k^2(\rho_i - \rho_e)}{lBR^2(\rho_i + \rho_e)}. \tag{5.58}$$

Using this result and Equations (5.13) and (5.55), we obtain

$$\frac{\partial^3 Y_1}{\partial z^2 \partial \psi} + \frac{\omega^2}{C_k^2}\frac{\partial Y_1}{\partial \psi} = \left(\frac{2\omega^2(\rho_i - \rho_e)}{lBR^2(\rho_i + \rho_e)} - \frac{\partial \lambda_1}{\partial \psi}\right)\frac{XY_1(\psi_1, 0)}{C_k^2}. \tag{5.59}$$

Multiplying Equation (5.59) by X, integrating the obtained equation with respect to z, and using Equation (5.5), (5.20), and (5.37) yields

$$\Delta = -\left.\frac{\partial \lambda_1}{\partial \psi}\right|_{\psi=\psi_1} = -\frac{2\omega^2 J}{lBR^2 I}, \quad J = \int_{-L/2}^{L/2} \frac{(\rho_i - \rho_e)X^2}{(\rho_i + \rho_e)C_k^2}\, dz. \tag{5.60}$$

Then, using Equations (5.54) – (5.56) and (5.60), and the relation $\rho(\psi_1) = \frac{1}{2}(\rho_i + \rho_e)$, we obtain from Equation (5.32)

$$\Gamma = \frac{\pi}{4} l\omega^2 |J|. \tag{5.61}$$

We employ dimensionless variables proposed in Chapter 3. We solve a linear problem. Hence, we can fix A at the initial instant arbitrary. If we take $A(0) = 1$, then $A(t)$ is the ratio of the current oscillation amplitude to its value at the initial time. We substitute X for S_0 in Equation (5.5). Then, using Equations (3.40), (3.41)–(3.43), and the relation $BR^2 = \text{const}$, we obtain

$$\frac{\partial^2 X}{\partial Z^2} + \frac{\varpi^2 \Lambda^4 X}{4(\zeta+1)} \left[\zeta \exp\left(-\kappa e^{\tau} \cos\frac{\pi z}{2}\right) + \exp\left(-\kappa \cos\frac{\pi z}{2}\right) \right] = 0, \tag{5.62}$$

Since the loop is symmetric with respect to the apex point, and we consider the fundamental mode, we can solve Equation (5.62) using the boundary conditions

$$\frac{\partial X}{\partial Z} = 0 \quad \text{at} \;\; Z = 0, \quad X = 0 \quad \text{at} \;\; Z = 1. \tag{5.63}$$

The function $X(Z)$ takes maximum at $Z = 0$, so we can reduce the condition $\max_z X(z) = 1$ to $X(0) = 1$. This boundary value problem determines ϖ and $X(Z)$.

Using Equations (3.22), (3.41), (3.41), (3.43), (5.34), (5.60) and (5.61) we obtain

$$\frac{d(\varpi \Pi_+ A^2)}{dt} = -\alpha \varpi^2 |\Pi_-| A^2, \tag{5.64}$$

where

$$\Pi_\pm = \int_0^1 X^2 \Lambda^4 \left[\zeta \exp\left(-\kappa e^{\tau} \cos\frac{\pi z}{2}\right) \pm \exp\left(-\kappa \cos\frac{\pi z}{2}\right) \right] dZ, \tag{5.65}$$

$$\alpha = \frac{\pi l C_f t_{cool}}{4L}. \tag{5.66}$$

The parameter α determines the relative strength of resonant damping and amplification caused by cooling. We see that the dependence of the oscillation amplitude is determined by five non-dimensional parameters: α, ζ, κ, and ϑ.

Numerical solution was obtained using software packages from Wolfram Mathematica 11.3. To obtain the solution to the eigenvalue problem constituted by Equation (5.62) with the boundary conditions (5.63) we used the program NDEigenesystem that calculates the eigenvalue τ and the eigenfunction $X(\tau, z)$. Then, we substituted τ and $X(\tau, z)$ in Equation (5.64) and integrated this equation numerically using the program NIntegrate. By default, this program uses the Global adaptive method that automatically chooses a numerical method that minimises the error. As a result, we calculated the dependence of A on τ.

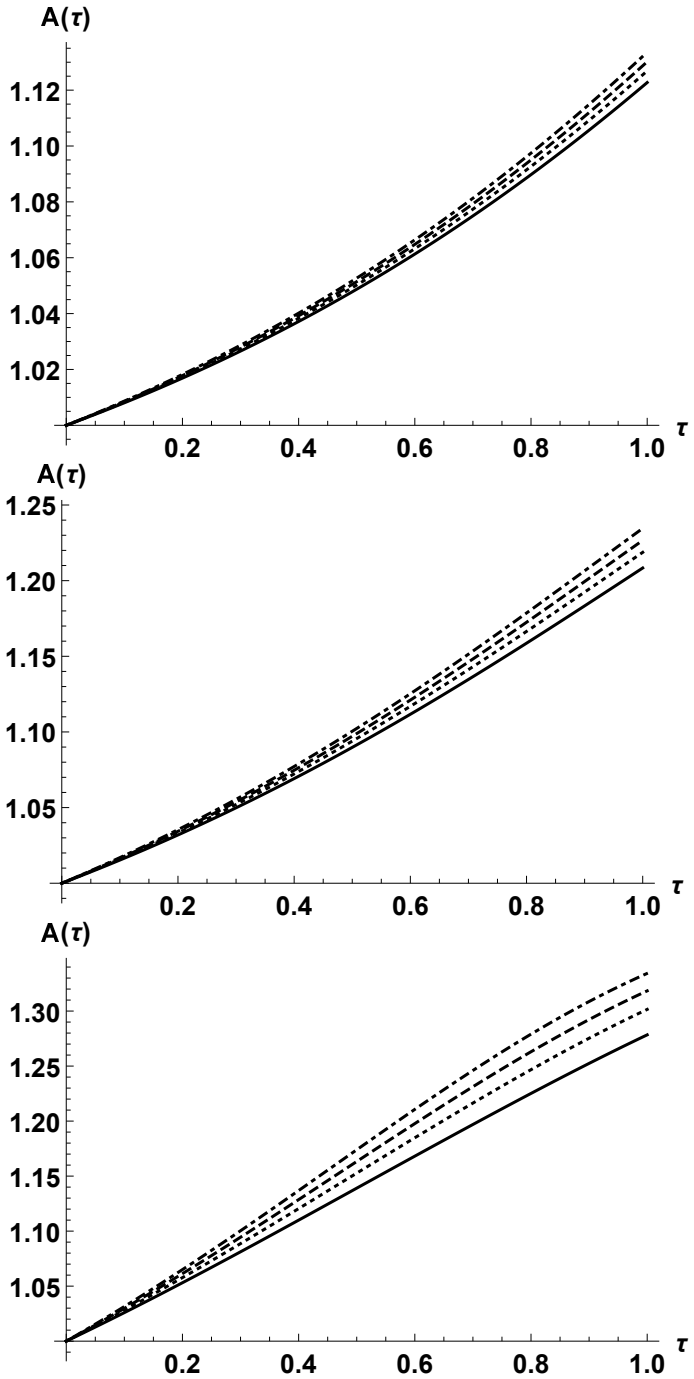

Figure 5.1: The dependence of dimensionless amplitude A of the fundamental mode on the dimensionless time τ for $\zeta = 3$ and $L/L_c = 6$ and $\alpha = 0$. The upper, middle, and lower panels correspond to $\kappa = 0.5$, 1, and 2 , respectively. The solid, dotted, dashed, and dashed-dotted lines correspond to $\vartheta = 1$, 1.15, 1.3, and 1.5.

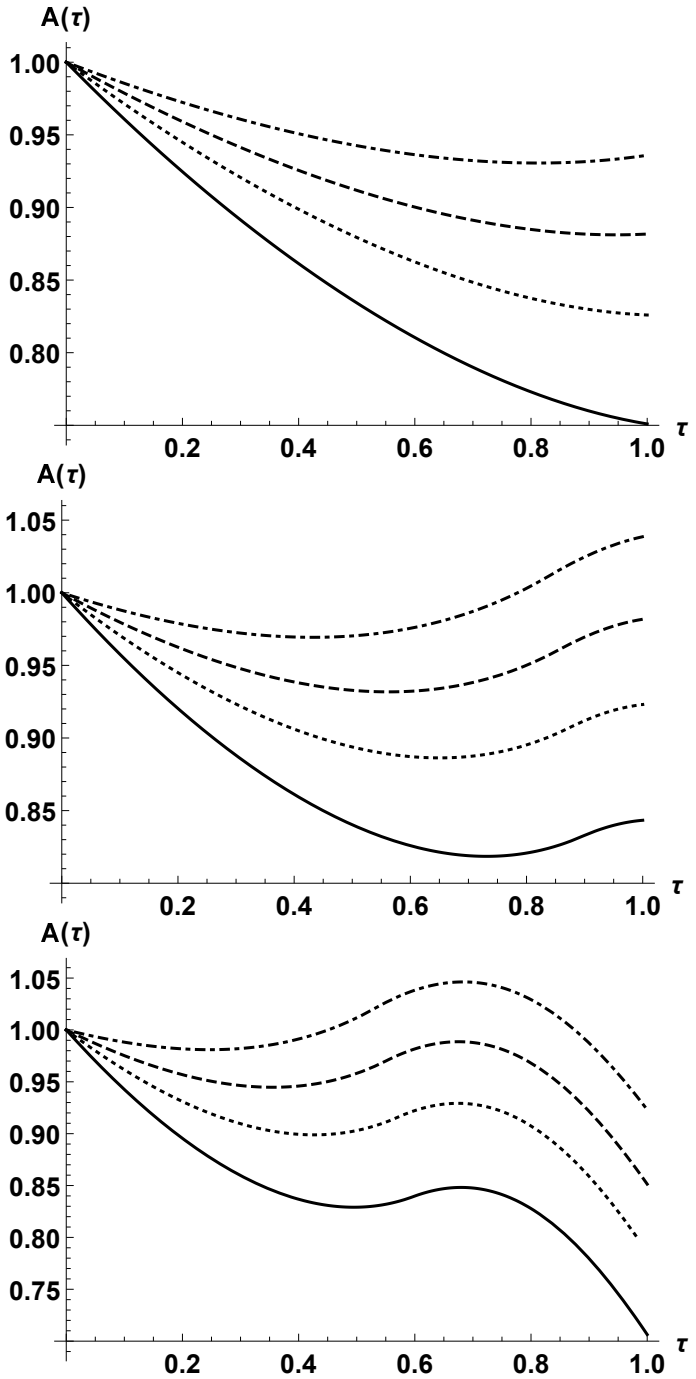

Figure 5.2: The dependence of dimensionless amplitude A of the fundamental mode on the dimensionless time τ for $\zeta = 3$ and $L/L_c = 6$ and $\alpha = 0.5$. The upper, middle, and lower panels correspond to $\kappa = 0.5$, 1, and 2 , respectively. The solid, dotted, dashed, and dashed-dotted lines correspond to $\vartheta = 1$, 1.15, 1.3, and 1.5.

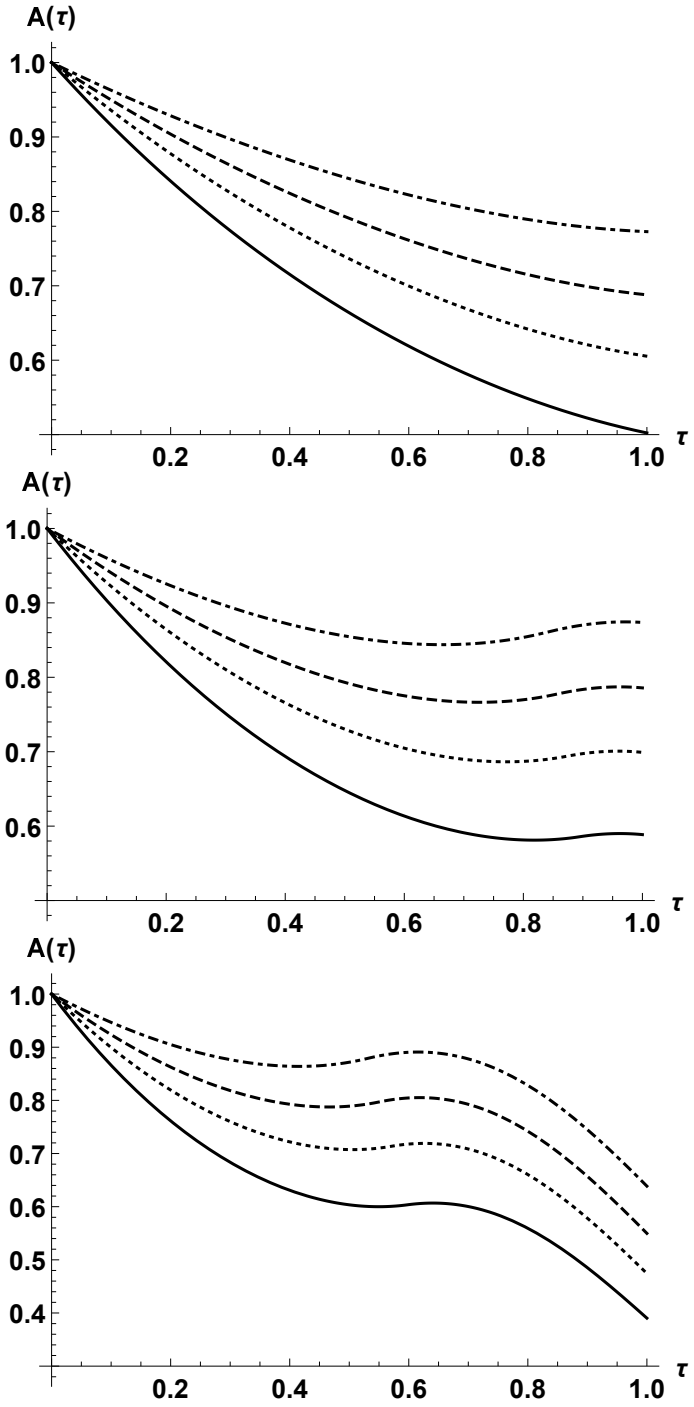

Figure 5.3: The dependence of dimensionless amplitude A of the fundamental mode on the dimensionless time τ for $\zeta = 3$ and $L/L_c = 6$ and $\alpha = 1$. The upper, middle, and lower panels correspond to $\kappa = 0.5$, 1, and 2 , respectively. The solid, dotted, dashed, and dashed-dotted lines correspond to $\vartheta = 1$, 1.15, 1.3, and 1.5.

In our calculations we took $\zeta = 3$ similarly to Ruderman (2011b) and Ruderman et al. (2017) and $L/L_c = 6$. The latest asumption enables us to cover whole range of reallistic expansion factors ϑ. The function $A(t)$ is calculated numerically for various values of α, κ and ϑ. The results of these calculations are presented in Figures 5.1–5.3. We see that when there is no resonant absorption ($\alpha = 0$) cooling results in the amplification of oscillations. This result is in a perfect agreement with that obtained by Ruderman (2011a), Ruderman (2011b), and Ruderman et al. (2017).

As we have already pointed out, our analysis describes competition between the amplification of oscillations due to cooling and damping of oscillations caused by resonance absorption. We found that the magnetic tube expansion enhances the amplification. As a result, when there is no resonant absorption the larger the tube expansion the faster the oscillation amplitude grows. When resonant absorption is present, the larger the tube expansion the slower the oscillation amplitude decays. For particular values of parameters the tube expansion we even can have the oscillation damping in a non-expanding tube, and the oscillation amplification in an expanding tube.

Another interesting results is that the amplification due to cooling may result in local increase of the amplitude for particular values of parameter, with overall damping of kink oscillation. Those the presence of cooling may be the good candidate for physical mechanism of recently found kink oscillations with varying amplitude profile (see e.g. Pascoe et al., 2016).

Now, we introduce the critical value of α defined by the condition that $A(1) = A(0)$ for $\alpha = \alpha_c$. That means that the oscillation amplitude at $t = t_{cool}$ is equal to its initial amplitude. Similarly, we introduce the critical value of transitional layer thickness, l_c, given by

$$l_c = \frac{4\alpha_c L}{\pi C_f t_{cool}}. \tag{5.67}$$

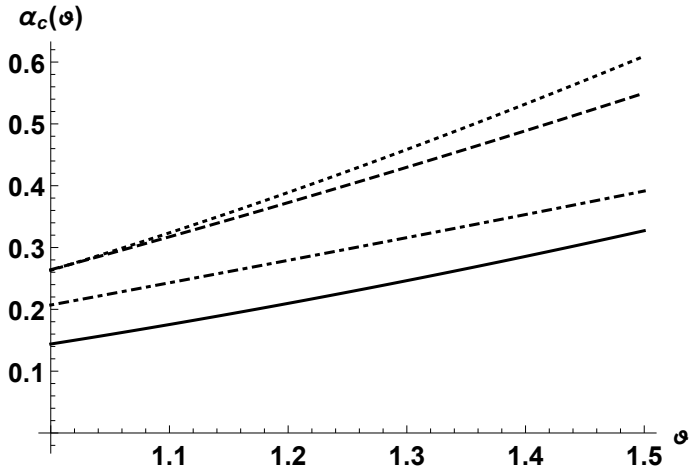

Figure 5.4: Dependence of critical value α_c on expansion factor ϑ. The solid, dotted, dashed, and dash-dotted lines correspond to $\kappa = 0.5$, 1, 1.5, and 2, respectively.

When $l = l_c$ the damping due to resonant absorption is balanced by amplification due to cooling. Figure 5.4 shows the dependence of α_c on ϑ for various values of κ. Again, we see that the tube expansion enhances the effect of the amplitude amplification. What is also interesting, is that the dependence of this effect on κ is not monotonic. The effect increases when κ changes from 0.5 to 1, and then is becoming weaker when κ further increases.

§ 5.4 Summary

Here, we summarise results obtained in Chapter 5. First, we returned to the original equilibrium configuration proposed in Chapter 2. We then used WKB approximation and results presented in Chapter 4. As a result, we obtained jumps of pressure and displacement across transitional layer to close the system of main governing equations. That enabled us to proceed further with the theoretical analysis, to obtain equations for decrement, frequency and time evolution of amplitude of kink oscillations of coronal loops (Equations (5.32) – (5.35)). In case of analogous to Chapter 4 density stratification, the ratio of decrement of kink oscillations to oscillation frequency coincides with one obtained in Chapter 4.

Then we employed the model of loop cross-section variation proposed by Ruderman et al. (2008). That enabled us to numerically solve the Equation (5.34), which describes the time evolution of amplitude. We concluded that the loop expansion acts in favour of oscillation amplification. In the absence of damping due to the resonant absorption, the increase in loop expansion causes the faster growth of the oscillation amplitude. The similar conclusion was obtained in Chapter 3. In case the resonant absorption is present there are three possible scenarios of the oscillation amplitude behaviour. First, coronal loop expansion can reduce the damping rate. Secondly, expansion can balance out the damping, so that the amplitude before and after cooling stays the same. Thirdly, the most interesting result is that loop expansion may amplify the amplitude of loop oscillation, even in the presence of resonant absorption. These results have a particular interest to the coronal seismology. First of all, it presents that cooling is a good candidate for a mechanisms for the recently observed non-damped and amplified kink oscillations of cooling coronal loops. Secondly, it suggests that expansion and the ratio of tube length to scale height have significant effect on the amplitude profile for kink oscillations and thus have a particular importance to be taken in consideration. Finally, this model allows to obtain the estimate for the length of the transitional layer for various profiles of a kink oscillations amplitude evolution.

We introduced the relative strength of resonant damping and amplification caused by cooling. Then we defined its critical value for which the oscillation amplitude before and after cooling does not change. Finally, we numerically found the dependence of this critical value on the expansion factor. We concluded that increase in expansion factor amplifies the critical value of the relative strength of resonant damping and amplification caused by cooling.

Chapter 6

Conclusion

§ 6.1 Summary

This thesis is built on my earlier works published as Ruderman et al. (2017), Shukhobodskiy and Ruderman (2018), and Shukhobodskiy et al. (2018). Chapter 2 and 3 are mainly based on Ruderman et al. (2017). Chapter 4 is mainly based on Shukhobodskiy and Ruderman (2018). Finally Chapter 5 is based on Shukhobodskiy et al. (2018). In this thesis we studied kink oscillations of coronal loops. The plasma structure was considered as straight cylindrical magnetic flux tube with a background flow inside them. The magnetic flux tube was divided in core and transitional region of thickness l. In the transitional region the density was assumed to decrease from a higher value inside the tube to the lower value in surrounding plasma. This model was studied throughout this thesis analytically and numerically.

In Chapter 2 we derived the main governing equations of this thesis. Equations (2.75) and (2.76) are used throughout this thesis to study various effects on kink oscillations of magnetic flux tube, such as damping of oscillation amplitude due to resonant absorption, oscillation amplitude amplification during the cooling process and the effect of background flow on oscillation frequency and amplitude.

Note that we only kept terms of the order of the constant determining the thickness of transitional layer, $l \ll 1$, when deriving Equation (2.76), while we neglected terms of higher order with respect to l. When there is no transitional layer ($l = 0$) we have $\mathcal{L} = 0$ and Equation (2.75) governs the kink oscillations of a thin expanding magnetic tube with a background field-aligned flow. However, in the presence of the transitional layer the system of Equations (2.75) and (2.76) is not closed. To close the system one needs to express the jump of plasma displacement across transitional layer divided by the tube radius, $\delta\eta$, and the jump of plasma pressure across the transitional layer, δP, in terms of plasma displacement of the magnetic flux tube boundary divide by its radius η.

When there is no flow ($U = 0$) and no transitional region ($l = 0$) Equation (2.75) reduces to the equation describing the kink oscillations of a thin expanding magnetic tube derived by Ruderman et al. (2008). On the other hand, when there is no expansion ($R = \text{const}$), Equations (2.75) and (2.76) reduce to Equations (23) and (24) in Ruderman (2011a) describing resonantly damped kink oscillations of a thin magnetic tube with non-stationary density and flow. Note that the expression for $\mathcal{L}$ given by Equation (2.76) is slightly different from that given by Equations (24) in Ruderman (2011a). However, it is straightforward to show using Equation (2.75) that the difference between $R\mathcal{L}$ with $\mathcal{L}$ given by Equation (2.76) and $\mathcal{L}$ given by Equations (24) in Ruderman (2011a) is of the order of l^2.

In Chapter 3 we used the governing equations derived in Chapter 2 to study the effect of background flow on kink oscillations. We assumed that there is no transitional layer, which implies that the oscillations are described by Equation (2.75). First we studied the general properties of the eigenvalue problem governing the kink oscillations and proved that the frequencies of all eigenmodes are real. Then, we numerically studied the effect of siphon flows on the fundamental frequency and on the ratio of the frequencies of the first overtone and fundamental mode of kink oscillations of a

loop with a half-circle shape. The general conclusion is that the effect of a realistic background flow, with flow speed not exceeding 100 kms^{-1}, is weak (see e.g. Schrijver, 2001). Depending on the tube and flow parameters, the background flow can either increase or decrease both the fundamental frequency and the ratio of the frequencies of the first overtone and fundamental mode of kink oscillations of a loop. An interesting result is that for sufficiently strong tube expansion the ratio of frequencies exceeds two. This result is related to the fact that the tube expansion reduces the magnitude of the magnetic field. For sufficiently strong tube expansion this reduction of the magnetic field magnitude dominates the decrease of the density with height due to gravitational stratification. As a result, the kink speed decreases from its value of the tube footpoint to its apex.

Then we used the WKB method to derive the expression for adiabatic invariant, which is the quantity that is conserved while the plasma density changes. We assumed that the plasma density inside the loop depends exponentially. Then we numerically calculated the time dependence of the fundamental mode frequency, the ratio of frequencies of the first overtone and fundamental mode, and the oscillation amplitude.

The numerical results can be summarised as follows. Cooling causes an increase in the oscillation frequency and a decrease in the ratio of frequencies of the first overtone and fundamental mode. This is a generalisation of the results previously obtained by Morton and Erdélyi (2009, 2010) and Ruderman (2011b). Cooling also causes the enhancement of the oscillation amplitude. Previously, this result was obtained by Ruderman (2011b) for non-expanding loops. The amplitude enhancement due to cooling becomes stronger when the loop expansion increases. This effect is more pronounced for longer loops. However, amplitude enhancement due to cooling is very moderate even for loops where the height is equal to the two times the initial atmospheric scale height.

In Chapter 4, we studied resonant damping of kink oscillations of thin expanding and stratified magnetic flux tubes. Our analysis is based on the equations describing kink oscillations of expanding flux tubes derived by in Chapter 2. This system is not closed because it contains the jumps of the magnetic pressure and plasma displacement across the transitional layer where the plasma density decreases from its value in the tube core region to that in the surrounding plasma. We derived expressions for these quantities thus closing the system.

We used the obtained jumps across the transitional layer to calculate the decrements of eigenmodes of the tube kink oscillations. We generalised the definition of homogeneous stratification formulated by Dymova and Ruderman (2006a). We defined homogeneous stratification as the condition that the ratio of densities in the tube core region and outside the tube does not vary along the tube, and the density in the transitional layer can be factorised and written as a product of two function, one depending on the coordinate along the tube and the other depending on the magnetic flux function. Although at first sight this assumption looks artificial, in fact it is quite viable. If the temperature does not change across the tube and in its vicinity, then the density variation along a magnetic line in the tube and in its vicinity is the same along this arbitrary line, while its absolute value can change from line to line. The main result

is that, under the assumption of homogeneous stratification, the ratio of decrement and oscillation frequency is independent of a particular form of the density and tube cross-section radius variation along the tube, and it is also the same for any oscillation eigenmode. This result has an important implication for coronal seismology. The finding enables us not to care about the coronal loop expansions and density variation along the loops when using the observed damping of kink oscillations to obtain information about the radial structure of the loops.

In Chapter 5, we studied the process of resonant damping of kink oscillations of cooling coronal magnetic loops. A coronal magnetic loop is modelled by a thin straight magnetic tube with the plasma density and the cross-section radius varying along the tube. The equilibrium plasma density is approximately independent of the radial coordinate inside the core of the tube and outside of the tube. However, it varies in the radial direction from its value in the core region to its value outside of the tube in a thin transitional layer. This density variation results in the presence of resonant absorption. We use the system of two equations describing oscillations of non-stationary magnetic tubes in the presence of resonance absorption in the thin tube approximation that were derived by Ruderman et al. (2017). This system contains three dependent variables: the tube displacement η, the jumps of the plasma displacement and the magnetic pressure perturbation across the transitional layer in a cold plasma.

The system is not closed. To close it, we need to express the jumps of the plasma displacement and the magnetic pressure perturbation in terms of η. Shukhobodskiy and Ruderman (2018) has done this. The derivation of jumps was shown in Chapter 4 in the case of static magnetic tubes, under the assumption that the density in the transitional layer can be factorised and written as a product of two functions, one depending on the coordinate along the tube and the other depending on the magnetic flux function. However, we cannot make this assumption here, when a loop is dynamic, because even if the condition is initially satisfied it will not be valid later because the density is changing with time. Hence, we adapted the derivation given by Shukhobodskiy and Ruderman (2018) and shown in Chapter 4. Eventually, we derived Equation (5.34) describing the evolution of the oscillation amplitude. In the absence of transitional layer Equation (5.34) reduces to the conservation of an adiabatic invariant previously derived by Ruderman et al. (2017). The derivation was also shown in Chapter 3, where there is no resonant absorption.

We studied the evolution of amplitude of kink oscillation of a cooling coronal magnetic loop. The cooling causes the amplification of loop oscillation, while resonant absorption causes its decay. Hence, the governing equation for the oscillation amplitude describes the competition between the amplification and damping. This equation was solved numerically. There are numerous observations of expanding coronal loops. However the effect of expansion is not fully understood. Our main aim was to study the effect of the loop expansion on the evolution of the amplitude of transversal oscillations. We found that the loop expansion acts in favour of oscillation amplification. When there is no damping due to resonant absorption the larger the loop expansion the faster the oscillation amplitude growths. If resonant absorption is present then the loop expansion either reduces the damping rate, or even can turn it into the amplification

of oscillation.

We also considered the possibility of oscillations that are not amplified and also do not decay. We define such oscillations as those with the amplitude at the cooling time $t_{\rm cool}$ equal to its initial value. In this case, there is the balance between the amplification due to cooling and decay due to resonant absorption. Again, we found that the loop expansion acts in favour of amplification. As a result, the larger the loop expansion the stronger resonant absorption can be counterbalanced by cooling with the same cooling rate.

§ 6.2 Discussion

In this thesis we studied kink oscillation of straight magnetic flux tube in a presence of bulk flow. There are several possibilities to improve such a model which we considered here. As we know from observations, the coronal loops are not straight magnetic flux tubes. This is one of simplifications used to be able to proceed with theoretical results more easily. The simplification is in agreement with some observations. However, Dymova and Ruderman (2006b) showed that the effect of the geometry on the ratio of periods of the fundamental mode and first overtone is considerable for the non-expanding magnetic flux tube with circular shape. Therefore, it will be interesting to understand how the expansion of cross-section will affect kink oscillations for various geometrical shapes of the magnetic flux tube. For example we may consider the same model, however instead of the straight magnetic flux tube we may consider half-circular shape of an expanding coronal loop and take into account the effect of gravity.

Another option is to consider the different shape of coronal loop cross-section. In this thesis we considered circular cross-section as its symmetry considerably simplifies theoretical analysis. However, this shape might be not the only one that is applicable for modelling loop oscillations. It will be of great interest to consider also coronal loops of other cross-section shape. One of the options is the elliptic cross-section option (see e.g. Ruderman, 2003). The effect of resonant damping on kink oscillations of such shape for straight non-expanding magnetic flux tube was studied by Ruderman (2003). This study showed that there are only two kink modes and the other are fluting. With one kink mode polarised on semi-major half axis and another polarised on semi-minor half-axis. The decrements of such oscillation is not much different in case the ratio of semi major half axis on semi manor half axis does not exceed 2. As a result, it will be of a great interest to consider elliptic shape of cross-section for expanding tube. Nevertheless, there are several potential difficulties which may arise. First, in case of an elliptic shape, expansion will not only depend on the vertical component of straight magnetic flux tube but also on the azimuthal component. The second difficulty is that the tube is not symmetric, it is not clear what kind of expansion is appropriate to consider. One option is to consider the uniform expansion of cross-section. That means, the expansion which varies in a uniform manner around the original footpoint of a elliptic shape cross-section. Another option is to consider expansion which varies only along the semi-major or semi minor lines of elliptical cross-section.

Finally, observations suggest that some of the coronal loops are magnetically twisted.

Such twist may arise due to electric current moving along the tube. Such a model was firstly introduced by Alfvén (1950). Erdélyi and Fedun (2010) studied propagating magneto-acustic waves in the weakly twisted magnetic flux tubes, for sausage, kink and fluting modes. Erdélyi and Fedun (2010) found out that the fast kink modes of propagting waves under photospheric conditions are either none existent, or very small. One of more recent theoretical results for standing waves include the model introduced by Ruderman (2007). In this model the twist has not affected the ratio of frequencies of fundamental mode on first overtone for standing kink oscillations. In the model proposed by Ruderman and Terradas (2015) twist indeed does affect the ratio of frequencies of fundamental mode on first overtone for standing kink oscillations. Thus, it will be of a particular interest to theoretically analyse the combined effect of magnetic field twist and cross-section expansion of a mangetic flux tube. One of such possibilities is to modify the model proposed in this thesis by adding twist to the background magnetic field. The potential difficulty is that even for the case of straight magnetic flux tube theoretical analysis is complicated. Adding another level of complexity will complicate analysis even further.

References

Abedini, A. (2018). Observations of Excitation and Damping of Transversal Oscillations in Coronal Loops by AIA/SDO. *Solar Physics*, 293:22.

Al-Ghafri, K. S., Ruderman, M. S., Williamson, A., and Erdélyi, R. (2014). Longitudinal Magnetohydrodynamics Oscillations in Dissipative, Cooling Coronal Loops. *The Astrophysical Jouranl*, 786:36.

Alfvén, H. (1950). Discussion of the Origin of the Terrestrial and Solar Magnetic Fields. *Tellus*, 2:74–82.

Anfinogentov, S., Nisticò, G., and Nakariakov, V. M. (2013). Decay-less kink oscillations in coronal loops. *Astronomy & Astrophysics*, 560:A107.

Aschwanden, M. J., Fletcher, L., Schrijver, C. J., and Alexander, D. (1999). Coronal Loop Oscillations Observed with the Transition Region and Coronal Explorer. *The Astrophysical Jouranl*, 520:880–894.

Aschwanden, M. J. and Schrijver, C. J. (2011). Coronal Loop Oscillations Observed with Atmospheric Imaging AssemblyKink Mode with Cross-sectional and Density Oscillations. *The Astrophysical Journal*, 736:A102.

Aschwanden, M. J. and Terradas, J. (2008). The Effect of Radiative Cooling on Coronal Loop Oscillation. *The Astrophysical Journal*, 686:L127–L130.

Bender, C. M. and Orszag, S. A. (1978). *Advanced Mathematical Methods for Scientists and Engineers*. New York: McGraw-Hill, 1978.

Braginskii, S. I. (1965). A reinterpretation of the energy balance in active region loops following new results from Hinode EIS. *Review Plasma Physics*, 1:205–210.

Chae, J., Ahn, K., Lim, E.-K., Choe, G. S., and Sakurai, T. (2008). Persistent Horizontal Flows and Magnetic Support of Vertical Threads in a Quiescent Prominence. *The Astrophysical Journall*, 689:L73.

Coddington, E. A. and Levinson, N. (1955). *Theory of Ordinary Differential Equations*. New York: McGraw-Hill.

Duckenfield, T., Anfinogentov, S. A., Pascoe, D. J., and Nakariakov, V. M. (2018). Detection of the Second Harmonic of Decay-less Kink Oscillations in the Solar Corona. *The Astrophysical Journal*, 854:L5.

Dymova, M. V. and Ruderman, M. S. (2005). Non-Axisymmetric Oscillations of Thin Prominence Fibrils. *Solar Physics*, 229:79–94.

Dymova, M. V. and Ruderman, M. S. (2006a). Resonantly damped oscillations of longitudinally stratified coronal loops. *Astronomy & Astrophysics*, 457:1059–1070.

Dymova, M. V. and Ruderman, M. S. (2006b). The geometry effect on transverse oscillations of coronal loops. *Astronomy & Astrophysics*, 459:241–244.

Eddy, J., Ise, R., and Center, G. C. M. S. F. (1979). *A New Sun: The Solar Results from Skylab*. NASA SP. Scientific and Technical Information Office, National Aeronautics and Space Administration.

Edwin, P. M. and Roberts, B. (1983). Wave propagation in a magnetic cylinder. *Solar Physics*, 88:179–191.

Erdélyi, R., Ballai, I., and Goossens, M. (2001). Nonlinear resonant absorption of fast magnetoacoustic waves due to coupling into slow continua in the solar atmosphere. *Astronomy & Astrophysics*, 368:662–675.

Erdélyi, R. and Fedun, V. (2010). Magneto-Acoustic Waves in Compressible Magnetically Twisted Flux Tubes. *Solar Physics*, 263:63–85.

Erdélyi, R. and Goossens, M. (1995). Resonant absorption of Alfven waves in coronal loops in visco-resistive MHD. *Astronomy & Astrophysics*, 294:575–586.

Erdélyi, R. and Taroyan, Y. (2008). Hinode EUV spectroscopic observations of coronal oscillations. *Astronomy & Astrophysics*, 489:L49–L52.

Goossens, M., Andries, J., Arregui, I., Doorsselaere, T. V., and Poedts, S. (2005). Solar coronal loop oscillations: theory of resonantly damped oscillations and comparison with observations. *AIP Conference Proceedings*, 784(1):114–128.

Goossens, M., Andries, J., and Aschwanden, M. J. (2002). Coronal loop oscillations. An interpretation in terms of resonant absorption of quasi-mode kink oscillations. *Astonomy & Astrophysics*, 394:L39–L42.

Goossens, M., Erdélyi, R., and Ruderman, M. S. (2011). Resonant MHD waves in the solar atmosphere. *Space Science Review*, 158:289–338.

Goossens, M., Hollweg, J. V., and Sakurai, T. (1992). Resonant behaviour of MHD waves on magnetic flux tubes. III - Effect of equilibrium flow. *Solar Physics*, 138:233–255.

Goossens, M., Ruderman, M. S., and Hollweg, J. V. (1995). Dissipative MHD solutions for resonant Alfven waves in 1- dimensional magnetic flux tubes. *Solar Physics*, 157:75–102.

Hollweg, J. V. and Yang, G. (1988). Resonant-absorption of compressible magnetohydrodynamic waves at thin surfaces. *Computer Phys. Rep.*, 93:5423–5436.

Klimchuk, J. A. (2000). Cross-sectional properties of coronal loops. 193:53–75.

Korn, G. and Korn, T. (1961). *Mathematical Handbook for Scientists and Engineers*. New York: McGraw-Hill.

Morton, R. J. and Erdélyi, R. (2009). Transverse Oscillations of a Cooling Coronal Loop. *The Astrophysical Journal*, 707:750–760.

Morton, R. J. and Erdélyi, R. (2010). Application of the theory of damping of kink oscillations by radiative cooling of coronal loop plasma. *Astronomy & Astrophysics*, 519:A43.

Naimark, M. A. (1967). *Linear Differential Equations, Part I*. New York: Frederic Ungar Publ. Co.

Nakariakov, V. M., Ofman, L., Deluca, E. E., Roberts, B., and Davila, J. M. (1999). TRACE observation of damped coronal loop oscillations: Implications for coronal heating. *Science*, 285:862–864.

Nisticò, G., Nakariakov, V. M., and Verwichte, E. (2013). Decaying and decayless transverse oscillations of a coronal loop. *Astronomy & Astrophysics*, 552:A57.

Ofman, L., Davila, J. M., and Steinolfson, R. S. (1994). Coronal heating by the resonant absorption of Alfven waves: The effect of viscous stress tensor. *The Astrophysical Journal*, 421:360–371.

Ofman, L. and Wang, T. J. (2008). Hinode observations of transverse waves with flows in coronal loops. *Astronomy & Astrophysics*, 482:L9–L12.

Pascoe, D. J., Goddard, C. R., and Nakariakov, V. M. (2016). Spatially resolved observation of the fundamental and second harmonic standing kink modes using SDO/AIA. *Astronomy & Astrophysics*, 593:A53.

Priest, E. (2014). *Magnetohydrodynamics of the Sun*. Cambridge, UK: Cambridge University Press.

Priest, E. R. (1999). Heating the solar corona by magnetic reconnection. In Büchner, J., Axford, I., Marsch, E., and Vasyliūnas, V., editors, *Plasma Astrophysics And Space Physics*, pages 77–100, Dordrecht. Springer Netherlands.

Roberts, B. (2000). Waves and oscillations in the corona – (invited review). *Solar Physics*, 193(1):139–152.

Ruderman, M. S. (2003). The resonant damping of oscillations of coronal loops with elliptic cross-sections. *Astronomy & Astrophysics*, 409:287–297.

Ruderman, M. S. (2007). Nonaxisymmetric Oscillations of Thin Twisted Magnetic Tubes. *Solar Physics*, 246:119–131.

Ruderman, M. S. (2010). The Effect of Flows on Transverse Oscillations of Coronal Loops. *Solar Physics*, 267:377–391.

Ruderman, M. S. (2011a). Resonant damping of kink oscillations of cooling coronal magnetic loops. *Astronomy & Astrophysics*, 534:A78.

Ruderman, M. S. (2011b). Transverse Oscillations of Coronal Loops with Slowly Changing Density. *Solar Physics*, 271:41–54.

Ruderman, M. S. and Erdélyi, R. (2009). Transverse Oscillations of Coronal Loops. *Space Science Reviews*, 149:199–228.

Ruderman, M. S., Petrukhin, N. S., and Pelinovsky, E. (2016). On the Ratio of Periods of the Fundamental Harmonic and First Overtone of Magnetic Tube Kink Oscillations. *Solar Physics*, 291:1143–1157.

Ruderman, M. S. and Roberts, B. (2002). The Damping of Coronal Loop Oscillations. *Astrophysical Journal*, 577:475–486.

Ruderman, M. S., Shukhobodsky, A. A., and Erdélyi (2017). Kink oscillations of cooling coronal loops with variable cross-section. *Astronomy & Astrophysics*, 602:A50.

Ruderman, M. S. and Terradas, J. (2015). Standing kink oscillations of thin twisted magnetic tubes with continuous equilibrium magnetic field. *Astronomy & Astrophysics*, 580:A57.

Ruderman, M. S., Tirry, W., and Goossens, M. (1995). Non-stationary resonant Alfvén surface waves in one-dimensional magnetic plasmas. *Journal of Plasma Physics*, 54:129–148.

Ruderman, M. S., Verth, G., and Erdélyi, R. (2008). Transverse Oscillations of Longitudinally Stratified Coronal Loops with Variable Cross Section. *The Astrophysical Journal*, 686:694–700.

Ryutov, D. D. and Ryutova, M. P. (1976). Sound oscillations in a plasma with "magnetic filaments". *Sov. Phys. – JETP*, 43:491–000.

Sakurai, H., Goossens, S., and Hollweg, Y. (1991). Resonant behaviour of MHD waves on magnetic flux tubes. I - Connection formulae at the resonant surfaces. *Solar Physics*, 133:227–245.

Schrijver, C. J. (2001). Catastrophic cooling and high-speed downflow in quiescent solar coronal loops observed with TRACE. *Solar Physics*, 198:325–345.

Shukhobodskiy, A. A. and Ruderman, M. S. (2018). Resonant damping of kink oscillations of thin expanding magnetic tubes. *Astronomy & Astrophysics*, 615:A156.

Shukhobodskiy, A. A., Ruderman, M. S., and Erdélyi, R. (2018). Resonant damping of kink oscillations of thin cooling and expanding coronal magnetic loops. *Astronomy & Astrophysics*, 619:A173.

Su, W., Guo, Y., Erdélyi, R., Ning, Z. J., Ding, M. D., Cheng, X., and Tan, B. L. (2018). Period Increase and Amplitude Distribution of Kink Oscillation of Coronal Loop. *Nature Scientific Reports*, 8:4471.

Terradas, S., Oliver, R., and Ballester, J. L. (2006). Damping of kink oscillation in curved loops. *Astrophysical Journal*, 650:L91–L94.

Tirry, W. J. and Goossens, M. (1996). Quasi-Modes as Dissipative Magnetohydrodynamic Eigenmodes: Results for One-dimensional Equilibrium States. *The Astrophysical Journal*, 471:501.

Tsuneta, S., Ichimoto, K., Katsukawa, Y., Lites, B. W., Matsuzaki, K., Nagata, S., Orozco Suárez, D., Shimizu, T., Shimojo, M., Shine, R. A., Suematsu, Y., Suzuki, T. K., Tarbell, T. D., and Title, A. M. (2008). The Magnetic Landscape of the Sun's Polar Region. *The Astrophyiscal Journal*, 688:1374–1381.

Van Doorsselaere, T., Debosscher, A., Andries, J., and Poedts, S. (2004). The effect of curvature on quasi-modes in coronal loops. *Astronomy & Astrophysics*, 424:1065–1074.

Van Doorsselaere, T., Nakariakov, V. M., and Verwichte, E. (2007). Coronal loop seismology using multiple transverse loop oscillation harmonics. *Astronomy & Astrophysics*, 473:959–966.

Verth, G. and Erdélyi, R. (2008). Effect of longitudinal magnetic and density inhomogeneity on transversal coronal loop oscillations. *Astronomy & Astrophysics*, 486:1015–1022.

Verwichte, E., Nakariakov, V. M., Ofman, L., and Deluca, E. E. (2004). Characteristics of transverse oscillations in a coronal loop arcade. *Solar Physics*, 223:77–94.

Wang, T., Ofman, L., Davila, J. M., and Su, Y. (2012). Growing Transverse Oscillations of a Multistranded Loop Observed by SDO/AIA. *The Astrophysical Journall*, 751:L27.

Watko, J. A. and Klimchuk, J. A. (2000). Width Variations along Coronal Loops Observed by TRACE. *Solar Physics*, 193:77–93.

Appendices

Appendix A

Derivation of Governing Equation

§ A.1 Total Derivative in Lagrangian representation

Let $\mathbf{a}$ be a position of Lagrangian particle defined by position vector a. The trajectory of this particle is given by $\boldsymbol{x} = \boldsymbol{x}(t, \mathbf{a})$, such that $\boldsymbol{x}(0, \mathbf{a}) = a$. Let us assume that two points have two positions $\mathbf{a}$ and $\mathbf{a} + d\mathbf{a}$. Then

$$\boldsymbol{x} = \boldsymbol{x}(t, \mathbf{a}), \tag{A.1}$$

$$\boldsymbol{x} + d\boldsymbol{x} = \boldsymbol{x}(t, \mathbf{a} + d\mathbf{a}). \tag{A.2}$$

In addition it follows from chain rule that for vector

$$dx_i = \frac{\partial x_i}{\partial a_j} da_j, \tag{A.3}$$

where indices $i, j \in [1, n]$ $\forall n \in \mathbb{N}$ indicate the respectful scalar components of vector. As a result, it follows from Equations (A.1) – (A.3) and the chain rule that,

$$\frac{dx_i}{dt} = \frac{\partial v_i}{\partial a_j} da_j, \tag{A.4}$$

where

$$\mathbf{v} = \frac{\partial \boldsymbol{x}}{\partial t}. \tag{A.5}$$

Therefore, Equation (A.4) can be rewritten as

$$\frac{d(d\boldsymbol{x})}{dt} = (d\boldsymbol{x} \cdot \nabla)\mathbf{v}. \tag{A.6}$$

§ A.2 Transformation of Governing Equations

We define $\xi_\parallel$ and $\xi_\perp$ as

$$\xi_\parallel = \frac{\xi_r B_r + \xi_z B_z}{B}, \tag{A.7}$$

$$\xi_\perp = \frac{\xi_r B_z - \xi_z B_r}{B}. \tag{A.8}$$

Thus, following definitions in Chapter 2 we have from Equations (A.7) and (A.8) that

$$\boldsymbol{\xi} = \xi_\perp \left(\hat{\boldsymbol{\phi}} \times \boldsymbol{b}_0\right) + \xi_\phi \hat{\boldsymbol{\phi}} + \xi_\parallel \boldsymbol{b}_0 \tag{A.9}$$

and

$$\boldsymbol{\xi}_1 = \xi_\perp \left(\hat{\boldsymbol{\phi}} \times \boldsymbol{b}_0\right) + \xi_\phi \hat{\boldsymbol{\phi}}, \tag{A.10}$$

where $\hat{\boldsymbol{\phi}}$ is the unit vector in the azimuthal direction. Also, rearranging (A.9) and (A.10), we have

$$\xi_r = \xi_\parallel b_{0r} + \xi_\perp b_{0z} \tag{A.11}$$

and

$$\xi_z = \xi_\parallel b_{0z} - \xi_\perp b_{or}. \tag{A.12}$$

Similarly for the parallel and perpendicular components of the velocity change $\boldsymbol{u}$ are

$$u_\parallel = \frac{u_r B_r + u_z B_z}{B} \tag{A.13}$$

and

$$u_\perp = \frac{u_r B_z - u_z B_r}{B}. \tag{A.14}$$

Therefore, we obtain from Equations (A.13) and (A.14) that

$$\boldsymbol{u} = u_\perp \left(\hat{\boldsymbol{\phi}} \times \boldsymbol{b}_0\right) + u_\phi \hat{\boldsymbol{\phi}} + u_\parallel \boldsymbol{b}_0 \tag{A.15}$$

and we define

$$\boldsymbol{u}_1 = u_\perp \left(\hat{\boldsymbol{\phi}} \times \boldsymbol{b}_0\right) + u_\phi \hat{\boldsymbol{\phi}}, \tag{A.16}$$

Then, rewriting Equations (A.13) and (A.14), yields

$$u_r = u_\parallel b_{0r} + u_\perp b_{0z} \tag{A.17}$$

and

$$u_z = u_\parallel b_{0z} - u_\perp b_{0r}. \tag{A.18}$$

Applying Equations (A.11) and (A.12) on terms on the right hand side of Equation (2.16), we have

$$\xi_\parallel (\nabla \cdot \boldsymbol{U}) = \xi_\parallel \left(\frac{1}{r}\frac{\partial r U_r}{\partial r} + \frac{\partial U_z}{\partial z}\right), \tag{A.19}$$

$$U\left(\nabla\cdot\boldsymbol{\xi}\right)=U\Bigg[\frac{1}{r}\frac{\partial}{\partial r}\left(r\left(b_{0z}\xi_{\perp}+\xi_{\parallel}b_{0r}\right)\right)+\frac{1}{r}\frac{\partial\xi_{\phi}}{\partial\phi}+\frac{\partial}{\partial z}\left(\xi_{\parallel}b_{0z}-\xi_{\perp}b_{0r}\right)\Bigg] \tag{A.20}$$

and

$$\frac{1}{B}\nabla\cdot\left(BU\boldsymbol{\xi}_{1}\right)=\frac{1}{B}\Bigg[\frac{1}{r}\frac{\partial}{\partial r}\left(rB_{z}U\xi_{\perp}\right)+\frac{BU}{r}\frac{\partial\xi_{\phi}}{\partial\phi}-\frac{\partial}{\partial z}\left(B_{r}U\xi_{\perp}\right)\Bigg]. \tag{A.21}$$

Therefore, using Equations (A.19) – (A.21), Equation (2.17) becomes

$$\begin{aligned}\frac{\partial\xi_{\parallel}}{\partial t}=&\frac{1}{B}\Bigg[\frac{1}{r}\frac{\partial}{\partial r}\left(rB_{z}U\xi_{\perp}\right)+\frac{BU}{r}\frac{\partial\xi_{\phi}}{\partial\phi}-\frac{\partial}{\partial z}\left(B_{r}U\xi_{\perp}\right)\Bigg]\\&+\xi_{\parallel}\left(\frac{1}{r}\frac{\partial(rU_{r})}{\partial r}+\frac{\partial U_{z}}{\partial z}\right)-U\Bigg[\frac{1}{r}\frac{\partial}{\partial r}\left(r\left(b_{0z}\xi_{\perp}+\xi_{\parallel}b_{0r}\right)\right)\\&+\frac{1}{r}\frac{\partial\xi_{\phi}}{\partial\phi}+\frac{\partial}{\partial z}\left(\xi_{\parallel}b_{0z}-\xi_{\perp}b_{0r}\right)\Bigg].\end{aligned} \tag{A.22}$$

Then, rewriting Equation (A.22) yields

$$\begin{aligned}\frac{\partial\xi_{\parallel}}{\partial t}=&b_{0z}\frac{\partial(U_{0}\xi_{\perp})}{\partial r}+\frac{U_{0}\xi_{\perp}}{B_{0}r}\frac{\partial(rB_{0z})}{\partial r}+\frac{U_{0}}{r}\frac{\partial\xi_{\phi}}{\partial\phi}-b_{0r}\frac{\partial(U_{0}\xi_{\perp})}{\partial z}\\&-\frac{U_{0}\xi_{\perp}}{B_{0}}\frac{\partial B_{0r}}{\partial z}+\xi_{\parallel}\left(\frac{1}{r}\frac{\partial(rU_{r})}{\partial r}+\frac{\partial U_{z}}{\partial z}\right)-\frac{U_{0}\xi_{\perp}}{r}\frac{\partial(rb_{0z})}{\partial r}-b_{0z}U_{0}\frac{\partial\xi_{\perp}}{\partial r}\\&-\frac{U_{0}}{r}\frac{\partial(r\xi_{\parallel}b_{0r})}{\partial r}-\frac{U_{0}}{r}\frac{\partial\xi_{\phi}}{\partial\phi}-U_{0}\frac{\partial(\xi_{\parallel}b_{0z})}{\partial z}+U_{0}\xi_{\perp}\frac{\partial b_{0r}}{\partial z}+U_{0}b_{0r}\frac{\partial\xi_{\perp}}{\partial z}.\end{aligned} \tag{A.23}$$

Expanding Equation (A.23) we obtain

$$\begin{aligned}\frac{\partial\xi_{\parallel}}{\partial t}=&b_{0z}\xi_{\perp}\frac{\partial U}{\partial r}+b_{0z}U\frac{\partial\xi_{\perp}}{\partial r}+\frac{U\xi_{\perp}b_{0z}}{B}\frac{\partial B}{\partial r}+\frac{U\xi_{\perp}}{r}\frac{\partial(rb_{0z})}{\partial r}\\&-\xi_{\perp}b_{0r}\frac{\partial U}{\partial z}-Ub_{0r}\frac{\partial\xi_{\perp}}{\partial z}-U_{0}\xi_{\perp}\frac{\partial b_{0r}}{\partial z}-\frac{U\xi_{\perp}b_{0r}}{B}\frac{\partial B}{\partial z}\\&+\xi_{\parallel}\left(\frac{1}{r}\frac{\partial(rU_{r})}{\partial r}+\frac{\partial U_{z}}{\partial z}\right)-\frac{U\xi_{\perp}}{r}\frac{\partial(rb_{0z})}{\partial r}-b_{0z}U\frac{\partial\xi_{\perp}}{\partial r}-\frac{U\xi_{\parallel}}{rB}\frac{\partial(rB_{r})}{\partial r}\\&-UB_{r}\frac{\partial}{\partial r}\left(\frac{\xi_{\parallel}}{B}\right)-\frac{U\xi_{\parallel}}{B}\frac{\partial B_{z}}{\partial z}-UB_{z}\frac{\partial}{\partial z}\left(\frac{\xi_{\parallel}}{B}\right)+U_{0}\xi_{\perp}\frac{\partial b_{0r}}{\partial z}\\&+U_{0}b_{0r}\frac{\partial\xi_{\perp}}{\partial z}.\end{aligned} \tag{A.24}$$

Then, applying Equations (2.12) and (2.12) on Equation (A.24), we have

$$\begin{aligned}\frac{\partial\xi_{\parallel}}{\partial t}=&\frac{\xi_{\perp}}{B_{0}}\left(b_{0z}\frac{\partial}{\partial r}(BU)-b_{0r}\frac{\partial}{\partial z}(BU)\right)\\&-U^{2}\left[b_{or}\frac{\partial}{\partial r}\left(\frac{\xi_{\parallel}}{U}\right)+b_{0z}\frac{\partial}{\partial z}\left(\frac{\xi_{\parallel}}{U}\right)\right].\end{aligned} \tag{A.25}$$

Now, employing Equations (A.11) and (A.12) on Equation (2.25), it follows that magnetic pressure perturbation is described by

$$P = -\frac{1}{\mu_0 r}\frac{\partial}{\partial r}\left(rB_z w\right) - \frac{B^2}{\mu_0 r}\frac{\partial \xi_\phi}{\partial \phi} + \frac{1}{\mu_0}\frac{\partial}{\partial z}\left(B_r w\right), \tag{A.26}$$

where $w = B_0\xi_\perp$.

Let us consider the right-hand side of equation (2.26). Rewriting it in cylindrical coordinates, we obtain

$$\boldsymbol{\xi} \times \boldsymbol{B} = \xi_\phi B_z \hat{\boldsymbol{r}} - \xi_\perp B\hat{\boldsymbol{\phi}} - \xi_\phi B_r \hat{\boldsymbol{z}}, \tag{A.27}$$

where $\hat{\boldsymbol{r}}$ is a unit vector in radial direction and $\hat{\boldsymbol{z}}$ is a unit vector in z direction. It follows from equation (A.27) that

$$\begin{aligned}\nabla \times (\boldsymbol{\xi} \times \boldsymbol{B}) = &\left(-\frac{B_r}{r}\frac{\partial \xi_\phi}{\partial \phi} + \frac{\partial w}{\partial z}\right)\hat{\boldsymbol{r}} + \left(\frac{\partial(\xi_\phi B_z)}{\partial z} + \frac{\partial(\xi_\phi B_r)}{\partial r}\right)\hat{\boldsymbol{\phi}} \\ &- \frac{1}{r}\left(\frac{\partial(rw)}{\partial r} + B_z\frac{\partial \xi_\phi}{\partial \phi}\right)\hat{\boldsymbol{z}}.\end{aligned} \tag{A.28}$$

Taking curl of Equation (A.28), yields

$$\begin{aligned}\nabla \times \nabla \times (\boldsymbol{\xi} \times \boldsymbol{B}) = &\left[\frac{1}{r}\frac{\partial}{\partial \phi}\left(-\frac{1}{r}\left(\frac{\partial}{\partial r}(rw) + B_z\frac{\partial \xi_\phi}{\partial \phi}\right)\right) - \frac{\partial}{\partial z}\left(\frac{\partial(\xi_\phi B_z)}{\partial z}\right.\right. \\ &\left.\left. + \frac{\partial(\xi_\phi B_r)}{\partial r}\right)\right]\hat{\boldsymbol{r}} + \left[\frac{\partial}{\partial z}\left(-\frac{1}{r}\frac{\partial(\xi_\phi B_r)}{\partial \phi} + \frac{\partial w}{\partial z}\right)\right. \\ &\left. + \frac{\partial}{\partial r}\left(\frac{1}{r}\left(\frac{\partial}{\partial r}(rw) + B_z\frac{\partial \xi_\phi}{\partial \phi}\right)\right)\right]\hat{\boldsymbol{\phi}} \\ &+ \frac{1}{r}\left[\frac{\partial}{\partial r}\left(r\left(\frac{\partial(\xi_\phi B_z)}{\partial z} + \frac{\partial(\xi_\phi B_r)}{\partial r}\right)\right)\right. \\ &\left. - \frac{\partial}{\partial \phi}\left(-\frac{1}{r}\frac{\partial(\xi_\phi B_r)}{\partial \phi} + \frac{\partial w}{\partial z}\right)\right]\hat{\boldsymbol{z}}.\end{aligned} \tag{A.29}$$

Considering the $\hat{\boldsymbol{r}}$ component term of Equation (A.29) and employing Equations (2.2) and (2.4), we obtain

$$\begin{aligned}&\frac{1}{r}\frac{\partial}{\partial \phi}\left(\frac{1}{r}\left(\frac{\partial}{\partial r}(rw) + B_z\frac{\partial \xi_\phi}{\partial \phi}\right)\right) + \frac{\partial}{\partial z}\left(\frac{\partial(\xi_\phi B_z)}{\partial z} + \frac{\partial(\xi_\phi B_r)}{\partial r}\right) = \\ &\frac{1}{r^2}\left[\frac{\partial}{\partial r}\left(rB\frac{\partial \xi_\perp}{\partial \phi}\right) + B_z\frac{\partial^2 \xi_\phi}{\partial \phi^2}\right] + \frac{\partial}{\partial z}\left(B_r\frac{\partial \xi_\phi}{\partial r} + B_z\frac{\partial \xi_\phi}{\partial z} - \frac{B_r}{r}\xi_\phi\right).\end{aligned} \tag{A.30}$$

Using Equations (2.2) and (2.4) we rewrite the term with $\hat{\boldsymbol{\phi}}$ in Equation (A.29) as follows

$$\begin{aligned}&\frac{\partial}{\partial z}\left[\frac{\partial w}{\partial z} - \frac{B_r}{r}\frac{\partial \xi_\phi}{\partial \phi}\right] + \frac{\partial}{\partial r}\left[\frac{1}{r}\frac{\partial}{\partial r}(rw) + \frac{B_z}{r}\frac{\partial \xi_\phi}{\partial \phi}\right] = \frac{\partial^2 w}{\partial z^2} \\ &+ \frac{\partial}{\partial r}\left(\frac{1}{r}\frac{\partial}{\partial r}(rw)\right) - \frac{B_r}{r}\frac{\partial^2 \xi_\phi}{\partial \phi \partial z} + B_z\frac{\partial}{\partial r}\left(\frac{1}{r}\frac{\partial \xi_\phi}{\partial \phi}\right).\end{aligned} \tag{A.31}$$

Then, using Equation (2.2) and (2.4) on the $\hat{\boldsymbol{z}}$-component term of Equation (A.29), the multiple of $1/r$ in $\hat{\boldsymbol{z}}$ component term becomes

$$\frac{\partial}{\partial r}\left[r\left(\frac{\partial(B_z\xi_\phi)}{\partial z}+\frac{\partial(B_r\xi_\phi)}{\partial r}\right)\right]-\frac{\partial}{\partial\phi}\left[\frac{\partial w}{\partial z}-\frac{B_r}{r}\frac{\partial\xi_\phi}{\partial\phi}\right]= \\ \frac{\partial}{\partial r}\left[r^2B_r\frac{\partial}{\partial r}\left(\frac{\xi_\phi}{r}\right)+rB_z\frac{\partial\xi_\phi}{\partial z}\right]-\frac{\partial^2 w}{\partial\phi\partial z}+\frac{B_r}{r}\frac{\partial^2\xi_\phi}{\partial\phi^2}. \tag{A.32}$$

As a result, it follows from Equations (A.30) – (A.32) that Equation (A.29) turns into

$$\begin{aligned}\nabla\times\nabla\times(\boldsymbol{\xi}\times\boldsymbol{B})=&-\left\{\frac{1}{r^2}\left[\frac{\partial^2(rw)}{\partial\phi\partial r}+B_z\frac{\partial^2\xi_\phi}{\partial\phi^2}\right]+\frac{\partial}{\partial z}\left[rB_r\frac{\partial}{\partial r}\left(\frac{\xi_\phi}{r}\right)\right.\right.\\&\left.\left.+B_z\frac{\partial\xi_\phi}{\partial z}\right]\right\}\hat{\boldsymbol{r}}+\left\{\frac{\partial}{\partial r}\left(\frac{1}{r}\frac{\partial}{\partial r}(rw)\right)+\frac{\partial^2 w}{\partial z^2}\right.\\&+B_z\frac{\partial}{\partial r}\left(\frac{1}{r}\frac{\partial\xi_\phi}{\partial\phi}\right)-\frac{B_r}{r}\frac{\partial^2\xi_\phi}{\partial\phi\partial z}\Big\}\hat{\boldsymbol{\phi}}+\left\{\frac{1}{r}\frac{\partial}{\partial r}\Big[r^2\right.\\&\times B_r\frac{\partial}{\partial r}\left(\frac{\xi_\phi}{r}\right)+rB_z\frac{\partial\xi_\phi}{\partial z}\Big]-\frac{1}{r}\frac{\partial^2 w}{\partial\phi\partial z}\\&\left.+\frac{B_r}{r^2}\frac{\partial^2\xi_\phi}{\partial\phi^2}\right\}\hat{\boldsymbol{z}}.\end{aligned} \tag{A.33}$$

Now, we have

$$\nabla\times\boldsymbol{u}=\left(\frac{1}{r}\frac{\partial u_z}{\partial\phi}-\frac{\partial u_\phi}{\partial z}\right)\hat{\boldsymbol{r}}+\left(\frac{\partial u_r}{\partial z}-\frac{\partial u_z}{\partial r}\right)\hat{\boldsymbol{\phi}}+\frac{1}{r}\left(\frac{\partial(ru_\phi)}{\partial r}-\frac{\partial u_r}{\partial\phi}\right)\hat{\boldsymbol{z}}. \tag{A.34}$$

Considering the $\hat{\boldsymbol{\phi}}$ component term of Equation (A.34) and employing Equations (A.18) and (A.19), we obtain

$$\frac{\partial}{\partial z}\left(\frac{u_\parallel B_r+u_\perp B_z}{B}\right)-\frac{\partial}{\partial r}\left(\frac{u_\parallel B_z-u_\perp B_r}{B}\right)=B_r\Big[r\frac{\partial}{\partial r}\left(\frac{u_\perp}{rB}\right) \\ +\frac{\partial}{\partial z}\left(\frac{u_\parallel}{B}\right)\Big]+B_z\Big[\frac{\partial}{\partial z}\left(\frac{u_\perp}{B}\right)-\frac{\partial}{\partial r}\left(\frac{u_\parallel}{B}\right)\Big]. \tag{A.35}$$

Then, using Equations (2.2), (A.18), (A.19) and (A.35), Equation (A.34) becomes

$$\begin{aligned}\nabla\times\boldsymbol{u}=&\left\{\frac{1}{r}\left(b_{0z}\frac{\partial u_\parallel}{\partial\phi}-b_{0r}\frac{\partial u_\perp}{\partial\phi}\right)-\frac{\partial u_\phi}{\partial z}\right\}\hat{\boldsymbol{r}}+\left\{B_r\Big[r\frac{\partial}{\partial r}\left(\frac{u_\perp}{rB}\right)\right.\\&\left.+\frac{\partial}{\partial z}\left(\frac{u_\parallel}{B}\right)\Big]+B_z\Big[\frac{\partial}{\partial z}\left(\frac{u_\perp}{B}\right)-\frac{\partial}{\partial r}\left(\frac{u_\parallel}{B}\right)\Big]\right\}\hat{\boldsymbol{\phi}}+\frac{1}{r}\left\{\frac{\partial(ru_\phi)}{\partial r}\right.\\&\left.-b_{0r}\frac{\partial u_\parallel}{\partial\phi}-b_{0z}\frac{\partial u_\perp}{\partial\phi}\right\}\hat{\boldsymbol{z}}.\end{aligned} \tag{A.36}$$

It follows from Equations (A.33) and (A.36) that

$$
\begin{aligned}
U\nabla\times\boldsymbol{u}-\frac{B}{\mu_0\rho}\nabla\times\nabla\times(\boldsymbol{\xi}\times\boldsymbol{B}) &= \left\{U\left[\frac{1}{r}\left(b_{0z}\frac{\partial u_{\parallel}}{\partial\phi}-b_{0r}\frac{\partial u_{\perp}}{\partial\phi}\right)-\frac{\partial u_{\phi}}{\partial z}\right)\right] \\
&+\frac{B}{\mu_0\rho}\left[\frac{1}{r^2}\left(\frac{\partial^2(wr)}{\partial\phi\partial r}+B_z\frac{\partial^2\xi_{\phi}}{\partial\phi^2}\right)+\frac{\partial}{\partial z}\left(rB_r\frac{\partial}{\partial r}\left(\frac{\xi_{\phi}}{r}\right)+B_z\frac{\partial\xi_{\phi}}{\partial z}\right]\right\}\hat{\boldsymbol{r}} \\
&+\left\{U\left[B_r\left(r\frac{\partial}{\partial r}\left(\frac{u_{\perp}}{rB}\right)+\frac{\partial}{\partial z}\left(\frac{u_{\parallel}}{B}\right)\right)+B_z\left(\frac{\partial}{\partial z}\left(\frac{u_{\perp}}{B}\right)-\frac{\partial}{\partial r}\left(\frac{u_{\parallel}}{B}\right)\right)\right]\right. \\
&\left.-\frac{B}{\mu_0\rho}\left[\frac{\partial}{\partial r}\left(\frac{1}{r}\frac{\partial(rw)}{\partial r}\right)+\frac{\partial^2 w}{\partial z^2}+B_{0z}\frac{\partial}{\partial r}\left(\frac{1}{r}\frac{\partial\xi_{\phi}}{\partial\phi}\right)-\frac{B_r}{r}\frac{\partial^2\xi_{\phi}}{\partial\phi\partial z}\right]\right\}\hat{\boldsymbol{\phi}} \\
&+\left\{\frac{U}{r}\left[\frac{\partial(ru_{\phi})}{\partial r}-b_{0r}\frac{\partial u_{\parallel}}{\partial\phi}-b_{0z}\frac{\partial u_{\perp}}{\partial\phi}\right]-\frac{B}{\mu_0\rho}\left[\frac{1}{r}\frac{\partial}{\partial r}\left(r^2B_r\frac{\partial}{\partial r}\left(\frac{\xi_{\phi}}{r}\right)\right.\right.\right. \\
&\left.\left.\left.+rB_z\frac{\partial\xi_{\phi}}{\partial z}\right)-\frac{1}{r}\frac{\partial^2 w}{\partial\phi\partial z}+\frac{B_r}{r^2}\frac{\partial^2\xi_{\phi}}{\partial\phi^2}\right]\right\}\hat{\boldsymbol{z}}. \qquad \text{(A.37)}
\end{aligned}
$$

Let

$$
\boldsymbol{Q}=U\nabla\times\boldsymbol{u}-\frac{1}{\mu_0\rho}\nabla\times\nabla\times(\boldsymbol{\xi}\times\boldsymbol{B})\,. \qquad \text{(A.38)}
$$

Then, applying Equation (A.38) on Equation (2.26), we have

$$
\frac{\partial\boldsymbol{u}}{\partial t}=\boldsymbol{b}_0\times\boldsymbol{Q}=-b_{0z}Q_{\phi}\hat{\boldsymbol{r}}+\left(b_{0z}Q_r-b_{0r}Q_z\right)\hat{\boldsymbol{\phi}}+b_{0r}Q_{\phi}\hat{\boldsymbol{z}}. \qquad \text{(A.39)}
$$

Using Equations (2.2), (2.4), (A.37) and (A.38) we rewrite the $\hat{\boldsymbol{\phi}}$ component term of Equation (A.39) as

$$
\begin{aligned}
b_{0z}Q_r-b_{0r}Q_z = U_0\left[\frac{1}{r}\left(\frac{\partial u_{\parallel}}{\partial\phi}-b_{0r}\frac{\partial(ru_{\phi})}{\partial r}\right)-b_{0z}\frac{\partial u_{\phi}}{\partial z}\right]+\frac{B}{\mu_0\rho}\left[\frac{B}{r^2}\frac{\partial^2\xi_{\phi}}{\partial\phi^2}\right. \\
+\frac{b_{0z}}{r^2}\frac{\partial^2(rw)}{\partial\phi\partial r}-\frac{b_{0r}}{r}\frac{\partial^2 w}{\partial\phi\partial z}+\frac{b_{0r}}{r}\frac{\partial}{\partial r}\left(r^2B_{0r}\frac{\partial}{\partial r}\left(\frac{\xi_{\phi}}{r}\right)\right. \\
\left.\left.+rB_z\frac{\partial\xi_{\phi}}{\partial z}\right)+b_{0z}\frac{\partial}{\partial z}\left(rB_r\frac{\partial}{\partial r}\left(\frac{\xi_{\phi}}{r}\right)+B_z\frac{\partial\xi_{\phi}}{\partial z}\right)\right]. \qquad \text{(A.40)}
\end{aligned}
$$

Substituting Equation (A.40) to Equation (A.39), we obtain

$$
\begin{aligned}
\frac{\partial\boldsymbol{u}}{\partial t} = -b_{0z}Q_{\phi}\hat{\boldsymbol{r}}+\left\{U_0\left[\frac{1}{r}\left(\frac{\partial u_{\parallel}}{\partial\phi}-b_{0r}\frac{\partial(ru_{\phi})}{\partial r}\right)-b_{0z}\frac{\partial u_{\phi}}{\partial z}\right]+\frac{B_0}{\mu_0\rho}\left[\frac{B_0}{r^2}\frac{\partial^2\xi_{\phi}}{\partial\phi^2}\right.\right. \\
+\frac{b_{0z}}{r^2}\frac{\partial^2(rw)}{\partial\phi\partial r}-\frac{b_{0r}}{r}\frac{\partial^2 w}{\partial\phi\partial z}+\frac{b_{0r}}{r}\frac{\partial}{\partial r}\left(r^2B_{0r}\frac{\partial}{\partial r}\left(\frac{\xi_{\phi}}{r}\right)+rB_{0z}\frac{\partial\xi_{\phi}}{\partial z}\right) \\
\left.\left.+b_{0z}\frac{\partial}{\partial z}\left(rB_{0r}\frac{\partial}{\partial r}\right)\left(\frac{\xi_{\phi}}{r}+B_{0z}\frac{\partial\xi_{\phi}}{\partial z}\right)\right]\right\}\hat{\boldsymbol{\phi}}+b_{0r}Q_{\phi}\hat{\boldsymbol{z}}. \qquad \text{(A.41)}
\end{aligned}
$$

Next, we assume that $u_{\parallel} = 0$ at $t = 0$. As a result Equation (A.41) can be rewritten as

$$\begin{aligned}\frac{\partial \boldsymbol{u}}{\partial t} = &-b_{0z}\Bigg\{U\left[rB_r\frac{\partial}{\partial r}\left(\frac{u_\perp}{rB}\right) + B_z\frac{\partial}{\partial z}\left(\frac{u_\perp}{B}\right)\right] - \frac{B}{\mu_0\rho}\left[\frac{\partial}{\partial r}\left(\frac{1}{r}\frac{\partial(rw)}{\partial r}\right)\right.\\ &\left.+ \frac{\partial^2 w}{\partial z^2} + B_z\frac{\partial}{\partial r}\left(\frac{1}{r}\frac{\partial \xi_\phi}{\partial \phi}\right) - \frac{B_r}{r}\frac{\partial^2 \xi_\phi}{\partial \phi \partial z}\right]\Bigg\}\hat{\boldsymbol{r}} + \Bigg\{U\left[\frac{-b_{0r}}{r}\frac{\partial(ru_\phi)}{\partial r}\right.\\ &\left.- b_{0z}\frac{\partial u_\phi}{\partial z}\right] + \frac{B}{\mu_0\rho}\left[\frac{B}{r^2}\frac{\partial^2 \xi_\phi}{\partial \phi^2} + \frac{b_{0z}}{r^2}\frac{\partial^2(rw)}{\partial \phi \partial r} - \frac{b_{0r}}{r}\frac{\partial^2 w}{\partial \phi \partial z}\right.\\ &+ \frac{b_{0r}}{r}\frac{\partial}{\partial r}\left(r^2 B_r\frac{\partial}{\partial r}\left(\frac{\xi_\phi}{r}\right) + rB_z\frac{\partial \xi_\phi}{\partial z}\right) + b_{0z}\frac{\partial}{\partial z}\left(rB_{0r}\frac{\partial}{\partial r}\left(\frac{\xi_\phi}{r}\right)\right.\\ &\left.\left.+ B_z\frac{\partial \xi_\phi}{\partial z}\right)\right]\Bigg\}\hat{\boldsymbol{\phi}} + b_{0r}\Bigg\{U\left[rB_r\frac{\partial}{\partial r}\left(\frac{u_\perp}{rB}\right) + B_z\frac{\partial}{\partial z}\left(\frac{u_\perp}{B}\right)\right]\\ &- \frac{B}{\mu_0\rho}\left[\frac{\partial}{\partial r}\left(\frac{1}{r}\frac{\partial(rw)}{\partial r}\right) + \frac{\partial^2 w}{\partial z^2} + B_z\frac{\partial}{\partial r}\left(\frac{1}{r}\frac{\partial \xi_\phi}{\partial \phi}\right) - \frac{B_r}{r}\frac{\partial^2 \xi_\phi}{\partial \phi \partial z}\right]\Bigg\}\hat{\boldsymbol{z}}. \qquad \text{(A.42)}\end{aligned}$$

Expressing Equation (A.42) in components, we obtain

$$\begin{aligned}\frac{\partial u_\phi}{\partial t} = &-U\left[\frac{b_{0r}}{r}\frac{\partial(ru_\phi)}{\partial r} + b_{0z}\frac{\partial u_\phi}{\partial z}\right] + \frac{B}{\mu_0\rho}\left[\frac{B}{r^2}\frac{\partial^2 \xi_\phi}{\partial \phi^2} + \frac{b_{0z}}{r^2}\frac{\partial^2(rw)}{\partial \phi \partial r}\right.\\ &- \frac{b_{0r}}{r}\frac{\partial^2 w}{\partial \phi \partial z} + \frac{b_{0r}}{r}\frac{\partial}{\partial r}\left(r^2 B_r\frac{\partial}{\partial r}\left(\frac{\xi_\phi}{r}\right) + rB_z\frac{\partial \xi_\phi}{\partial z}\right)\\ &\left.+ b_{0z}\frac{\partial}{\partial z}\left(rB_r\frac{\partial}{\partial r}\left(\frac{\xi_\phi}{r}\right) + B_z\frac{\partial \xi_\phi}{\partial z}\right)\right], \qquad \text{(A.43)}\end{aligned}$$

$$\begin{aligned}\frac{\partial u_\perp}{\partial t} = &-U\left[rB_r\frac{\partial}{\partial r}\left(\frac{u_\perp}{rB}\right) + B_z\frac{\partial}{\partial z}\left(\frac{u_\perp}{B}\right)\right] + \frac{B}{\mu_0\rho}\left[\frac{\partial}{\partial r}\left(\frac{1}{r}\frac{\partial(rw)}{\partial r}\right)\right.\\ &\left.+ \frac{\partial^2 w}{\partial z^2} + B_z\frac{\partial}{\partial r}\left(\frac{1}{r}\frac{\partial \xi_\phi}{\partial \phi}\right) - \frac{B_r}{r}\frac{\partial^2 \xi_\phi}{\partial \phi \partial z}\right]. \qquad \text{(A.44)}\end{aligned}$$

Also, by the means of using Equation (2.4), Equation (2.25) becomes

$$P = -\frac{1}{\mu_0}\left(\frac{B_{0z}}{r}\frac{\partial(rw)}{\partial r} + \frac{B_0^2}{r}\frac{\partial \xi_\phi}{\partial \phi} - B_{0r}\frac{\partial w}{\partial z}\right). \qquad \text{(A.45)}$$

Applying Equation (A.45) on Equations (A.43), we obtain

$$\begin{aligned}\frac{\partial u_\phi}{\partial t} = &-U\left[\frac{b_{0r}}{r}\frac{\partial(ru_\phi)}{\partial r} + b_{0z}\frac{\partial u_\phi}{\partial z}\right] + \frac{1}{\rho}\left[-\frac{\partial}{\partial \phi}\left(\frac{P}{r}\right) + \frac{B_r}{r\mu_0}\frac{\partial}{\partial r}\left(r^2 B_r\right.\right.\\ &\left.\left.\times\frac{\partial}{\partial r}\left(\frac{\xi_\phi}{r}\right) + rB_z\frac{\partial \xi_\phi}{\partial z}\right) + \frac{B_z}{\mu_0}\frac{\partial}{\partial z}\left(rB_r\frac{\partial}{\partial r}\left(\frac{\xi_\phi}{r}\right) + B_z\frac{\partial \xi_\phi}{\partial z}\right)\right]. \qquad \text{(A.46)}\end{aligned}$$

Appendix B

WKB Approximation

Here, we show the detailed expansion of the governing Equations (2.75) and (2.76) using Wentzel-Krammers-Brillounin (WKB) method (see, eg. Bender and Orszag, 1978). First, we introduce the scaled magnetic field $\tilde{B} = \epsilon B$, then we rewrite Equations (2.75) and (2.76) as follows

$$\rho_i\left(\frac{\partial}{\partial t} + \frac{U_i}{R^2}\frac{\partial}{\partial z}R^2\right)\left(\frac{\partial \eta}{\partial t} + U_i\frac{\partial \eta}{\partial z}\right) + \rho_e\left(\frac{\partial}{\partial t} + \frac{U_e}{R^2}\frac{\partial}{\partial z}R^2\right)\left(\frac{\partial \eta}{\partial t} + U_e\frac{\partial \eta}{\partial z}\right) - \frac{2\epsilon^{-2}\tilde{B}^2}{\mu_0}\frac{\partial^2 \eta}{\partial z^2} = \mathcal{L}, \tag{B.1}$$

$$\mathcal{L} = \frac{\delta P}{R^2} + \frac{\epsilon^{-2}\tilde{B}^2}{\mu_0}\frac{\partial^2(l\eta + \delta\eta)}{\partial z^2} - \rho_e\left(\frac{\partial}{\partial t} + \frac{U_e}{R^2}\frac{\partial}{\partial z}R^2\right)\left(\frac{\partial}{\partial t} + U_e\frac{\partial}{\partial z}\right) \times (l\eta + \delta\eta). \tag{B.2}$$

In accordance with WKB method, we seek the solution to this Equations (B.1) and (B.2) in the form of

$$\eta = S(t, z)\exp[i\epsilon^{-1}\theta(t)]. \tag{B.3}$$

We expand S in the series

$$S = S_0 + \epsilon S_1 + \cdots . \tag{B.4}$$

Since $\tilde{B} = \epsilon B$, using Equation (2.38), we have $P \sim \epsilon^{-2}$ and thus it follows from Equation (2.73) that $\delta P \sim \epsilon^{-2}$. Substituting Equation (B.3) to Equations (B.1) and (B.2), yields

$$\rho_i\left(\frac{\partial}{\partial t} + \frac{U_i}{R^2}\frac{\partial}{\partial z}R^2\right)\left(\frac{\partial}{\partial t}\left(S(t, z)e^{-i\epsilon^- 1\theta(t)}\right) + U_i\frac{\partial}{\partial z}\left(S(t, z)e^{-i\epsilon^- 1\theta(t)}\right)\right) + \rho_e\left(\frac{\partial}{\partial t} + \frac{U_e}{R^2}\frac{\partial}{\partial z}R^2\right)\left(\frac{\partial}{\partial t}\left(S(t, z)e^{-i\epsilon^- 1\theta(t)}\right) + U_e\frac{\partial}{\partial z}\left(S(t, z)e^{-i\epsilon^{-1}\theta(t)}\right)\right) - \frac{2\epsilon^{-2}\tilde{B}^2}{\mu_0}\frac{\partial^2}{\partial z^2}\left(S(t, z)e^{-i\epsilon^{-1}\theta(t)}\right) = \mathcal{L}, \tag{B.5}$$

$$\mathcal{L} = \frac{\epsilon^{-1}\delta\tilde{P}}{R^2} + \frac{\epsilon^{-2}e^{i\epsilon^{-1}\theta(t)}\tilde{B}^2}{\mu_0}\frac{\partial^2(lS(t,z)+\epsilon\delta\tilde{S})}{\partial z^2}$$
$$- \rho_e e^{i\epsilon^{-1}\theta(t)}\left(\frac{\partial}{\partial t} + \frac{U_e}{R^2}\frac{\partial}{\partial z}R^2\right)\left(\frac{\partial}{\partial t} + U_e\frac{\partial}{\partial z}\right) \times (lS(t,z)+\epsilon\delta\tilde{S}), \tag{B.6}$$

where

$$\delta\eta = \delta S\exp(i\epsilon^{-1}\theta(t)), \quad \delta\tilde{S} = \epsilon^{-1}\delta S, \quad \delta\tilde{P} = \epsilon\delta P. \tag{B.7}$$

We expand the first term (term containing elements with subscript i) of equation (B.5), to obtain

$$\rho_i\left(\frac{\partial}{\partial t} + \frac{U_i}{R^2}\frac{\partial}{\partial z}R^2\right)\left(\frac{\partial}{\partial t}\left(S(t,z)e^{-i\epsilon^{-1}\theta(t)}\right) + U_i\frac{\partial}{\partial z}\left(S(t,z)e^{-i\epsilon^{-1}\theta(t)}\right)\right)$$
$$= \rho_i\Bigg[e^{i\epsilon^{-1}\theta(t)}\frac{\partial^2 S(t,z)}{\partial t^2} + i\epsilon^{-1}e^{i\epsilon^{-1}\theta(t)}\frac{\partial S(t,z)}{\partial t}\frac{\partial\theta(t)}{\partial t}$$
$$- \epsilon^{-2}e^{i\epsilon^{-1}\theta(t)}S(t,z)\left(\frac{\partial\theta(t)}{\partial t}\right)^2 + i\epsilon^{-1}e^{i\epsilon^{-1}\theta(t)}\frac{\partial S(t,z)}{\partial t}\frac{\partial\theta(t)}{\partial t}$$
$$+ i\epsilon^{-1}S(t,z)e^{i\epsilon^{-1}\theta(t)}\frac{\partial^2\theta(t)}{\partial t^2} + e^{i\epsilon^{-1}\theta(t)}\frac{\partial U_i}{\partial t}\frac{\partial S(t,z)}{\partial z}$$
$$+ e^{i\epsilon^{-1}\theta(t)}U_i\frac{\partial^2}{\partial z\partial t}(S(t,z)) + i\epsilon^{-1}e^{i\epsilon^{-1}\theta(t)}U_i\frac{\partial S(t,z)}{\partial z}\frac{\partial\theta(t)}{\partial t}$$
$$+ \frac{2U_i}{R}\frac{\partial R}{\partial z}\left(e^{i\epsilon^{-1}\theta(t)}\frac{\partial S(t,z)}{\partial t} + i\epsilon^{-1}e^{i\epsilon^{-1}\theta(t)}S(t,z)\frac{\partial\theta(t)}{\partial t} + e^{i\epsilon^{-1}\theta(t)}U_i\frac{\partial S(t,z)}{\partial z}\right)$$
$$+ U_i\Bigg(e^{i\epsilon^{-1}\theta(t)}\frac{\partial^2(S(t,z))}{\partial z\partial t} + i\epsilon^{-1}e^{i\epsilon^{-1}\theta(t)}\frac{\partial S(t,z)}{\partial z}\frac{\partial\theta(t)}{\partial t}$$
$$+ e^{i\epsilon^{-1}\theta(t)}\frac{\partial U_i}{\partial z}\frac{\partial S(t,z)}{\partial z} + e^{i\epsilon^{-1}\theta(t)}U_i\frac{\partial^2 S(t,z)}{\partial z^2}\Bigg)\Bigg]. \tag{B.8}$$

Similarly, we expand the second term (term containing elements with subscript e) of Equation (B.5), to obtain

$$\rho_e\left(\frac{\partial}{\partial t} + \frac{U_e}{R^2}\frac{\partial}{\partial z}R^2\right)\left(\frac{\partial}{\partial t}\left(S(t,z)e^{-i\epsilon^{-1}\theta(t)}\right) + U_e\frac{\partial}{\partial z}\left(S(t,z)e^{-i\epsilon^{-1}\theta(t)}\right)\right)$$
$$= \rho_e\Bigg[e^{i\epsilon^{-1}\theta(t)}\frac{\partial^2 S(t,z)}{\partial t^2} + i\epsilon^{-1}e^{i\epsilon^{-1}\theta(t)}\frac{\partial S(t,z)}{\partial t}\frac{\partial\theta(t)}{\partial t}$$

$$
\begin{aligned}
&- \epsilon^{-2} e^{i\epsilon^{-1}\theta(t)} S(t,z) \left(\frac{\partial \theta(t)}{\partial t}\right)^2 + i\epsilon^{-1} e^{i\epsilon^{-1}\theta(t)} \frac{\partial S(t,z)}{\partial t} \frac{\partial \theta(t)}{\partial t} \\
&+ i\epsilon^{-1} S(t,z) e^{i\epsilon^{-1}\theta(t)} \frac{\partial^2 \theta(t)}{\partial t^2} + e^{i\epsilon^{-1}\theta(t)} \frac{\partial U_e}{\partial t} \frac{\partial S(t,z)}{\partial z} \\
&+ e^{i\epsilon^{-1}\theta(t)} U_e \frac{\partial^2}{\partial z \partial t} \left(S(t,z)\right) + i\epsilon^{-1} e^{i\epsilon^{-1}\theta(t)} U_e \frac{\partial S(t,z)}{\partial z} \frac{\partial \theta(t)}{\partial t} \\
&+ \frac{2U_e}{R} \frac{\partial R}{\partial z} \left(e^{i\epsilon^{-1}\theta(t)} \frac{\partial S(t,z)}{\partial t} + i\epsilon^{-1} e^{i\epsilon^{-1}\theta(t)} S(t,z) \frac{\partial \theta(t)}{\partial t} + e^{i\epsilon^{-1}\theta(t)} U_e \frac{\partial S(t,z)}{\partial z} \right) \\
&+ U_e \Bigg(e^{i\epsilon^{-1}\theta(t)} \frac{\partial^2 (S(t,z))}{\partial z \partial t} + i\epsilon^{-1} e^{i\epsilon^{-1}\theta(t)} \frac{\partial S(t,z)}{\partial z} \frac{\partial \theta(t)}{\partial t} \\
&+ e^{i\epsilon^{-1}\theta(t)} \frac{\partial U_e}{\partial z} \frac{\partial S(t,z)}{\partial z} + e^{i\epsilon^{-1}\theta(t)} U_e \frac{\partial^2 S(t,z)}{\partial z^2} \Bigg) \Bigg]. \qquad \text{(B.9)}
\end{aligned}
$$

Finally, expanding Equation (B.6), we have

$$
\begin{aligned}
\mathcal{L} = &\frac{\epsilon^{-1} \delta \tilde{P}}{R^2} + \frac{\epsilon^{-2} l \tilde{B}^2 e^{i\epsilon^{-1}\theta(t)}}{\mu_0} \frac{\partial^2 S(t,z)}{\partial z^2} + \frac{\epsilon^{-1} \tilde{B}^2 e^{i\epsilon^{-1}\theta(t)}}{\mu_0} \frac{\partial^2 \delta \tilde{S}}{\partial z^{\prime 2}} \\
&- \rho_e l \Bigg[e^{i\epsilon^{-1}\theta(t)} \frac{\partial^2 S(t,z)}{\partial t^2} + i\epsilon^{-1} e^{i\epsilon^{-1}\theta(t)} \frac{\partial S(t,z)}{\partial t} \frac{\partial \theta(t)}{\partial t} \\
&- \epsilon^{-2} e^{i\epsilon^{-1}\theta(t)} S(t,z) \left(\frac{\partial \theta(t)}{\partial t}\right)^2 + i\epsilon^{-1} e^{i\epsilon^{-1}\theta(t)} \frac{\partial S(t,z)}{\partial t} \frac{\partial \theta(t)}{\partial t} \\
&+ i\epsilon^{-1} S(t,z) e^{i\epsilon^{-1}\theta(t)} \frac{\partial^2 \theta(t)}{\partial t^2} + e^{i\epsilon^{-1}\theta(t)} \frac{\partial U_e}{\partial t} \frac{\partial S(t,z)}{\partial z} \\
&+ e^{i\epsilon^{-1}\theta(t)} U_e \frac{\partial^2}{\partial z \partial t} \left(S(t,z)\right) + i\epsilon^{-1} e^{i\epsilon^{-1}\theta(t)} U_e \frac{\partial S(t,z)}{\partial z} \frac{\partial \theta(t)}{\partial t} \\
&+ \frac{2U_e}{R} \frac{\partial R}{\partial z} \left(e^{i\epsilon^{-1}\theta(t)} \frac{\partial S(t,z)}{\partial t} + i\epsilon^{-1} e^{i\epsilon^{-1}\theta(t)} S(t,z) \frac{\partial \theta(t)}{\partial t} + e^{i\epsilon^{-1}\theta(t)} U_e \frac{\partial S(t,z)}{\partial z} \right) \\
&+ U_e \Bigg(e^{i\epsilon^{-1}\theta(t)} \frac{\partial^2 (S(t,z))}{\partial z \partial t} + i\epsilon^{-1} e^{i\epsilon^{-1}\theta(t)} \frac{\partial S(t,z)}{\partial z} \frac{\partial \theta(t)}{\partial t} \\
&e^{i\epsilon^{-1}\theta(t)} \frac{\partial U_e}{\partial z} \frac{\partial S(t,z)}{\partial z} + e^{i\epsilon^{-1}\theta(t)} U_e \frac{\partial^2 S(t,z)}{\partial z^2} \Bigg) \Bigg] \\
&- \rho_e \Bigg[\epsilon e^{i\epsilon^{-1}\theta(t)} \frac{\partial^2 \delta \tilde{S}}{\partial t^2} + i e^{i\epsilon^{-1}\theta(t)} \frac{\partial \delta \tilde{S}}{\partial t} \frac{\partial \theta(t)}{\partial t} - \epsilon^{-1} e^{i\epsilon^{-1}\theta(t)} \delta \tilde{S} \left(\frac{\partial \theta(t)}{\partial t}\right)^2 \\
&+ i e^{i\epsilon^{-1}\theta(t)} \frac{\partial \delta \tilde{S}}{\partial t} \frac{\partial \theta(t)}{\partial t} + i e^{i\epsilon^{-1}\theta(t)} \delta \tilde{S} \frac{\partial^2 \theta(t)}{\partial t^2} + e^{i\epsilon^{-1}\theta(t)} \frac{\partial U_e}{\partial t} \frac{\partial \delta \tilde{S}}{\partial z} \\
&+ \epsilon e^{i\epsilon^{-1}\theta(t)} U_e \frac{\partial^2 \delta \tilde{S}}{\partial z \partial t} + i e^{i\epsilon^{-1}\theta(t)} U_e \frac{\partial \delta \tilde{S}}{\partial z} \frac{\partial \theta(t)}{\partial t} + \frac{2U_e}{R} \frac{\partial R}{\partial z} \left(\epsilon e^{i\epsilon^{-1}\theta(t)} \frac{\partial \delta \tilde{S}}{\partial t} \right.
\end{aligned}
$$

$$+ ie^{i\epsilon^{-1}\theta(t)}\delta\tilde{S}\frac{\partial\theta(t)}{\partial t} + \epsilon e^{i\epsilon^{-1}\theta(t)}U_e\frac{\partial\delta\tilde{S}}{\partial z}\Bigg) + U_e\Bigg(\epsilon e^{i\epsilon^{-1}\theta(t)}\frac{\partial^2\delta\tilde{S}}{\partial z\partial t}$$
$$+ ie^{i\epsilon^{-1}\theta(t)}\frac{\partial\delta\tilde{S}}{\partial z}\frac{\partial\theta(t)}{\partial t} + \epsilon e^{i\epsilon^{-1}\theta(t)}\frac{\partial U_e}{\partial z}\frac{\partial\delta\tilde{S}}{\partial z} + \epsilon e^{i\epsilon^{-1}\theta(t)}U_e\frac{\partial^2\delta\tilde{S}}{\partial z^2}\Bigg)\Bigg]. \tag{B.10}$$

Appendix C

Compatibility condition

Here, we present the calculations of Compatibility condition used in Chapters 3 – 5. We start from writing down the governing Equations (2.75) and (2.76) obtained under approximation of geometrical optics

$$\frac{\partial^2 S_0}{\partial z^2} + \frac{\Omega^2}{\tilde{C}_k^2} S_0 = 0, \quad \tilde{C}_k = \frac{2\tilde{B}^2}{\mu_0(\rho_i + \rho_e)}, \tag{C.1}$$

$$S_0 = 0 \quad \text{at} \quad z = \pm L/2. \tag{C.2}$$

Then, we recall the governing equation obtained under approximation of physical optics

$$\begin{aligned}\frac{\partial^2 S_1}{\partial z^2} + \frac{\Omega^2}{\tilde{C}_k^2} S_1 = \frac{1}{\tilde{C}_k^2(\rho_i + \rho_e)} \Bigg[\frac{1}{2}\Omega^2(\rho_i - \rho_e) S_0 - \rho_e \left(\Omega^2 \delta\tilde{S} + \tilde{V}_{Ae} \frac{\partial^2 \delta\tilde{S}}{\partial z^2} \right) \\ - \frac{\delta\tilde{P}}{R^2} e^{-i\epsilon^{-1}\theta(t)} \Bigg] + \frac{2i\Omega}{\tilde{C}_k^2} \left[\frac{\partial S_0}{\partial t} + \frac{\rho_i U_i + \rho_e U_e}{\rho_i + \rho_e} \left(\frac{\partial S_0}{\partial z} + \frac{S_0}{R} \frac{\partial R}{\partial z} \right) + \frac{S_0}{2\Omega} \frac{\partial \Omega}{\partial t} \right],\end{aligned} \tag{C.3}$$

where

$$V_{Ae} = \epsilon^{-2} \tilde{V}_{Ae} = \frac{2B^2}{\mu_0 \rho_e}, \tag{C.4}$$

with the boundary condition

$$S_1 = 0 \quad \text{at} \quad z = \pm L/2. \tag{C.5}$$

Note, that in case $l = 0$, the right-hand side of Equation (C.3) only the last term remains. The homogeneous counterpart of Equation (C.3) with the boundary conditions given by Equation (C.5) has a non-trivial solution $S_1 = S_0$. As a result, the boundary value problem, which determines S_1, has a solution only if the right-hand side of Equation (C.3) satisfies the compatibility condition, meaning that it is orthogonal to S_0 . To obtain this condition we multiply Equation (C.3) by S_0 and apply boundary

condition Equation (C.5). Thus, we have

$$\frac{1}{\tilde{C}_k^2(\rho_i+\rho_e)}\left[\frac{1}{2}\Omega^2(\rho_e-\rho_i)S_0^2+\rho_e\left(\Omega^2\delta\tilde{S}+\tilde{V_{Ae}}\frac{\partial^2\delta\tilde{S}}{\partial z^2}\right)S_0+\frac{\delta\tilde{P}}{R^2}e^{-i\epsilon^{-1}\theta(t)}S_0\right]$$
$$=\frac{2i\Omega}{\tilde{C}_k^2}\left[S_0\frac{\partial S_0}{\partial t}+\frac{\rho_iU_i+\rho_eU_e}{\rho_i+\rho_e}\left(S_0\frac{\partial S_0}{\partial z}+\frac{S_0^2}{R}\frac{\partial R}{\partial z}\right)+\frac{S_0^2}{2\Omega}\frac{\partial\Omega}{\partial t}\right]. \tag{C.6}$$

Using the first and the last term of the right-hand side of Equation (C.6), we obtain

$$\frac{2i\Omega}{\tilde{C}_k^2}\left(S_0\frac{\partial S_0}{\partial t}+\frac{S_0^2}{2\Omega}\frac{\partial\Omega}{\partial t}\right)=\frac{i}{\tilde{C}_k^2}\frac{\partial S_0^2\Omega}{\partial t}. \tag{C.7}$$

It follows from Equations (C.1) and (C.7) that Equation (C.6) can be written as

$$\frac{1}{\tilde{C}_k^2}\frac{\partial S_0^2\Omega}{\partial t}=\frac{i}{\tilde{C}_k^2(\rho_i+\rho_e)}\left[\frac{1}{2}\Omega^2(\rho_i-\rho_e)S_0^2-\rho_e\left(\Omega^2\delta\tilde{S}+\tilde{V}_{Ae}\frac{\partial^2\delta\tilde{S}}{\partial z^2}\right)\right.$$
$$\left.-\frac{\delta\tilde{P}}{R^2}e^{-i\epsilon^{-1}\theta(t)}S_0\right]-\frac{\mu_0\Omega}{\tilde{B}^2}\left[(\rho_iU_i+\rho_eU_e)\left(S_0\frac{\partial S_0}{\partial z}+\frac{S_0^2}{R}\frac{\partial R}{\partial z}\right)\right]. \tag{C.8}$$

Rewriting the last term of the Equation (C.8), we obtain the following

$$\frac{\mu_0\Omega}{\tilde{B}^2}\left[\left(\rho_iU_i+\rho_eU_e\right)\left(S_0\frac{\partial S_0}{\partial z}+\frac{S_0^2}{R}\frac{\partial R}{\partial Z}\right)=\frac{\mu_0\Omega}{2\tilde{B}^2R^2}\left[\left(\rho_iU_i+\rho_eU_e\right)\frac{\partial S_0^2R^2}{\partial z}\right]\right. \tag{C.9}$$

Recalling that the mass conservation law, outside the transitional layer and not far away from the magnetic flux, may be written as

$$\frac{\partial\rho}{\partial t}+\frac{1}{R^2}\frac{\partial\rho R^2U}{\partial z}=0. \tag{C.10}$$

Therefore, integrating equation (C.8), using integration by parts, and employing equations (C.2), (C.10) and $\tilde{B}R^2=\text{const}$, we have

$$\int_{-L/2}^{L/2}\frac{1}{\tilde{C}_k^2}\frac{\partial S_0^2\Omega}{\partial t}dz=\int_{-L/2}^{L/2}\frac{i}{\tilde{C}_k^2(\rho_i+\rho_e)}\left[\frac{1}{2}\Omega^2(\rho_i-\rho_e)S_0^2-\rho_e\left(\Omega^2\delta\tilde{S}\right.\right.$$
$$\left.\left.+\tilde{V}_{Ae}^2\frac{\partial^2\delta\tilde{S}}{\partial z^2}\right)S_0-\frac{\delta\tilde{P}}{R^2}e^{-i\epsilon^{-1}\theta(t)}S_0\right]dz+\frac{\mu_0\Omega}{2}\int_{-L/2}^{L/2}\frac{S_0^2}{\tilde{B}^2R^2}\frac{\partial}{\partial z}\left(R^2(\rho_iU_i+\rho_eU_e)\right)dz. \tag{C.11}$$

Note that in the case of $l=0$, the first integral term on the right-hand side of Equation (C.11) disappears.